E.O. Paton Electric Welding Institute of the National Academy of Science of Ukraine
International Association «Welding»

The Paton Welding Journal

09
2023

International Scientific-Technical and Production Journal ◊ Founded in January 2000 (12 Issues Per Year)

Address of Editorial Board
E.O. Paton Electric Welding Institute, 11 Kazymyr Malevych Str., 03150, Kyiv, Ukraine
Tel./Fax: (38044) 205 23 90, E-mail: journal@paton.kiev.ua
https://patonpublishinghouse.com/eng/journals/tpwj

State Registration Certificate 24933-14873 ПР from 13.08.2021
ISSN 0957-798X, DOI: http://dx.doi.org/10.37434/tpwj

Subscriptions, 12 issues per year:
$384 — annual subscription for the printed (hard copy) version, air postage and packaging included;
$312 — annual subscription for the electronic version (sending issues in pdf format or providing access to IP addresses).

Representative Office of «The Paton Welding Journal» in China:
China-Ukraine Institute of Welding, Guangdong Academy of Sciences
Address: Room 210, No. 363 Changxing Road, Tianhe, Guangzhou, 510650, China.
Zhang Yupeng, Tel: +86-20-61086791, E-mail: patonjournal@gwi.gd.cn

The content of the Journal includes articles received from authors from around the world in the field of welding, cutting, cladding, soldering, brazing, coating, 3D additive technologies, electrometallurgy, material science, NDT and selectively includes translations into English of articles from the following journals, published in Ukrainian:
• Automatic Welding (https://patonpublishinghouse.com/eng/journals/as);
• Electrometallurgy Today (https://patonpublishinghouse.com/eng/journals/sem);
• Technical Diagnostics & Nondestructive Testing (https://patonpublishinghouse.com/eng/journals/tdnk).

CONTENTS

ORIGINAL ARTICLES

*Translated Article(s) from “Automatic Welding”, No. 9, 2023.

DOI: https://doi.org/10.37434/tpwj2023.09.01

CRYSTALLOGRAPHIC AND DIMENSIONAL CHARACTERISTICS OF STRUCTURE ELEMENTS IN WELDS OF HIGH-TEMPERATURE NICKEL ALLOY SINGLE CRYSTALS

I.S. Gakh, B.O. Zaderyi, G.V. Zviagintseva, A.V. Zavdoveyev, Yu.V. Oliinyk

E.O. Paton Electric Welding Institute of the NASU
11 Kazymyr Malevych Str., 03150, Kyiv, Ukraine

ABSTRACT

Crystallographic-orientational and dimensional-morphological features of microstructure in welded joints of high-temperature nickel alloy single crystals are considered, depending on the initial crystallographic orientation and its change over the weld solidification macrofront. EBSD analysis and optical metallography methods were used to study the structural features of individual zones of welded joints of high-temperature nickel alloy single crystals. Their dependence on the initial crystallographic orientation of the welded joint and its change over the weld pool solidification macrofront is established. It is shown that alongside the predominant inheritance of base metal crystallographic orientation by the weld metal, formation of a grain structure of different crystallographic orientation, morphology, dimensions and nature, namely solidification and deformation-induced, can be in place. The mechanisms of formation of grains of the specified nature are considered. Boundaries of solidification type grains are the junction of dendrite blocks with different crystallographic orientation. Deformation type grains are the result of relaxation of microstresses at the stage of welded joint cooling, and they form in areas where the direction of acting stresses is the closest to the crystallographic orientation of easy slip. It was also found that deformation type grains can form both in the weld metal, and in the HAZ. At the same temperature conditions of making the welded joints, the quantitative and dimensional-orientational parameters of deformation structure of the HAZ metal correlate with similar parameters of weld structure elements. The possibility to produce welds without cracks with perfect single crystal structure is indicated.

KEYWORDS: single crystals, high-temperature nickel alloys, welded joints, EBSD-analysis, crystallographic orientation, structure parameters, grain nature, weld pool, solidification macrofront

INTRODUCTION

The work is related to constantly growing demand for improvement of tactical and technical, service, production and ecological characteristics of gas turbine engines (GTE), and power units (GTU) of both military and civil applications [1–3]. As is known, improvement of thermodynamic characteristics of GTE and GTU is achieved mainly due to increase of gas temperature at the turbine inlet and lowering the rotor metal content and weight that requires creation and application of new high-temperature materials [4, 5]. Increase of high-temperature strength due to more complex alloying, application of alloys, particularly those with a single crystal structure, has now reached its limit, chiefly, in connection with the accompanying deterioration of their adaptability-to-manufacture. Therefore, the majority of designers and manufacturers choose the path of improvement of the turbine design, including application of welding [3, 6]. However, the higher the alloy high-temperature strength, the lower is their weldability, which is manifested in a high susceptibility of high-temperature nickel alloys to cracking and deterioration of the specially created structural state, especially single crystallinity, which ensures an optimal combination of the mechanical characteristics in a broad range of temperatures and loads.

The majority of publications on welding of single crystals of high-temperature nickel alloys (HTNA) consider the conditions of initiation and prevention of formation in the welds of the so-called defects of single crystal growth structure and cracks [7–10]. Results of studying the mechanical characteristics and features of welded joint formation [11, 12] point to the need for a more detailed study of the structure orientation changes, occurring as a result of thermodeformational impact in welding. This applies, in particular, to the crystallographic orientation spectrum, both as a whole, and as individual structural components: presence of local structures, microstresses and strains; nature, morphology and size of structural elements, boundaries and extent of their misorientation as factors, which determine the welded joint mechanical and service properties.

The objective of the work is determination of the influence of the sample initial crystallographic orientation on the structural features of HTNA single crystal welded joint and its change over the weld width.

INVESTIGATION PROCEDURE

Commercial high-temperature alloys with more than 61 % of the intermetallic dispersion-strengthening γ'-phase were selected for investigation performance.

These alloys are widely used as structural material in manufacture of blades of aviation GTE hot section.

Studies conducted by us [8, 9] and other authors [7, 10] of the crystallographic orientation of the joint and influence of the curvature of weld pool solidification macrofront on inheritance of the initial crystallographic orientation by the weld metal and perfection of its structure showed that in order to prevent grain and crack formation, it is necessary to ensure a deviation of the direction of temperature gradient passage through the solidification front from <001> direction. In terms of technology, it is achieved by the correspondence of the plane of welded butt joint edges to the high symmetry orientation {100} and formation of macroplanar front of weld pool solidification. Two main crystallographic combinations: {001}, <100> and {110}, <011> were selected at analysis of possible variants of crystallographic orientation in the welded sample joint (initial metal plane {UVW} and welding directions <hk1>. Collection of samples of the selected crystallographic orientations for welding was performed with up to 5° accuracy. Test samples of {110}, <011> orientation had deviations from the selected one within 10° in some cases, which during welding can result in different value of the angle of deviation of the maximal temperature gradient from <001> direction over the solidification front [8]: up to 15° — favourable conditions, above the indicated level — unfavourable conditions for single crystal structure formation. Samples of 2 mm thickness were cut out by electric spark method from single crystal castings produced by high-gradient directional solidification, with subsequent grinding and etching.

Electron beam welding was performed in modes ensuring stable formation of through-thickness uniform penetration and the temperature-time conditions of single crystal structure formation.

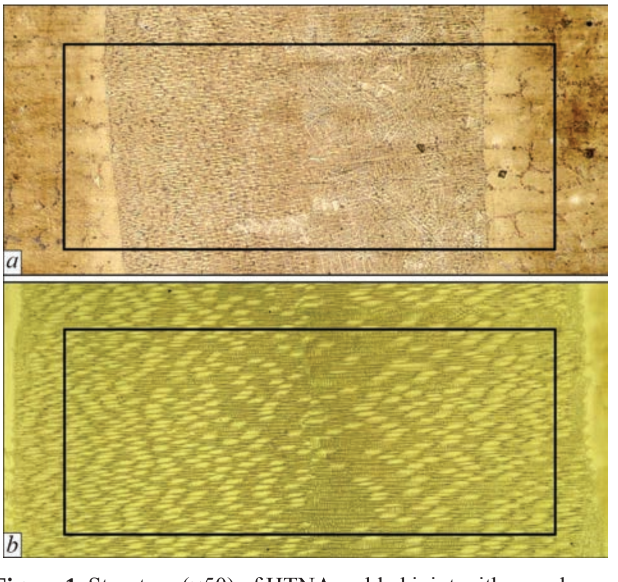

Figure 1. Structure (×50) of HTNA welded joint with sample surface close to (101) (*a*) and (001) (*b*) with outlined areas studied by EBSD

Over the recent years EBSD analysis is becoming successfully applied for evaluation of structural changes in single and polycrystalline materials as a result of technological and service effects, due to automated combination of step-by-step assessment of local (0.05–1.0 μm) structural-deformational changes and subsequent plotting of generalized patterns [13, 14]. Its application provides broader information, compared to the traditional methods of structure evaluation: X-ray structural, electron diffraction in TEM, neutron diffraction, optical metallography, etc., which are chiefly directed at detection and subsequent investigation of the main defects of single crystal growth structure, such as jet segregation, parasitic grains, surface carbides, etc. At the same time, it is known that optimization of HTNA structure parameters is one of the ways to meet the high requirements to the mechanical and service properties of these alloys [12–16]. Moreover, more detailed quantitative and qualitative evaluation of the structure and development of methods to control its formation in welding are becoming ever more urgent.

The advantages of EBSD analysis are especially evident, when studying the single crystal welded joints which are a composition of areas of different structure and crystallographic orientation. Its application provides a large scope of information, required for assessment of the joint structure evolution, important when solving both the theoretical and applied issues of structure formation and control during welding. One of the important advantages of EBSD analysis is the possibility to determine the type and ratio of structure elements and its formation mechanism. When studying the single crystals, the main object of research is the availability and characteristics of grain boundaries as the main factor determining the structure performance: their type, morphology, parameters of shape and dimensions, orientation and specific share of each type. A not less important factor and advantage of EBSD analysis of the welded joints is the clear presentation of the crystallographic orientation of both individual areas and elements of the structure by colour coding in the respective research maps and as a whole.

Investigations of structural-crystallographic state of the welded joints were performed on microsections taken from the sample surface with application of Neophot-32 optical microscope and Verios 460 XHL electron microscope with HKL Nordlys System attachment for EBSD analysis. The general area of scanning by the electron beam is 796×2000 μm, with 2×4 μm locality. Figure 1 illustrates the area studied

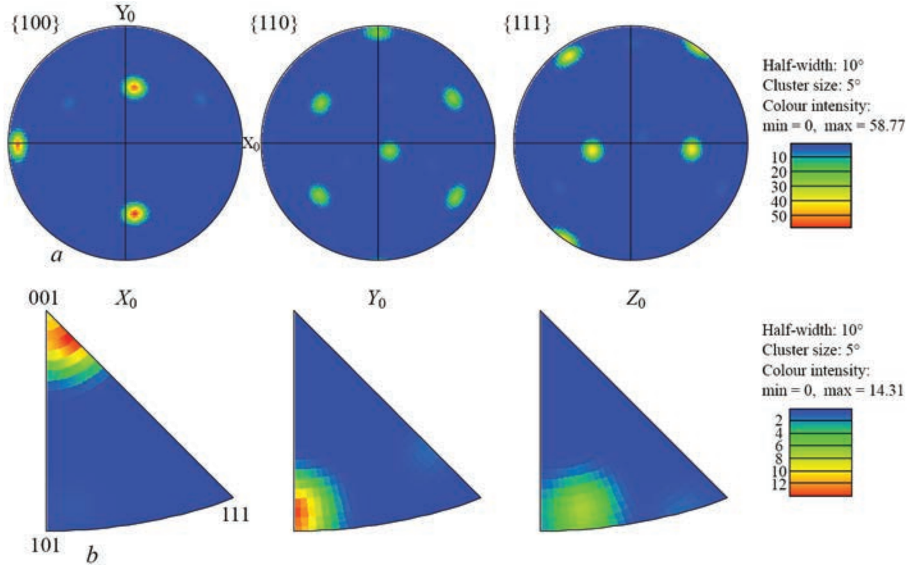

Figure 2. Straight (*a*) and inverse (*b*) pole figures of base metal of single crystal HTNA welded joint with sample surface close to (101)

by EBSD analysis on the welded joints. The characteristic areas of single crystal welded joints revealed during analysis [16, 17] were considered: base metal, HAZ, fusion line, epitaxial growth zone and weld areas with different deviations of the crystallographic orientation from the initial one.

In some cases the crystallographic orientation of the structure was evaluated by metallographic etching patterns. The structure was recorded using an optical microscope. Structure visualization was here performed by microsection surface etching.

Sample preparation for EBSD analysis included a special grinding-polishing technology [13, 14], which allows avoiding the sample surface cold hardening, ensuring a high accuracy of the results. During investigations, the focus was on the welded joints and their individual areas, for which the conditions of directional solidification of the single crystal and formation of a perfect single crystal structure were fulfilled or were not ensured [7–9, 16, 17]. The features of crystallographic orientation and dimensional-morphological characteristics of individual characteristic zones of welded joints, depending on fulfillment of the above-mentioned conditions were considered.

INVESTIGATION RESULTS

The base metal structure is characterized by a typical developed homogeneous coarse-dendritic architecture [15] with directional crystallographic orientation (Figures 2, 3), which corresponds to sample orientation as a whole, and which is determined by the conditions of high-gradient growing of the initial single crystal.

The HAZ metal preserves the initial crystallographic orientation. When moving closer to the fusion line, however, a change in the morphology and

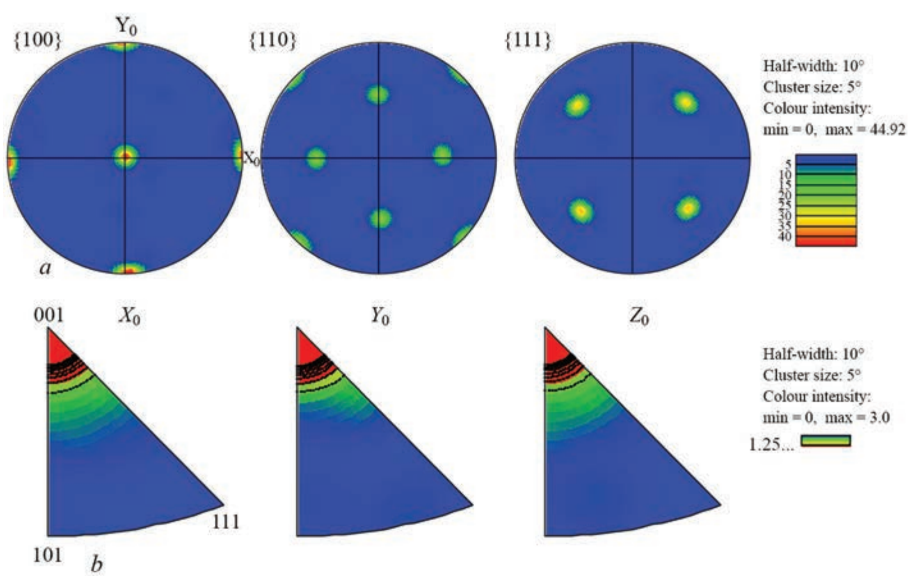

Figure 3. Straight (*a*) and inverse (*b*) pole figures of base metal of single crystal HTNA welded joint with (001) sample surface

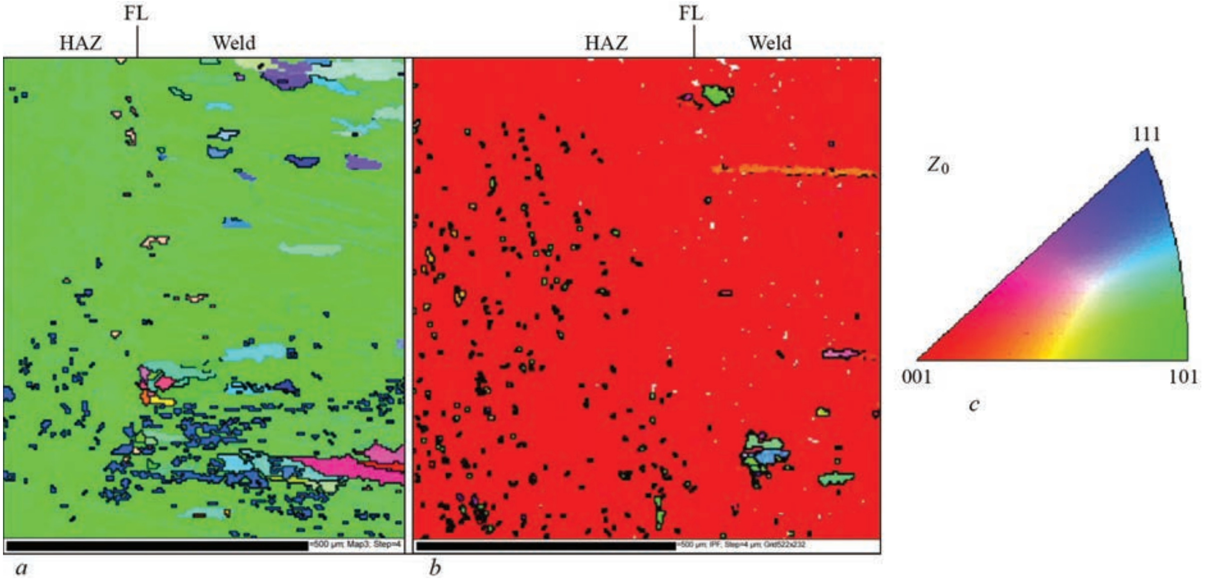

Figure 4. Orientation maps of epitaxial growth zone and HTNA sample fusion areas with surface close to (101) (*a*) and (001) (*b*) at compliance of initial crystallographic orientation (CGO) with directional solidification conditions. CGO is the legend for orientation map, HAZ is the heat-affected zone, FL is the fusion line

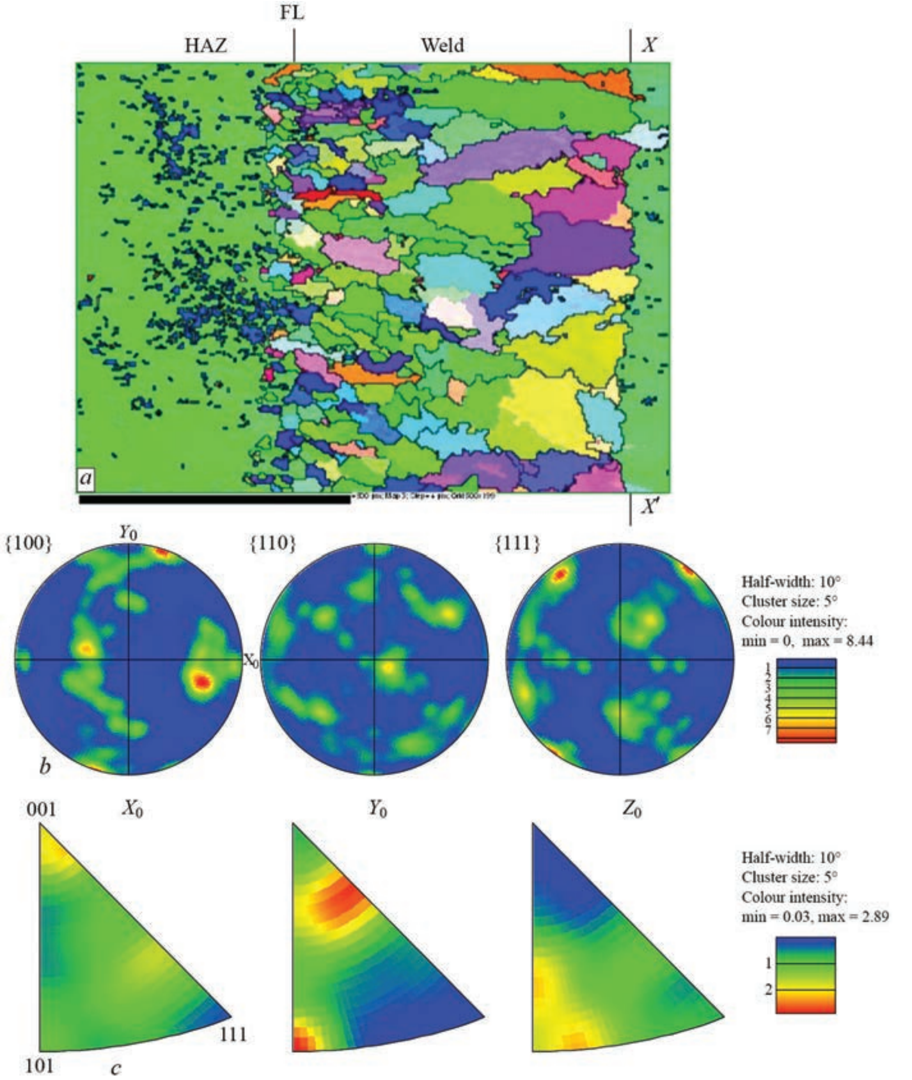

Figure 5. Orientation maps (*a*) of a welded joint area with sample surface close to (101), straight and inverse pole figures (*c*) at non-compliance of weld area with directional solidification conditions. CGO is the legend for orientation map (Figure 4, *c*), HAZ is the heat-affected zone, FL is the fusion line, *X*–*X*′ is the weld axis

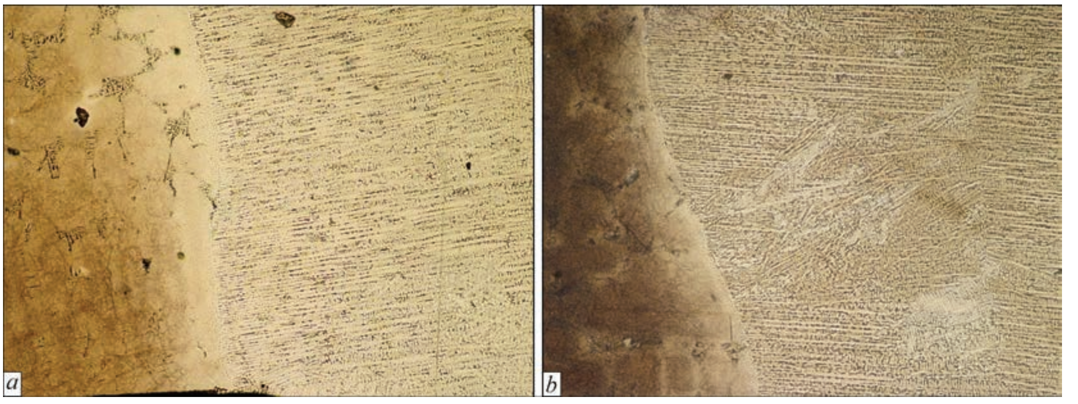

Figure 6. Microstructure (×100) of HTNA weld area near the rectilinear fusion zone (*a*) and local change of its geometry (*b*)

dimensions and distribution of the main strengthening component of the alloy, namely γ- γ′-phase is in place, which was discussed in detail in work [17]. In the HAZ microstructure of a sample with a favourable crystallographic orientation, formation of up to 10 % of scattered fine grains of up to 10 μm size of [111] orientation is observed for [101] initial orientation (Figure 4, *a*), and of [101] orientation — for [001] initial orientation (Figure 4, *b*), respectively, which may be indicative of their deformation nature. Alongside a certain crystallographic orientation, the deformation nature of the detected grains is indicated by their morphology, dimensions and results of comprehensive analysis of the maps of orientations and microstresses, as well as their location in the welded joint. The number of the grains, similar to their orientation, correlates with the degree of deviation of the initial crystallographic orientation from the high symmetry direction. Note that they were not revealed by metallography.

In case of noncompliance of the welded joint crystallographic orientation with the high-symmetry (Figure 5), the quantity of grains of [111] orientation in the HAZ grows to 20 % at a pronounced tendency to their concentration.

The fusion line zone is a transition area from the HAZ to the zone of weld metal epitaxial growth. Its structure is characterized by presence of partially melted dendrites and interdendritic gaps [17]. Partially melted dendrites take the shape of cells, a change in the crystallographic orientation being hardly noticeable. Now, in case of noncompliance of the welded joint crystallographic orientation with the high symmetry (Figure 5), this zone is characterized by a fine-grained structure (5–40 μm) with prevalence of the crystallographic orientation, corresponding to initial one and to orientation of deformation type grains.

The zone of epitaxial growth was defined from the very beginning of investigations as an area, which in metallographic presentation consists of orthogonal fusion lines of fine dendrites located in parallel [17]. In the case of a symmetrical welded joint, its structure points to preservation of the initial crystallographic orientation and presence of individual fine (5–40 μm) grains of [111] orientation (Figure 4, *a*) or [101] orientation (Figure 4, *b*). In case of noncompliance of crystallographic orientation of the welded joint or weld area with high symmetry (Figure 5, *a*) this zone is characterized by a fine-grained structure (40–70 μm).

For samples with a favourable crystallographic orientation, a certain increase of individual grain size

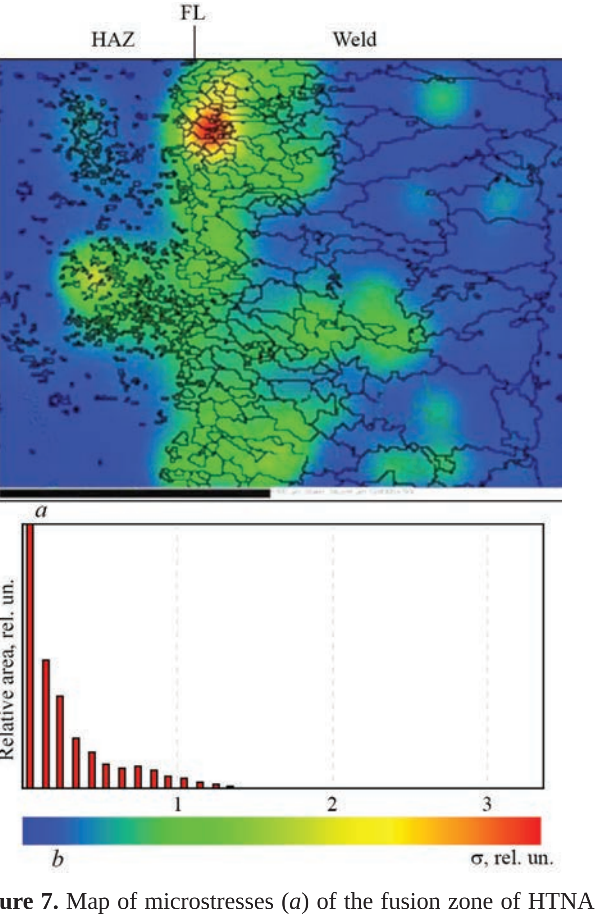

Figure 7. Map of microstresses (*a*) of the fusion zone of HTNA sample weld with surface close to (101) and frequency histogram (*b*) at noncompliance of the weld area to crystallographic conditions of directional solidification. HAZ is the heat-affected zone, FL is the fusion line

in the weld metal structure with preservation of base metal orientation (Figure 4, *a*, *b*) is possible, when moving closer to the axis.

For a sample with welded joint crystallographic orientation noncompliant with the high symmetry, the structure develops coarse grains of different size (up to 300 μm), predominantly oriented orthogonally to the weld pool solidification front, when moving closer to the axis, both in the metallographic and EBSD presentation. In addition to grain size increase, a violation of single crystallinity is clearly manifested. In the straight pole figures appearance of new reflexes, shifting and blurring of the main ones is observed; in reverse figures a decrease of the intensity and accent of the reflexes are found (Figure 5). Maximal increase of the dimensions and defectiveness of the structure, orientation deviation from the initial one are observed in the vicinity of the weld axis (Figure 5), where a local change in the curvature of weld pool solidification macrofront results in violation of the main condition of directional solidification — the relationship of crystal growth direction and its orientation [001]. It is exactly the area where hot cracking and destruction of the joint is the most often observed at high-temperature testing [7, 10, 11, 16]. A similar situation was also observed in the areas of local changes of weld geometry (Figure 6), as a result of different technological disturbances, or weld pool fluctuations even in crystallographic symmetry of the welded joint (Figure 4, *a*, *b*).

Note that appearance of a high concentration of deformation-induced fine grains with [111] orientation for the initial [101] orientation is found around formations of longitudinal solidification grains (Figure 4, *a*).

Clusters of fine grains of different crystallographic orientation, more often found in the zone of the fusion line, leads to microstress concentration (Figure 7), which has a negative influence on the performance of the joint as a whole.

Comparison of the results of EBSD-analysis and metallographic examination [9, 14, 17] points to the nature of grains of a different orientation, which can form in welding of HTNA single crystals: solidification and deformation-induced. The solidification grains boundaries form during metal solidification at abutment of weld dendrite blocks of different orientation, those of deformation-induced grains form as a result of stress relaxation at metal cooling by the mechanism of, most probably, polygonization and

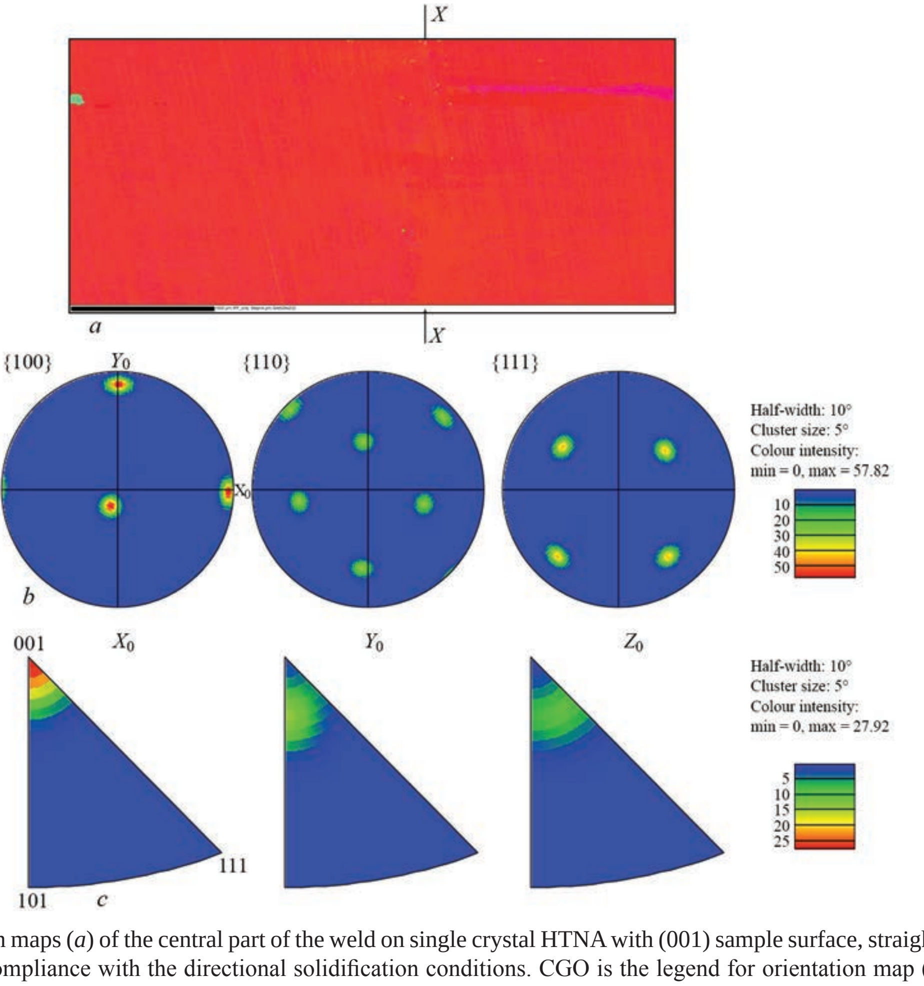

Figure 8. Orientation maps (*a*) of the central part of the weld on single crystal HTNA with (001) sample surface, straight (*b*) and inverse (*c*) pole figures at compliance with the directional solidification conditions. CGO is the legend for orientation map (see Figure 4, *c*), *X*–*X*′ is the weld axis

dynamic recrystallization. The deformation-induced grain boundaries can pass both through the interdendritic gaps and through the dendrite body, depending on the relative orientation of acting stresses and dendrites. Here, the dimensions, morphology and orientation of deformation-induced grains correlate with the respective parameters of the solidification grains and dendrites.

In view of the different nature of the considered grains, despite a certain similarity of their parameters, the technological paths for prevention of the above-mentioned grain formation will be different. However, the geometry of weld pool solidification front and crystallographic orientation of the joint line are of prevailing important.

It should be further noted that under the same temperature conditions of making the welded joint, the quantitative and dimensional-orientational parameters of the deformation structure of the HAZ metal have a certain correlation with similar parameters of the weld structure elements. The established dependencies can be indicative of the influence of the weld metal solidification structure on the nature of deformation distribution, also in the HAZ, at the welded joint cooling stage.

It should be emphasized that under favourable crystallographic conditions, due to formation of the appropriate geometry of the weld pool and technological guarantee of the values of temperature-time parameters [8, 16, 18] at the solidification front by the directional solidification conditions, it is possible to produce welds with satisfactory perfection of the single crystal structure (Figures 3, 8).

By the results of the conducted investigations with application of EBSD-analysis when studying the structural evolution of welded joints in HTNA single crystals, there is an obvious need to perform work on regulation of the dimensions, morphology, misorientation, number and nature of distribution of the structure components and expansion of the technological control methods.

CONCLUSIONS

1. One of the main factors, which determine the features of structure formation in welding HTNA single crystals, is not only the initial crystallographic orientation of the welded joint, but also its change over the weld pool solidification front.

2. The methods of EBSD-analysis and optical microscopy were used to show that deviation of the initial crystallographic orientation of welded joints in 2 mm single crystal HTNA by more than 5° and of the front of weld pool solidification by more than 15° from the direction of prevailing crystal growth of <001> leads to violation of the epitaxial inheritance of the initial orientation by the weld metal and to formation of grains of a different orientation.

3. To achieve the specified perfection of single crystal structure of the welded joints, in addition to following the main conditions of directional solidification (temperature-time and crystallographic-orientational), it is necessary to ensure limitation of local changes of weld pool geometry, which is determined by the joint design, service conditions, welding modes and scheme.

4. Failure to fulfill the crystallographic orientation and temperature-time conditions of formation of a perfect single crystal structure of weld metal leads to development of a grain structure of solidification and deformation origin (nature), of different morphology and dimensions. After a narrow zone 100–150 μm wide of fine equiaxed grains (up to 40–70 μm), a transformation of the structure into a directional coarse-grained one (40–300 μm) is found near the fusion line when moving closer to the weld axis, which is associated with a change of temperature-time and crystallographic orientation conditions of solidification over the joint cross-section. A correlation of the parameters of secondary (final) and solidification (initial) structure is found. Clustering of fine grains, particularly, in the zone of the fusion line, promotes a concentration of microstresses.

5. It is shown that under the same temperature parameters of making the welded joint, formation of deformation type grains is in place in the HAZ. Depending on orientation conditions, it is up to 10% under favourable, and up to 20 % under unfavourable conditions, which is attributable to different susceptibility of the metal to deformation localization.

6. The following structure elements are considered to be critical:

- transverse elongated grains of different crystallographic orientation in the weld central part, the boundaries of which are the crack initiation site during welding;
- concentration of fine grains of different orientation, particularly near the fusion line, where localization of stresses and strains occurs, thus increasing the susceptibility to destruction at high-temperature mechanical loads, and lowering the welded structure performance.

7. Results of the conducted studies improve our understanding of structure formation and its evolution, depending on the welding process factors, and they indicate the possibility of creation of industrial welded structures from HTNA single crystals.

REFERENCES

1. Logunov, A.V., Burov, M.N., Danilov, D.V. (2016) Development of power and marine engine construction in the world (Review). *Dvigatel*, **1,** 10–13 [in Russian].
2. Tsukagoshi, K., Muyama, A., Masada, J. et al. (2007) Mitsubishi Heavy Industries, Ltd. *Technical Review*, 44(**4**), 1.
3. (2019) XF9-1, the World's Best Standards Fighter Engine, Has Been Completed — Japan's Military Technology, Interview with the Developer, *Blogos*, Pt 1–2, 4.
4. Hino, T., Kobayashi, T., Koizumi, Y. et al. (2000) *Superalloys*. Eds by T.M. Pollock, R.D. Kissinger, R.R. Bowman et al. TMS: 2000.
5. Koizumi, Y., Kobayashi, T., Yokokawa, T. et al. (1998) *Cost Conf. Liege*, Pt 2, 1089.
6. Langston, L.S. (2014) *Global Gas Turbine News*, **9**, 76.
7. Park, J.W., Vitec, J.M., Babu, S.S., David, S.A. (2004) Stray grain formation, thermomechanical stress and solidification cracking single crystal nickel base superalloy welds. *Sci. and Technol. of Welding and Joining*, 9(**6**), 472–482. DOI: 10.1179/136217104225021841
8. Yushchenko, K.A., Gakh, I.S., Zadery, B.A. et al. (2013) Influence of weld pool geometry on structure of metal of welds on high-temperature nickel alloy single crystals. *The Paton Welding J.*, **5**, 45–50.
9. Yushchenko, K.A., Zadery, B.A., Karasevskaya, O.P. et al. (2009) On possibility of inheritance of single crystal structure of complex nickel alloys in nonequilibrium conditions of fusion welding. *Metallofizika i Novejshie Tekhnologii,* 31**(4)**, 473–485 [in Russian].
10. Anderson, T.D., Du Pont, J.N. (2011) Stray grain formation and solidification cracking susceptibility of single crystal Ni base superalloy CMSX-4. *Welding J.*, **2**, 27–31.
11. Karasevska, O.P., Yushchenko, K.A., Zaderiy, B.O. et al. (2021) Deformation and fracture of single crystals of high-strength nickel alloys with welded joints during tensile testing. *Metalofizyka. Novitni Tekhnol.,* 43(**7**), 939–957 [in Ukrainian].
12. Golubovsky, E.P., Svetlov, I.L., Epishin, A.I. (2005) Influence of crystallographic orientation on strength characteristics of single crystals of high-temperature nickel alloy. *Nauchnye Trudy MATI*, 80(**8**). Moscow, ITsMATI, 22–27 [in Russian].
13. Shvarts, A., Kumar, M., Adams, B. et al. (2004) *Diffraction method of reflected electrons in materials science.* Moscow, Tekhnosfera [in Russian].
14. Varyukhin, V.N.., Pashinskaya, E.G., Zavdoveev, A.V. et al. (2014) *Possibilities of diffraction method of back scattered electrons for analysis of structure of wrought materials.* Kyiv, Naukova Dumka [in Russian].
15. Shalin, R.E., Svetlov, I.L., Kachanov, E.B. et al. (1997*) Single crystals of high-temperature nickel alloys.* Moscow, Mashinostroenie [in Russian].
16. Gakh, I.S. (2011) *Physical-technological features of electron beam welding of high-nickel high-strength alloys with single crystal structure*: Syn. of Thesis for Cand. of Techn. Sci. Degree. Kyiv [in Ukrainian].
17. Yushchenko, K.A., Zadery, B.A., Gakh I.S. et al. (2021) Features of the microstructure of welded joints of single crystals of heat-resistant nickel alloys. *Metallofiz. Noveishie Tekhnol.*, 43(**9**), 1175–1193.
18. Yushchenko, K.A., Zadery, B.A., Gakh I.S. et al. (2016) Formation of weld metal structure in electron beam welding of single crystals of high-temperature nickel alloys. *The Paton Welding J.*, **8**, 15–22. DOI: doi.org/10.15407/tpwj2016.08.04

ORCID

I.S. Gakh: 0000-0001-8576-4234,
B.O. Zaderyi: 0000-0001-6695-6986,
G.V. Zviagintseva: 0000-0002-6450-4887;
G.V. Zviagintseva: 0000-0003-2811-0765,
Yu.V. Oliinyk: 0000-0002-9293-4315

CONFLICT OF INTEREST

The Authors declare no conflict of interest

CORRESPONDING AUTHOR

I.S. Gakh
E.O. Paton Electric Welding Institute of the NASU
11 Kazymyr Malevych Str., 03150, Kyiv, Ukraine.
E-mail: gakh@paton.kiev.ua

SUGGESTED CITATION

I.S. Gakh, B.O. Zaderyi, G.V. Zviagintseva, A.V. Zavdoveyev, Yu.V. Oliinyk (2023) Crystallographic and dimensional characteristics of structure elements in welds of high-temperature nickel alloy single crystals. *The Paton Welding J.*, **9**, 3–10.

JOURNAL HOME PAGE

https://patonpublishinghouse.com/eng/journals/tpwj

Received: 14.06.2023
Accepted: 09.10.2023

DOI: https://doi.org/10.37434/tpwj2023.09.02

STRUCTURE AND PROPERTIES OF WELDED JOINTS OF 06G2BDP STEEL

S.L. Zhdanov, V.D. Poznyakov, A.V. Zavdoveyev, A.M. Herasymenko, O.G. Synyeok, A.O. Maksymenko, V.D. Ryabokon

E.O. Paton Electric Welding Institute of the NASU
11 Kazymyr Malevych Str., 03150, Kyiv, Ukraine

ABSTRACT

Ensuring reliable operation of bridge metal structures requires solving a wide range of issues, in particular, development of new local materials with guaranteed characteristics, which would provide the required durability of bridge structures. Modern requirements to materials for building metal structures and bridges are met by high-strength sparsely-alloyed 06GB, 06G2B steels, which were the base for development of 06G2BDP steel of 355–500 MPa class with higher resistance to atmospheric corrosion. Application of the corrosion-resistant steel for fabrication of bridge metal structures will allow improvement of their reliability and service life. The work deals with the influence of welding technology parameters on the structure and properties of welded joints of 06G2BDP steel.

KEYWORDS: bridge metal structures, corrosion-resistant steel, structure, welded joints, welding consumables, mechanical properties

INTRODUCTION

At present there is the need in metal structure fabrication for high-strength sheet steels with high mechanical properties and increased resistance to atmospheric corrosion [1–3]. This is indicated by the results of inspection of such metal structures with concrete roadway, main girders and transverse beams of steel. They showed that the main type of their damage is reduction of the cross-section of the girths and webs of the beams as a result of corrosion, which significantly lowers the structure load-carrying capacity and bridge serviceability [4–7]. A combination of design and technology factors, as well as application of ordinary construction steels in earlier build bridges, having relatively low corrosion resistance, promote an accelerated development of this process [8]. Application of higher corrosion resistance steels in metal span structures of bridges is important in terms of extension of their service life and lowering the bridge operating costs.

At present sparsely-alloyed steels of 06GB, 06G2B grades have been introduced into construction of critical welded metal structures [9]. These steels have a higher strength and cold resistance and by these values they differ favourably from 09G2S, 10KhSND steels, which are usually applied in fabrication of local metal structures. At the same time, in order to increase the corrosion resistance of 06G2B steel, a new steel of 06G2BDP grade was developed on its base [10], which contains 0.04–0.12 % carbon, depending on the steel grade, 0.90–1.75 % manganese, 0.30–0.45 % copper, and ≤0.012 % sulphur. Higher phosphorus content, particularly in contact with copper, enables increasing the corrosion resistance, but it can impair the deformation properties of the metal and can cause its cold brittleness, so that phosphorus content in the steel is limited to 0.05 % (Table 1). A combination of high strength and high impact toughness of 06G2BDP steel (Table 2) was produced by modifying treatment and thermal improvement.

Table 1. Chemical composition of the studied steels, wt.%

Rolled stock/melt	Thickness, mm	C	Mn	Si	P	S	Cr	Ni	Mo	Cu	Al	Nb	Ti
06G2BDP experimental melt	13	0.068	1.36	0.082	0.053	0.011	0.30	0.14	0.15	0.47	0.018	0.056	0.004
06G2BDP TU U27-05416823-078:2006	8–50	0.04–0.08	1.10–1.40	0.15–0.35	0.030–0.050	0.012	Before 0.30	Before 0.30	0.02–0.05	0.30–0.45	0.02–0.05	0.010–0.030	Before 0.020
06G2B	–	0.08	1.3	0.25	0.025	0.01	–	–	0.1	0.3	0.02	–	–
10KhSND	–	≤0.12	0.8	0.8	0.03	0.035	0.6	0.5	–	0.4	–	–	–

Table 2. Mechanical properties of steels

Steel grade/class	σ_y, MPa	σ_t, MPa	δ_5, %	KCV^{-20}	KCV^{-40}
06G2B C390	390	490	22	–	98
06G2BDP C390	390	490	22	68	49
10KhSND C390	390	530–685	19	–	29
06G2BDP experimental melt	529–534	645–666	24.7–27.3	298–310	230–298

By the results of studying the static strength, ductility, impact toughness and corrosion resistance it is shown that 06G2BDP steel is promising in terms of its application for building bridges, and other critical structures [11].

INVESTIGATION PROCEDURE

In order to ensure reliable operation of the structure, the welded joint metal, including the weld and HAZ, should have sufficient strength and cold resistance. These characteristics are determined, on the one hand, by the chemical composition, heat treatment and thickness of the metal being welded, and on the other hand, by welding conditions: heat input, preheating, technique of making the joints, etc. The work is devoted exactly to this analysis.

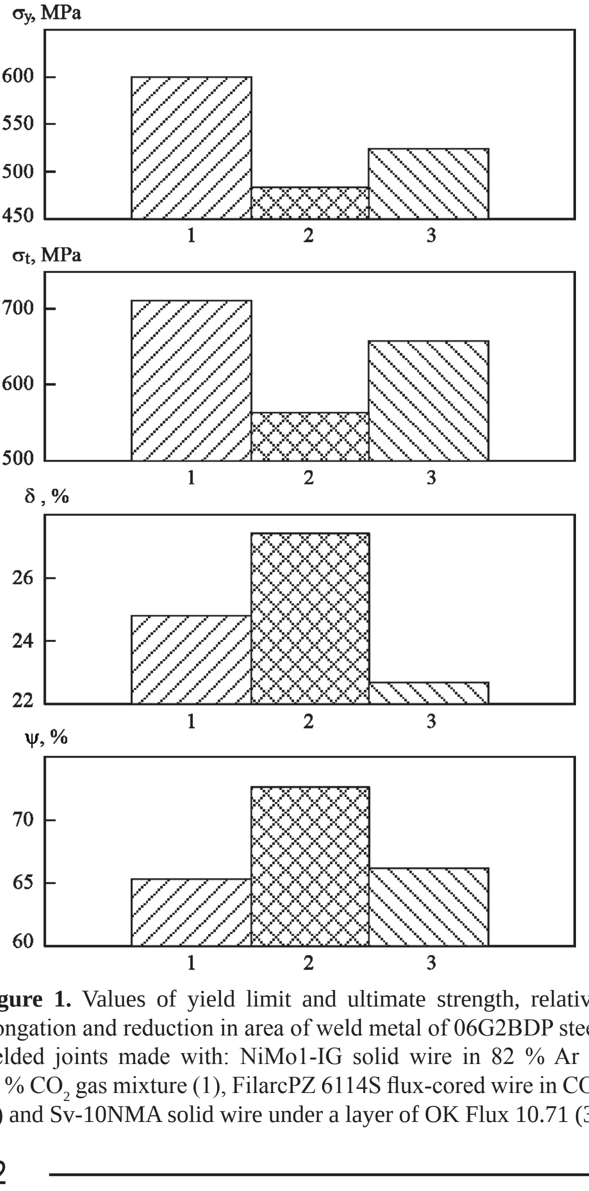

Figure 1. Values of yield limit and ultimate strength, relative elongation and reduction in area of weld metal of 06G2BDP steel welded joints made with: NiMo1-IG solid wire in 82 % Ar + 18 % CO_2 gas mixture (1), FilarcPZ 6114S flux-cored wire in CO_2 (2) and Sv-10NMA solid wire under a layer of OK Flux 10.71 (3)

For further development of arc welding technologies for fabrication of metal structures of bridge spans and engineering facilities from 06G2BDP steel, investigations were conducted using modern methods of light and electron metallography, and physical tests to study the influence of arc welding technologies on structure formation, mechanical properties and cold resistance of the HAZ metal. Flux-cored wire and solid wire for mechanized gas-shielded welding and solid wire for automatic submerged-arc welding were selected for these purposes.

Butt joints with V-shaped groove were made from 13 mm 06G2BDP steel for investigation performance. Mechanized welding in 82 % Ar + 18 % CO_2 gas mixture was performed with 1.2 mm Ni-Mo1-IG solid wire (Boehler Thyssen Company) and in CO_2 with 1.2 mm Filarc PZ 6114S flux-cored wire (ESAB Company). Welding modes were practically the same for both variants and were as follows: I_w = 190–220 A, U_a = 26–28 V, V_w = 14–16 m/h, shielding gas (mixture) flow rate was 15–18 l/min. Automatic submerged-arc welding with OK Flux 10.71 ceramic flux (ESAB Company) was performed with 4 mm Sv-10NMA solid wire in the following mode: I_w = 520–530 A, U_a = = 32 V, V_w = 28 m/h.

WORK RESULTS AND THEIR DISCUSSION

Building metal structures are usually made using mechanized gas-shielded and automatic submerged-arc welding. When mounting the structures, welding is most often performed by manual arc process, using coated electrodes.

Many years of experience showed that mechanized gas-shielded arc welding of structural steels of C390 grade is performed with Sv-08G2S solid wire, automatic submerged-arc welding is conducted with AN-348 or AN-47 flux with wires of Sv-08GA or Sv-10NMA grades, and manual arc welding — with electrodes of UONI-13/55 grade.

As regards welding steels of C500 and higher grade, to which 06G2BDP steel belongs, the normative documents on bridge building do not give any precise recommendations on selection of materials for their welding. Therefore, one of the main tasks of this study was substantiation of application of a par-

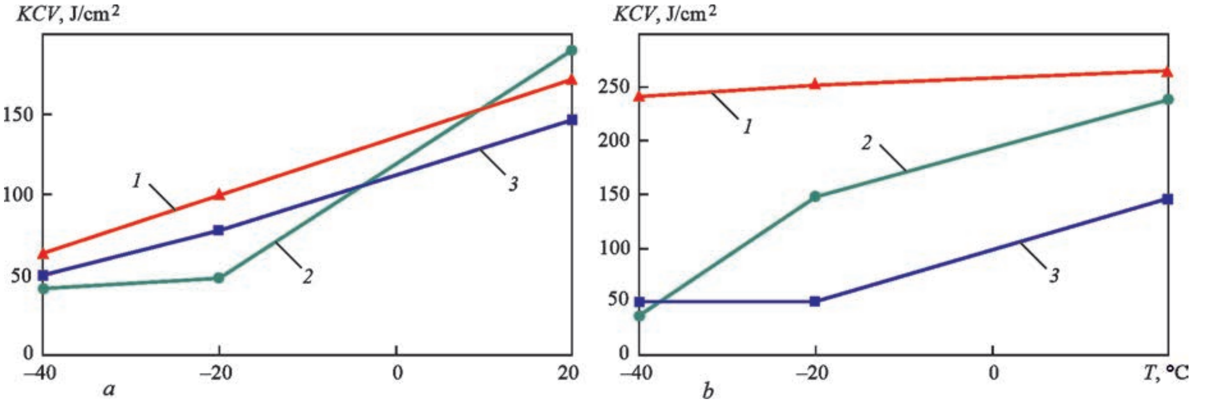

Figure 2. Impact toughness of weld metal (*a*) and HAZ metal (*b*) in 06G2BDP steel welded joints: *1* — NiMo1-IG wire, 82 % Ar + 18 % CO_2; *2* — FilarcPZ 6114S flux-cored wire, CO_2; *3* — Sv-10NMA wire, OK Flux 10.71

ticular material for welding metal of the above class. Obtained data on mechanical properties of the weld metal show (Figure 1) that the values of static strength and ductility of the weld metal, both in mechanized gas-shielded welding and in automatic submerged-arc process, are considerably higher than similar values of base metal of 06G2BDP steel of C390 class.

NiMo1-IG solid wire in combination with a shielding gas mixture of 82 % Ar + 18 % CO_2 and Sv-10NMA solid wire under a layer of OK Flux 10.71 ceramic flux ensure equivalent strength and 15–20 % higher σ_y and σ_t values of base metal of 06G2BDP steel of 500 class. Ductility values are also at a sufficiently high level, exceeding the standard values for steel.

By the static strength and ductility values the recommended welding processes and consumables ensure the required level of weld metal mechanical properties, and they can be used for fabrication of metal structures from 06G2BDP steel of C390 class, and they can be applied for welding steels of C500 class, except for Filarc PZ 6114S flux-cored wire.

Derived results of impact toughness studies (Figure 2) demonstrate that welds made with NiMo1-IG solid wire in 82 % Ar + 18 % CO_2 gas mixture and with Sv-10NMA solid wire under a layer of OK Flux 10.71 correspond to standard values ($KVC^{-20} \geq 68$ J/cm^2 and $KCV^{-40} \geq 49$ J/cm^2). In particular, in welding with NiMo1-IG wire in a gas mixture, *KCV* values of the metal of welds and HAZ exceed the base metal impact toughness 1.5–2.0 and 3.0–3.5 times, respectively.

High values of impact toughness are confirmed by fractographic studies of sample fractures after testing. So, at testing samples with a notch in the weld middle, the fracture mode at –40 °C temperature at the notch tip and in the final fracture zone is ductile with pit size d_p = 0.4–5 μm, being quasibrittle only in the zone of the main crack propagation (Figure 3). At the same temperature conditions in samples with a notch in the HAZ the fracture mode is 100 % ductile in all the zones with a large cluster of small pits of d_p = = 1–5 μm (Figure 4).

Contrarily, application of Filarc PZ 6114S flux-cored wire provides impact toughness of the metal of welds and HAZ of welded joints at the required level only at 20 °C testing temperature. At testing temperature lowering to –20 and –40 °C *KCV* values decrease, and in the weld metal they are even lower than the standard ones.

This is also indicated by the results of fractographic studies at similar temperatures of sample fractures with a notch both in the weld center, and in the HAZ. In the notch tip and in the final fracture zone for –40 °C temperature, a ductile fracture mode is observed in the weld metal with pit size d_p = 0.5–4 μm (Figure 5, *b*), and in the zone of the main crack prop-

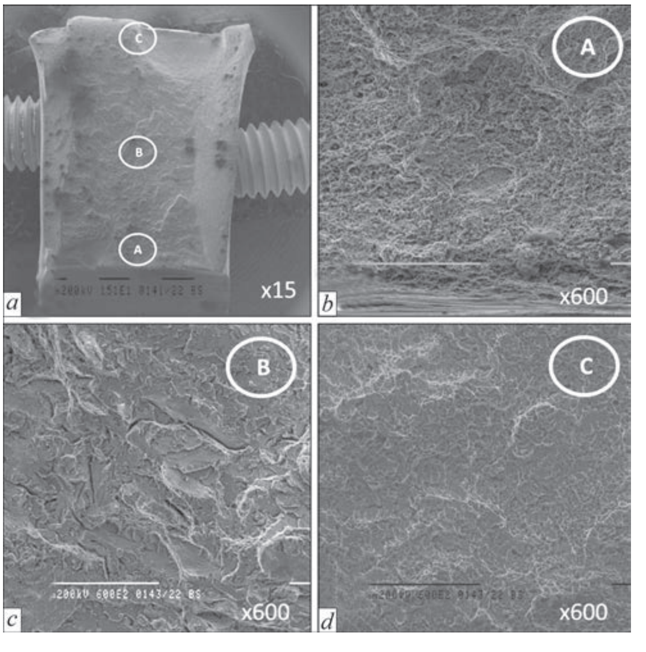

Figure 3. Appearance of sample fracture (*a*) after impact bend testing (T_{test} = –40 °C) of weld metal of 06G2BDP steel welded joint, made by NiMo1-IG solid wire in 82 % Ar + 18 % CO_2 gas mixture: A — area in the notch tip; B — area of the main crack propagation; C — final fracture area; *b* — fractograph of "A" area; *c* —fractograph of "B" area; *d* — fractograph of "C" area

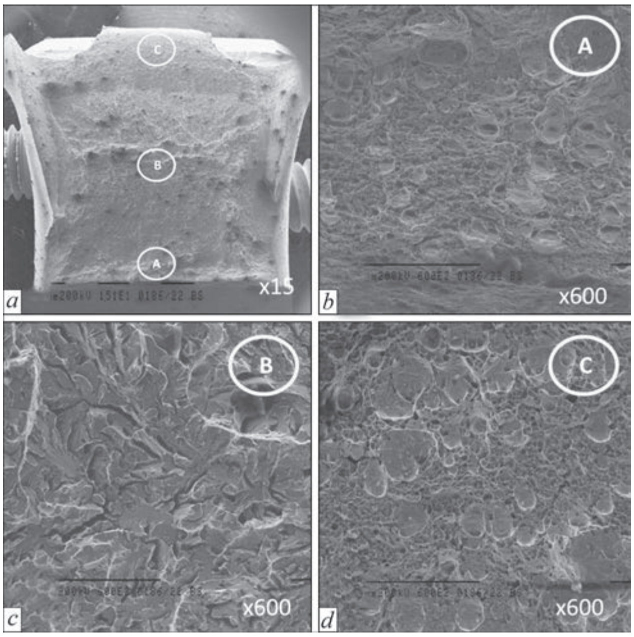

Figure 4. Appearance of sample fracture (*a*) after impact bend testing (T_{test} = –40 °C) of HAZ metal of 06G2BDP steel welded joint, made by NiMo1-IG solid wire in 82 % Ar + 18 % CO_2 gas mixture: A — area in the notch tip; B — area of the main crack propagation; C — final fracture area; *b* – fractograph of "A" area; *c* — fractograph of "B" area; *d* — fractograph of "C" area

agation brittle fracture prevails with cleavage facet diameter of 10–55 μm. Approximately the same situation is characteristic for fracture of samples with a notch in the HAZ at –20 °C testing temperature. At the same time, at temperature lowering to –40 °C, the quasibrittle and brittle fracture modes are observed at the notch tip and in the zone of the main crack propagation with cleavage facet size d_f = 8–30 μm (Fig-

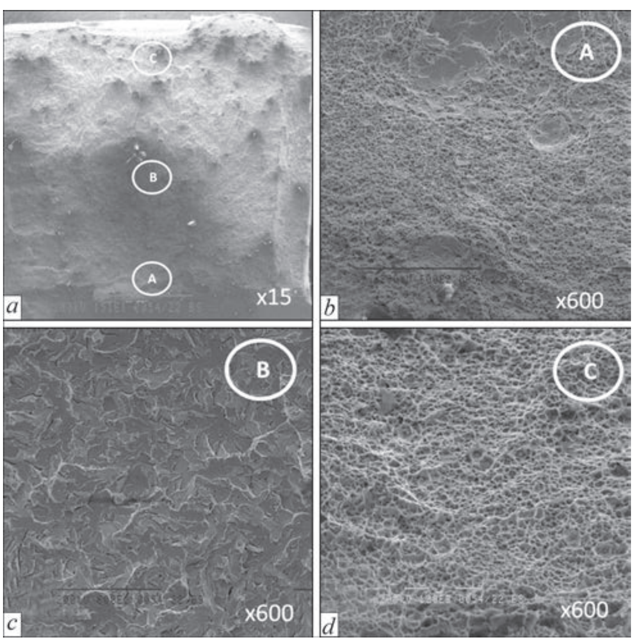

Figure 5. Structure of the weld upper layer in welding with stationary arc (*a*, *b*), in PAW (*c*, *d*) and in welding with pulsating arc (*d*, *e*): *a*, *c*, *e* — optical microscopy at ×500 (reduced 2 times); *b*, *d* — SEM

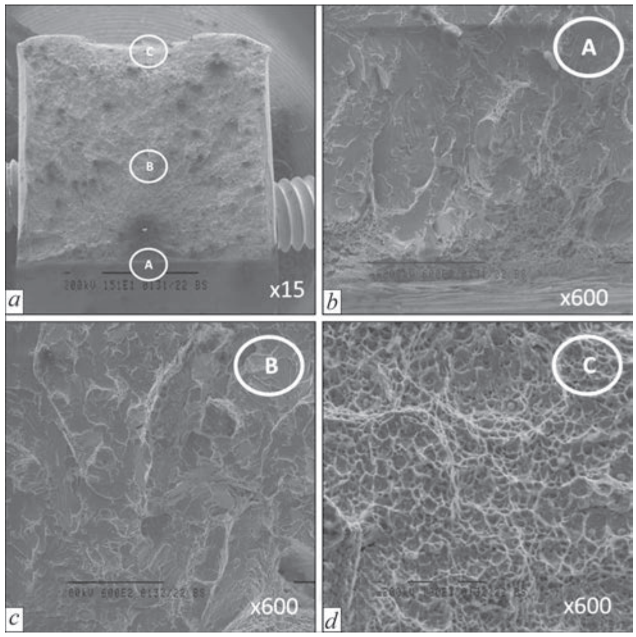

Figure 6. Macrosections of Tekken samples of 13KhGMRB steel joints made by PAW: *a* — without preheating; *b* — PT = 120 °C

ure 6, *c*). The fracture mode is ductile with small pit size d_p = 1–10 μm only in the final fracture zone (Figure 6, *d*).

By the results of fractographic investigations it was found that for all the studied variants of welding at low temperatures the HAZ metal ductility is somewhat higher than that of weld metal, which is ensured by dispersion of the structural components. Maximal values of impact toughness at all the testing temperatures are characteristic for 06G2BDP steel welded joints, made by mechanized welding with NiMo1-IG solid wire in 82 % Ar + 18 % CO_2 mixture.

Change of the values of mechanical properties and impact toughness is associated with structural transformations in the welded joint zones, both in the weld metal and in the HAZ metal.

At mechanized solid wire welding the most highly dispersed structure forms in the weld metal which consists of ferrite-carbide mixture with sparse hardly noticeable thin precipitates of hypoeutectoid ferrite along the primary grain boundaries of higher hardness of 2200 MPa (Figure 7, *a*). In the overheated subzone of the HAZ a fine structure of acicular ferrite forms with incomplete precipitation of hypoeutetoid ferrite. Hardness value of this zone is equal to 2500 MPa (Figure 7, *b*).

At mechanized flux-cored wire welding the weld metal forms a microstructure of acicular ferrite with a large fraction of coarse plates of hypoeutectoid ferrite, which precipitated from equidirectional coarse elongated ferrite grains of 2110 MPa microhardness, growing into the bulk (Figure 8, *a*). The HAZ metal forms a fine ferritic structure with hardness increase

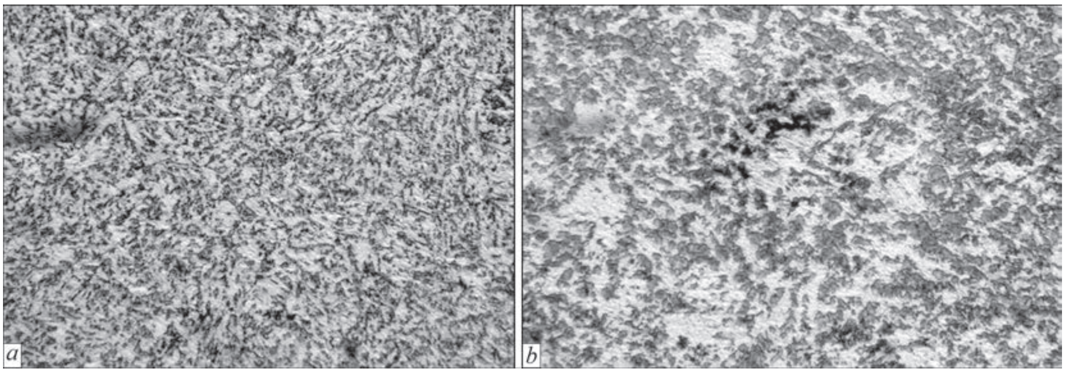

Figure 7. Microstructure (×500) of 06G2BDP steel welded joint made with NiMo1-IG solid wire in 82 % Ar + 18 % CO_2 gas mixture: *a* — weld; *b* — HAZ

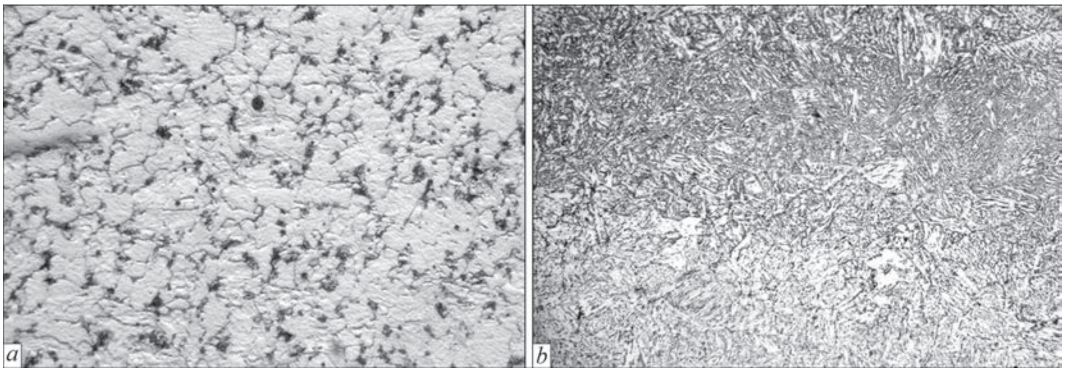

Figure 8. Microstructure (×500) of 06G2BDP steel welded joint made with FilarcPZ 6114S flux-cored wire in CO_2: *a* — weld; *b* — HAZ

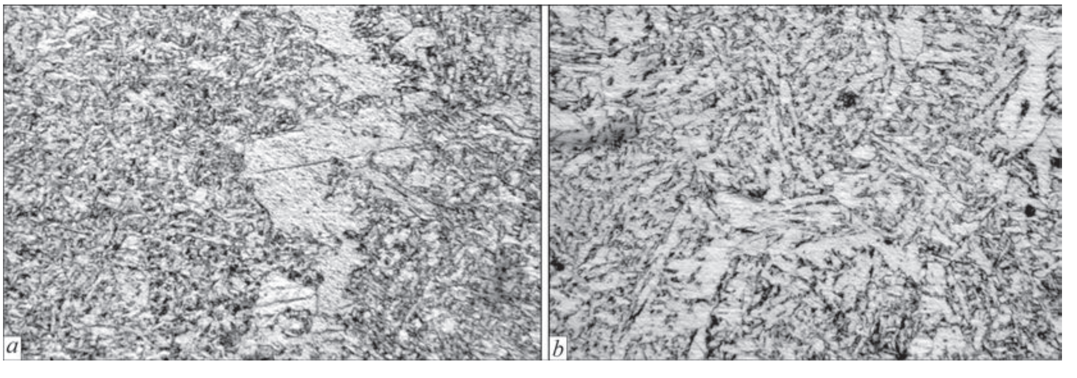

Figure 9. Microstructure (×500) of 06G2BDP steel welded joint made with Sv-10NMA solid wire under a layer of OK Flux 10.71: *a* — weld; *b* — HAZ

up to 2450 MPa in the overheated subzone and hardness lowering to 2100 MPa in the incomplete recrystallization subzone (Figure 8, *b*).

At automatic submerged-arc welding the weld metal develops an acicular ferritic structure with the most ramified network of pronounced hypoeutectoid ferrite along the boundaries of ferrite grains of a more round shape. Weld metal structure has the lowest microhardness of 2080 MPa. The fusion zone hardness is 2000 MPa (Figure 9, *a*). In the HAZ overheated subzone an acicular ferritic structure forms with coarse plates of hypoeutectoid ferrite and Widmanstaetten ferrite areas of 2050–2080 MPa hardness (Figure 9, *b*).

In addition, at automatic submerged-arc welding a tempered area of 6 mm width develops in the welded joint at 5 mm distance from the fusion line with a considerable hardness lowering to 1600–1800 MPa, and with emergence of a fine-grained ferritic-pearlitic structure.

In terms of formation of a dispersed ferritic-carbide structure and achieving high impact toughness values, the most favourable of the above-mentioned combinations of welding consumables is application of NiMo1-IG solid wire of Boehler Company at mechanized welding of 06G2BDP steel in 82 % Ar + 18 % CO_2 gas mixture.

CONCLUSIONS

Investigations of the influence of mechanized gas-shielded arc and automatic submerged-arc welding on the mechanical properties and structure of welded joints of 06G2BDP steel revealed the following:

● by the values of static strength and ductility the above-mentioned welding processes and welding consumables, namely NiMo1-IG solid wire in combination with 82 % Ar + 18 % CO_2 gas mixture, Filarc PZ 6114S flux-cored wire with CO_2 and Sv-10NMA solid wire in combination with OK Flux 10.71 provide the required level of weld metal mechanical properties, and they can be used for fabrication of metal structures from rolled stock of 06G2BDP steel of C390 class;

● on the other hand, the above-mentioned combinations of welding consumables, except for Filarc PZ 6114S flux-cored wire in CO_2, can be used for welding metal structures from 06G2BDP of C500 grade;

● metallographic investigations of microstructure of all the welded joint zones and fractographic studies of the sample fracture surfaces after impact bend testing showed that from the above-mentioned combinations of welding consumables application of NiMo1-IG solid wire of Boehler Company at mechanized welding in 82 % Ar + 18 % CO_2 gas mixture can be the most favourable in terms of formation of a dispersed ferritic-carbide structure and achieving high impact toughness values;

● application of the technology of automatic submerged-arc welding is rational at fabrication of metal structures, which will operate at temperatures not lower than –20 °C, and for products welded with flux-cored wire in CO_2 the working temperature range should only be positive (not lower than plus 20 °C), from the viewpoint of achieving impact toughness values higher than the standard values.

REFERENCES

1. Miki, C., Homma, K., Tominaga, T. (2002) High strength and high performance steels and their use in bridge structures. *J. of Constructional Steel Research*, 58(**1**), 3–20.
2. Albrecht, P., Hall Jr, T.T. (2003) Atmospheric corrosion resistance of structural steels. *J. of Materials in Civil Engineering*, 15(**1**), 2–24.
3. Bjorhovde, R. (2004) Development and use of high performance steel. *J. of Constructional Steel Research*, 60(**3–5**), 393–400.
4. Morcillo, M., Díaz, I., Cano, H. et. al. (2019) Atmospheric corrosion of weathering steels. Overview for engineers. Pt II: Testing, inspection, maintenance. *Construction and Building Materials*, **222**, 750–765. DOI: http://doi.org/10.1016/j.conbuildmat.2019.06.155
5. Shimanovskyi, O.V. (2020) *Essays on problems of nonconventional bridges*. Kyiv, Stal [in Ukrainian].
6. Shimanovskyi, O.V., Kotlubey, D.O., Shalinskyi, V.V. (2018) E.O.Paton bridge — current state and prospects. *Promyslove Budivnytstvo ta Inzhenerni Sporudy,* **1**, 2–9 [in Ukrainian].
7. Poznyakov, V.D., Dyadin, V.P., Davydov, Ye.O. (2021) Technical state of metal structures of main girders of E.O. Paton bridge across the Dnipro in Kyiv. *Promyslove Budivnytstvo ta Inzhenerni Sporudy,* **1**, 9–17 [in Ukrainian].
8. Kovtunenko, V.A., Sineok, A.G., Gerasimenko, A.M. et al. (2005) Typical damages of welded metal structures of bridges. *The Paton Welding J.*, **10**, 27–32.
9. Poznyakov, V.D., Zhdanov, S.L., Maksimenko, A.A. et. al. (2013) Weldability of sparcely-alloyed steels 06GBD and 06G2B. *The Paton Welding J.*, **4**, 8–14.
10. Kovtunenko, V.A., Gerasimenko, A.M., Petruchenko, A.A. et al. (2007) Steel rolled stock of increased weather resistance for welded building structures. *Dorogy i Mosty, Zbirnyk Nauk. Prats*, **7**, 297–304 [in Russian].
11. Zavdoveev, A.V., Poznyakov, V.D., Zhdanov, S.L. et al. (2020) Impact of thermal cycles of welding on formation of the structure and properties of corrosion-resistant steel 06G2BDP. *The Paton Welding J.*, **9**, 14–18. DOI: https://doi.org/10.37434/tpwj2020.09.02

ORCID

S.L. Zhdanov: 0003-3570-895X,
V.D. Poznyakov: 0000-0001-8581-3526,
A.V. Zavdoveyev: 0003-2811-0765

CONFLICT OF INTEREST

The Authors declare no conflict of interest

CORRESPONDING AUTHOR

A.V. Zavdoveyev
E.O. Paton Electric Welding Institute of the NASU
11 Kazymyr Malevych Str., 03150, Kyiv, Ukraine.
E-mail: avzavdoveev@gmail.com

SUGGESTED CITATION

S.L. Zhdanov, V.D. Poznyakov, A.V. Zavdoveyev, A.M. Herasymenko, O.G. Synyeok, A.O. Maksymenko, V.D. Ryabokon (2023) Structure and properties of welded joints of 06g2bdp steel. *The Paton Welding J.*, **9**, 11–16.

JOURNAL HOME PAGE

https://patonpublishinghouse.com/eng/journals/tpwj

Received: 07.07.2023
Accepted: 09.10.2023

DOI: https://doi.org/10.37434/tpwj2023.09.03

WELDING-TECHNOLOGICAL PROPERTIES OF FLUX-CORED WIRE WITH BORON-CONTAINING BINDER IN THE CHARGE

I.O. Ryabtsev, A.A. Babinets, I.P. Lentyugov

E.O. Paton Electric Welding Institute of the NASU
11 Kazymyr Malevych Str., 03150, Kyiv, Ukraine

ABSTRACT

In order to improve the performance of metal deposited with PP-Np-50Kh2MNSGF flux-cored wire, boron-containing FKhB-1 binder was added to the wire charge in such a way as to obtain boron content on the level of 0.01 % in the deposited metal. The effect of adding FKhB-1 binder to the flux-cored wire charge on its welding-technological properties was studied experimentally. It was found that application of boron-containing binder in the flux-cored wire charge does not impair its welding-technological properties, boron microalloying leading to refinement of the deposited metal structure and increasing its hardness from *HRC* 53–57 to *HRC* 60–62 at the same content of other alloying elements. Developed PP-Np-50Kh2MNSGF flux-cored wire is proposed for deposition of wear-resistant layers for protection of parts of special machines and mechanisms in mining, metallurgical and other industries, operating under the difficult conditions of abrasive wear in combination with intense shock loads.

KEYWORDS: arc surfacing, flux-cored wire, microalloying, welding-technological properties, deposited metal, deposited metal formation

INTRODUCTION

Analysis shows that boron is quite often used as microalloying element in production of various steels and alloys in order to improve their performance [1–6]. At the same time, boron application as a microalloying or modifying additive at surfacing (welding) is rather limited [7–10], which is related to difficulties of selection of the type and method of adding boron-containing components to the weld pool, boron assimilation processes, determination of its optimal concentrations, etc., as boron is capable of rather significantly influencing the properties of steels and alloys at its concentration in the range of hundredths and thousandths of a percent.

So in work [11] it was shown that microalloying of 25Kh5FMS deposited metal by boron in the range of 0.007–0.010 % leads to a considerable refinement of its microstructure and a certain increase of matrix microhardness, without detracting from the quality of deposited metal formation.

It has a positive effect on the performance of deposited metal microalloyed by boron: its heat- and wear-resistance increases 1.5–2.0 times. Increase of boron concentration in the deposited metal ≥ 0.02 % leads to further increase of microhardness of 25Kh5FMS steel. However, it has a negative influence on the metal crack resistance: it forms a considerable amount of cracks, which propagate through all the deposited metal layers.

The objective of the work consists in determination of the influence of boron microalloying on welding-technological properties of surfacing PP-Np-50Kh2MNSGF flux-cored wire designed for improvement of wear resistance of special machines and mechanisms in mining, metallurgical and other industries, working under the difficult conditions of abrasive wear in combination with intense high dynamic shock loads.

INVESTIGATION MATERIALS AND PROCEDURES

In order to protect the working surfaces of the above-mentioned parts, which include lining elements of screens, bins, dump truck bodies, blades and covering discs of draft blowers and similar parts, in this work it is proposed to deposit wear-resistant metal layers by submerged-arc surfacing with flux-cored wire of PP-Np-50Kh2MNSGF grade.

Total thickness of the deposited wear-resistant metal depends on the service conditions of a particular part, and it can be from 3 to 10 mm. Considering the high coefficient of deposited metal dilution by base metal (up to 50 %) in flux-cored wire arc surfacing, it is usually necessary to deposit 3 to 4 layers to achieve the specified chemical composition of the deposited metal. Proceeding from the need to ensure the specified chemical composition and properties already in the 1st–2nd layer of deposited metal in some cases, the charge composition of PP-Np-50Kh2MNSGF flux-cored wire was optimized, and FKhB-1 binder, containing 12 % boron, was further added to the charge.

The quantity of FKhB-1 binder, added directly to the charge of experimental flux-cored wire in the form

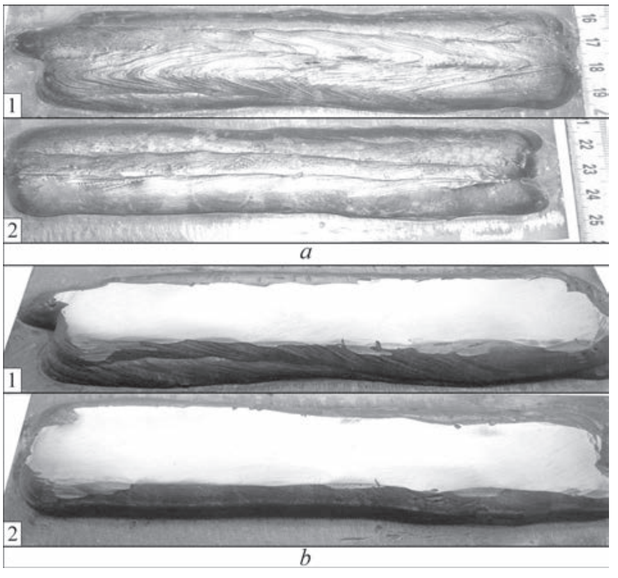

Figure 1. Appearance of beads deposited with PP-Np-50Kh2MNSGF wires of standard (1) and experimental (2) compositions immediately after deposition (*a*) and after mechanical scraping of the surface (*b*)

of powder during its manufacture, was calculated so as to obtain boron content on the level of 0.01 % in the deposited metal, taking into account the coefficients of wire filling and alloying element transition into the deposited metal. Such a concentration of boron in the deposited metal was selected in order to prevent cracking [11]. The flux-cored wire design is tubular with edge overlapping, 1.8 mm diameter and filling coefficient of 24 %.

Submerged-arc surfacing of test samples was performed by single beads with AN-26P flux in U-653 unit with VDU-506 power source in the following modes: 24 V voltage, 220 A current, 20 m/h deposition rate, 4 mm surfacing step, direct current, reverse polarity. Plates from 40Kh steel were used as base metal.

Two series of test samples were made. The first series was surfaced with wires of standard and experimental composition in four layers, which was followed by visual inspection of the processed surface before and after its mechanical cleaning. The second series of samples were surfaced stepwise in one, two and three layers. After that X-ray spectral method was used to determine the chemical composition of the deposited metal in the upper layer.

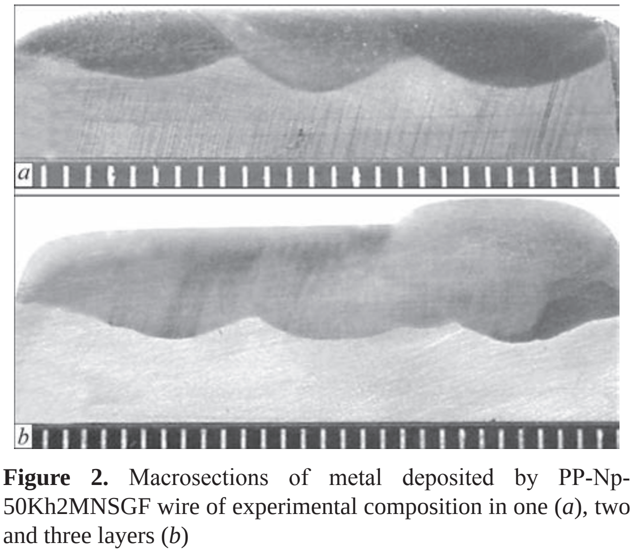

Figure 2. Macrosections of metal deposited by PP-Np-50Kh2MNSGF wire of experimental composition in one (*a*), two and three layers (*b*)

Welding-technological properties of experimental PP-Np-50Kh2MNSGF wire microalloyed by boron, compared to wire of the same grade of standard composition, were assessed by the following parameters:

- arc excitation mode (light, medium, complicated);
- melting characteristics (coefficients of melting, deposition, losses);
- arc burning stability (stable, satisfactory, unstable);
- quality of deposited bead formation (sound, satisfactory, poor);
- type and availability of defects in the deposited metal (absent, isolated, considerable number);
- quality of slag crust detachment (easy, satisfactory, complicated);
- compliance of deposited metal chemical composition and hardness with the specification (compliant, not compliant).

For calculation of the coefficients of melting (α_m), deposition (α_d) and losses (ψ) the plate and wire weight was determined before and after surfacing and deposition time was recorded. The respective coefficients were determined using common expressions:

$$\alpha_m = G_m/(I\cdot t), \qquad (1)$$

$$\alpha_d = G_d/(I\cdot t), \qquad (2)$$

$$\psi = ((\alpha_m - \alpha_d)/\alpha_m)\cdot 100\ \%, \qquad (3)$$

where G_m is the molten metal weight, g; G_d is the deposited metal weight, g; I is the welding current, A; t is the deposition time, h.

EXPERIMENTAL RESULTS AND THEIR DISCUSSION

Appearance of the first series of samples immediately after surfacing and after mechanical scraping of the processed surface is given in Figure 1. Templates were cut out of samples of the second series (Figure 2), microsections were prepared and structural studies of the samples were conducted at magnifications of ×240 (Figure 3, 4). Chemical composition and hardness of the metal deposited with standard and experimental PP-Np-50Kh2MNSGF flux-cored wires, as well as composition of 50Kh2MNSGF deposited metal according to the specification, is given in Table 1.

As one can see from Figure 1, boron microalloying at its concentration of 0.01 % in 50Kh2MNSGF

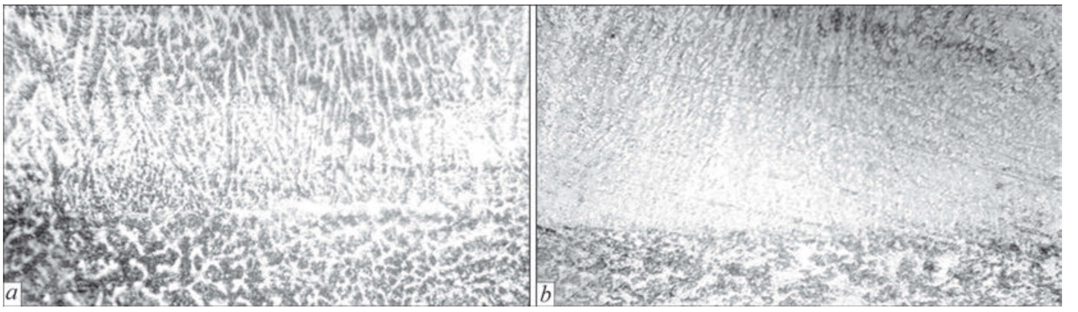

Figure 3. Microstructure (×240) of metal near the fusion line in samples surfaced with PP-Np-50Kh2MNSGF wire of standard (*a*) and experimental composition (*b*)

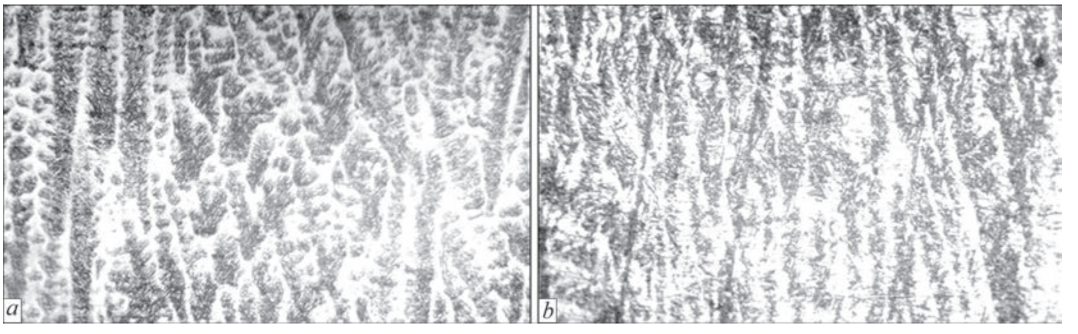

Figure 4. Microstructure (×240) of the central part of metal in samples surfaced with PP-Np-50Kh2MNSGF wire of standard (*a*) and experimental composition (*b*)

Table 1. Chemical composition and hardness of metal deposited with PP-Np-50Kh2MNSGF flux-cored wires of standard and experimental compositions

Deposited metal type	Number of deposited layers	Weight fraction of elements, %								Hardness, *HRC*
		C	Si	Mn	Cr	Ni	Mo	V	B	
50Kh2MNSGF (to specification)	3–5	0.3–0.5	0.4–1.0	0.4–1.0	1.5–2.5	0.8–1.6	0.3–0.6	0.3–0.6	–	55–60
50Kh2MNSGF (standard)	4	0.42	0.89	0.75	1.88	1.52	0.48	0.37	–	53–57
50Kh2MNSGF (experimental)	1	0.39	0.75	0.65	1.41	1.24	0.37	0.28	0.004	55–57
	2	0.43	0.83	0.72	1.86	1.47	0.43	0.35	0.005	57–60
	3	0.46	0.97	0.83	1.94	1.54	0.54	0.43	0.006	60–62

Table 2. Welding-technological properties of PP-Np-50Kh2MNSGF flux-cored wires of standard and experimental compositions

Parameter	Wire type	
	Standard	Experimental
Mode of arc excitation	Light	Light
Coefficients of: ● melting — α_m, g/A·h ● deposition — α_d, g/A·h ● losses — ψ, %	 17.56 17.04 2.96	 17.52 16.98 3.08
Arc burning stability	Stable	Stable
Quality of deposited bead formation	Sound	Sound
Presence of defects in the deposited metal	Absent	Absent
Quality of slag crust detachment	Satisfactory	Satisfactory
Compliance of deposited metal chemical composition and hardness with the specification	Compliant (standard)	Compliant

deposited metal does not impair its formation quality. Detachability of the slag crust remains on the same satisfactory level in all the samples, spinels on the sample surface are absent. Pores, cracks or other defects on the deposited metal surface are also absent.

Hardness of the metal deposited with experimental wire with microalloying additives of boron, is equal to *HRC* 57–60 already in the second layer, compared to hardness of metal deposited with wire of standard composition in the fourth layer — *HRC* 53–57 at the same concentration of other alloying elements.

As one can see from Figure 3, in samples deposited by wires of both types, the line of fusion of the deposited (above) and base metal (below) is clear, internal defects in the form of pores, cracks, and lacks of fusion are absent. Metal structure is quite homogeneous, here it is finer in the case of boron microalloying (Figure 4, *b*). Table 2 gives the generalized data on comparative assessment of welding-technological properties of the developed PP-Np-50Kh2MNSGF flux-cored wire of standard and experimental compositions.

It follows from the data given in Table 2 that welding-technological properties of experimental PP-Np-50Kh2MNSGF flux-cored wire with boron microalloying additives are at a high level by all the parameters and correspond to the characteristics of wire of standard composition of the same grade.

CONCLUSIONS

It was found that application of FKhB-1 binder with boron in the charge of PP-Np-50Kh2MNSGF flux-cored wire does not impair its welding-technological properties. Here, microalloying by boron in the quantity of 0.006–0.012 % leads to refinement of the deposited metal structure and allows its hardness to be increased from *HRC* 53–57 to *HRC* 60–62 at the same content of other alloying elements.

REFERENCES

1. Baker, T.N. (2016) Microalloyed steels. *Ironmaking & Steelmaking*, 43(**4**), 264–307. DOI: https://doi.org/10.1179/1743281215Y.0000000063
2. Lyakishev, N.P., Pliner, U.L., Lappo, S.I. (1986) *Boron-containing steels and alloys*. Moscow, Metallurgiya [in Russian].
3. Manyak, N.A., Manyak, L.K. (2002) Influence of boron on structure and toughness of low-alloyed steel. *Metall i Lityo Ukrainy*, **5–6**, 23–25 [in Russian].
4. Proidak, Yu.S., Manydyn, V.S., Isaieva, L.E. et al. (2020) Microalloying of low-carbon steel with boron and method of determination of dissolved boron effective concentration. *Teoriya i Praktyka Metalurgii*, **1**, 18–23 [in Ukrainian]. DOI: http://dx.doi.org/10.34185/tpm.1.2020.02
5. Mujagic, D., Imamovic, A., Hadzalic, M. (2021) The influence of microalloying with boron on properties of austenite stainless steel X8CrNiS18-9. *Int. J. of Adv. Res.*, **9**, 695–700. DOI: http://dx.doi.org/10.21474/IJAR01/13596
6. Xiao, L.-J., Qiu. S.-T., Liu, J.-Q., Gan, Y. (2008) Research and application status of boron microalloying in high quality steel plate. *J. of Iron and Steel Research*, 20(**5**), 1–4.
7. Zhudra, A.P., Krivchikov, S.Yu., Petrov, V.V. (2004) Selection of boron-containing charge materials for the core of flux-cored wire. *The Paton Welding J.*, **4**, 51–52.
8. Krivchikov, S.Yu. (2012) Modification by boron of deposited metal of white cast iron type. *The Paton Welding J.*, **6**, 19–21.
9. Maksimov, S.Yu., Machulyak. V.V., Sheremeta, A.V., Goncharenko, E.I. (2014) Investigation of influence of microalloying with titanium and boron of weld metal on its mechanical properties in underwater welding. *The Paton Welding J.*, **6–7**, 76–79. DOI: https://doi.org/10.15407/tpwj2014.06.15
10. Babinets, A.A., Ryabtsev, I.O. (2021) Influence of modification and microalloying on deposited metal structure and properties (Review). *The Paton Welding J.* DOI: https://doi.org/10.37434/as2021.10.01
11. Babinets, A.A., Ryabtsev, I.O., Lentyugov, I.P., Bogaichuk, I.L. (2022) Influence of microalloying with boron on the structure and properties of deposited metal of the type of tool steel 25Kh5FMS. *The Paton Welding J.*, **6**, 3–10. DOI: https://doi.org/10.37434/as2022.06.01

ORCID

I.O. Ryabtsev: 0000-0001-7180-7782,
A.A. Babinets: 0000-0003-4432-8879,
I.P. Lentyugov: 0000-0001-8474-6819

CONFLICT OF INTEREST

The Authors declare no conflict of interest

CORRESPONDING AUTHOR

I.O. Ryabtsev
E.O. Paton Electric Welding Institute of the NASU
11 Kazymyr Malevych Str., 03150, Kyiv, Ukraine.
E-mail: ryabtsev39@gmail.com

SUGGESTED CITATION

I.O. Ryabtsev, A.A. Babinets, I.P. Lentyugov (2023) Welding-technological properties of flux-cored wire with boron-containing binder in the charge. *The Paton Welding J.*, **9**, 17–20.

JOURNAL HOME PAGE

https://patonpublishinghouse.com/eng/journals/tpwj

Received: 30.06.2023
Accepted: 09.10.2023

DOI: https://doi.org/10.37434/tpwj2023.09.04

THERMAL CONDITIONS OF COATED ELECTRODE WELDING OF HEAT-RESISTANT LOW-ALLOY STEELS

S.I. Moravetskyi, A.K. Tsaryuk, V.Yu. Skulskyi, M.O. Nimko

E.O. Paton Electric Welding Institute of the NASU
11 Kazymyr Malevych Str., 03150, Kyiv, Ukraine

ABSTRACT

The objective of the work consisted in determination of admissible and critical thermal modes of manual arc welding of chromium-molybdenum-vanadium steels, based on the results of metallographic investigations and measurement of weld metal hardness in as-welded and as-heat treated condition. Experimental butt welded joints of 15Kh1M1F steel were obtained under different thermal conditions. Two parameters of the welding thermal mode were set: heat input equal to 5.21; 7.78 or 10.2 kJ/cm and temperature of preheating of the metal being welded, equal to 50; 160; 270 or 360 °C. Phoenix SH Kupfer 3 KC coated electrodes of EN ISO 3580-A – E ZCrMoV1 B 4 2 H5 type were used. The subject of research was metal of the welds of the above-mentioned welded joints. For all the combinations of the heat input and preheating temperature weld metal hardness was measured after welding and after high-temperature tempering. The structure of different zones of welded joint metal was studied to determine the presence of cracklike defects and nature of the microstructure. The main attention was given to weld metal structure. The critical and admissible thermal modes of welding 15Kh1M1F steel with the selected coated electrodes were determined by the quality criteria, namely nature of the microstructure and structural homogeneity, as well as degree of weld metal defectiveness.

KEYWORDS: welded joints, welding consumables, weld metal, metallographic investigations, microstructure, manual arc welding, hardness, welding thermal mode, heat-resistant steel, cold cracks

INTRODUCTION

The range of welded assemblies from traditional chromium-molybdenum-vanadium steels of 12Kh1MF, 20KhMFL, 15Kh1M1F, 15Kh1M1FL (furtheron referred to as Cr–Mo–V steels) in steam turbines, boiler units and other components of newly designed power equipment does not show any tendency to reduction. Owing to the need for reconstruction and continuation of operation of TPP and CHPP units, which have already worked off their fleet life, the scope of repair-restoration operations with involvement of coated-electrode manual welding is also increased. Therefore, improvement of the technologies of welding steels of this type remains an important and relevant goal.

Under the conditions in the recent years, difficult for providing the industry of Ukraine with energy carriers, in the cold season the air temperature even in assembly-welding shops of machine-building enterprises can drop to below zero values. In keeping with the standards [1], Cr–Mo–V steels are allowed to be welded at ambient air temperature from 0 to –15 °C, depending on steel grade and thickness. Here, however, an accelerated drop of temperature T_p of preheating of the products being welded is in place. Insufficiently fast transition between the operations of welding, monitoring of temperature and intermediate heating combined, possibly, with the human factor, can lead to the situation, when a certain volume of the deposited metal was produced, when the actual product temperature was lower than T_p range specified by the technological documentation. Welded joints where the weld contained metal deposited with insufficient product preheating, were subjected to the required postweld heat treatment and usually successfully passed all the kinds of nondestructive testing. At the same time, weld metal hardness in a single case showed that individual measurement results exceeded the maximum admissible values, although the average hardness value satisfied the current standards [1]. Such an inconsistency is not the basis for rejection of the product, but it requires coordination with the chief materials science organization ([1], Table 18.3, items 18.4.4, 18.4.5). In view of the above-said, the technologists are trying to not just specify the optimal T_p range during welding of Cr–Mo–V steels, but at least know a very accurate practically justified bottom line of the above range, and also know the key conditions and required measures for guaranteeing compliance with current norms of weld metal hardness.

Increase of the cooling rate and lowering of the temperature level, at which γ-α-transformation runs in the metal of the weld and HAZ of alloyed steels are known to lead to increase of the fraction of diffusionless products, stresses of 2nd and 3rd kinds, dislocation density, and hardness in as-welded state. Collectively, these phenomena are known as the “structural factor”, which has an essential influence on the delayed fracture mechanism in hardened steels welded joints. So, in this case the point is that the specified minimal T_p value should be characterized not by the category of optimality, but rather criticality in terms of the risk of development of metal defects, incompatible with the welded joint serviceability.

Alongside the preheating temperature, welding heat input Q also belongs to the parameters of welding thermal mode. Welder can influence Q mainly by varying welding current I_w (within optimal ranges for each coated electrode brand and diameter). It is possible to control Q through the arc movement speed and welding technique (transverse oscillations, "stringer" beads, etc).

For welded joints of Cr–Mo–V steels required T_p is recommended or specified in a rather broad range (from 450 to 100 °C), and not always with sufficient substantiation of this range [1–5]. In a number of cases, welded joints of 15Kh1M1FL steel are also produced without preheating [1, 6]. Proceeding from data of these and many other literature sources, it did not seem possible to determine the critically necessary T_p without additional experiments.

Weld metal hardness in finished products is controlled in as-heat treated state. Known are [7] the dispersion-hardening susceptibility of metal of Cr–Mo–V steel welded joints and the temperature-time ranges of this phenomenon. This prompted an investigation into the impact of welding thermal mode on weld metal structure and properties not only in as-welded state but also after high-temperature tempering.

Thus, the objective of the work consisted in studying the influence of the welding thermal mode on the nature of structure formation and change in the hardness of weld metal of Cr–Mo–V steel welded joints in as-welded and as-heat treated state, as well as in determination of the parameters of welding thermal mode critical for ensuring the technological strength and quality of the welded joints.

MATERIALS AND PROCEDURE

Plates of 25 mm thickness cut out of a forging of 15Kh1M1F steel were taken as the base metal for experimental welded joints. This material was selected as a typical well-studied and common pearlitic steel of Cr–Mo–V system. Spectral analysis performed in the specialized PWI laboratory revealed the following content of elements in its composition, wt.%: 0.15 C; 0.39 Si; 0.68 Mn; 1.32 Cr; 1.04 Mo; 0.35 V; 0.007 S; 0.023 P, which in general complies well with the requirements of standards and specifications for 15Kh1M1F steel [8].

A large number of electrode brands were developed for welding Cr–Mo–V steels, their current production being regulated by state or industry standards of the former USSR until recently. Among electrodes of E-09Kh1MF type (GOST 9467–75), identified by marketing search via the Internet, TML-3U, TsL-20, TsL-20B and TsL-39 brands can be regarded as widely accepted in the Ukrainian market. During previous years, the validity of normative acts of the Soviet era was gradually coming to an end. For instance [9], GOST 9467–75 was replaced by STU EN ISO 3580:2019 "Welding consumables. Coated electrodes for manual arc welding of creep-resisting steels. Classification". Contrarily, the certificates of suppliers or electrode descriptions often indicate that they were made by canceled GOSTs or specifications (for instance, TU U 25.9-31230196-004:2016, TU U 25.9-34142624-014:2017). Unfortunately, plant specifications are not readily available documents, making references to them questionable in terms of modern quality assurance systems. Under the conditions of electrode production adaptation to the new standardization system introduced in Ukraine, power equipment manufacturers began to give preference to products of European companies, which have been working under the EN ISO standard system for a long time, ensuring consistently reproducible quality of the coated electrodes.

So, two brand names of electrodes of European manufacturers were pretested: Boehler Fox DCMV and Phoenix SH Kupfer 3 KC. The electrodes belong to EN ISO 3580-A – E ZCrMoV1 B 4 2 H5 type, similar to E-09Kh1MF (GOST 9467–75). By the totality of the results of previous studies (soundly determined welding technology characteristics, chemical composition of pure deposited metal), there were practically no grounds for preferring a certain brand, considering the welding production requirements. However, Phoenix SH Kupfer 3 KC was chosen for this study, for which the typical and actual C, P, Si content in the deposited metal is somewhat higher (Table 1). This is closer to the critical conditions in terms of ensuring the technological strength of the welded joint and final hardness of the weld metal.

Welding was performed in the downhand position. Electrodes were applied after their rebaking (350 °C/2 h), and directly after their cooling to room temperature. Butt joints with a V-shaped groove (20° edge bevel angle, 3 mm root face, 3 mm gap) were assembled from 25×60×300 mm plates of 15Kh1M1F steel. Weld root zone metal was produced with 4 mm

Table 1. Chemical composition of deposited metal of electrodes of EN ISO 3580-A – E ZCrMoV1 B 4 2 H5 type

Brand	Data source	Element weight fraction, %							
		C	Si	Mn	Cr	Mo	V	S	P
Böhler Fox DCMV	[10]	0.12	0.3	0.9	1.2	1.0	0.22	≤0.025	≤0.030
	A*	0.13	0.35	0.90	1.24	1.10	0.25	0.006	0.015
Phoenix SH Kupfer 3 KC	[11]	0.13	0.4	1.0	1.4	1.05	0.25	≤0.025	≤0.030
	A	0.15	0.40	0.85	1.26	1.16	0.28	0.002	0.018

*A — spectral analysis of metal of 6th layer of the deposits made in keeping with [12].

electrodes of ISO 2560-A – E 46 3 B 5 3 H5 type. Butt preheating temperature during root pass welding was 200–300 °C. The purpose of this weld area was assembling the butts and giving them the initial rigidity, so that the weld root metal was not included into the study.

Groove filling was performed with Phoenix SH Kupfer 3 KS electrodes with maintenance of a combination of Q, T_p parameters, which was exactly what characterized the welding thermal mode (the format of thermal mode designation to be used further for concise presentation is related to it: n-T_p, where n is the welding mode 1, 2 or 3, Table 2). Change of Q level was ensured by I_w variation. From the viewpoint of avoiding defects (lacks of fusion, slagging) some passes in the low, narrow area of the groove were performed with small transverse oscillations. Above it the groove was filled by just stringer beads. I_w values were assigned and maintained by VDU-506 rectifier together with welding current regulator RDE-251U3.1, fitted with an ammeter. Values of arc voltage U_a and welding speed V_w were measured directly during welding the joints.

Heat input was calculated (Table 2), using V_w values averaged by the results of measurement in six arbitrarily selected passes in each mode, as well as value η of effective efficiency of metal heating by the arc, taken to be η = 0.775 [13].

Controlled preheating of welded joint metal was performed by gas-flame method up to temperatures of 160; 270 and 360 °C. Measurements were taken using a multimeter of MASTECH MS2101 model, fitted with chromel-alumel thermocouple. In addition, welded joints were produced, welding of which was started without preheating.

In the latter case, multipass welding leads to increase of base metal temperature due to self-heating, because of relatively small dimensions of experimental butt joints. At normal speed of bead deposition, already the 2nd pass should be performed with preheating up to ~100 °C. With higher pass number T_p grows, reaching values characteristic for thermal modes of the following levels, applied in this work (160 °C and higher). To avoid it, the welded joints without preheating were produced by significantly slowing down the bead deposition. Cooling of welded joint metal after each pass to room temperature required pauses of inacceptable duration. Therefore, each subsequent pass was performed after the metal temperature has reached the level of ~60–40 °C. For formal presentation of experimental results, this case was assigned the average temperature of concurrent heating T_p = 50 °C.

In the middle zone along the weld length, microsection blanks were cut out from the produced butt joints. The blanks were subjected to the following heat treatment: at 730 °C temperature optimal for welded joints of 15Kh1M1F steel [1], and at 690 °C temperature, selection of which is hypothetically possible, based on the data of [10]. Other parameters were the same for both the heat treatment variants: time of the furnace reaching the specified temperature — 2 h; time of soaking at this temperature — 3 h 20 min (20 min for equalizing of the temperature of blank metal and the furnace); cooling to room temperature with the furnace. All the microsection blanks (12 pcs) were tempered in one placement into the furnace and were mounted in it at a sufficient distance from one another.

Microsection preparation began from surface milling for 2 mm thickness, in order to eliminate the influence of the metal surface layer, decarbonized during high-temperature soaking. The milled surface was ground and polished by materials with successive reduction of abrasive particle size. The microsections were etched in 4 % solution of nitric acid in ethyl alcohol. As-welded blanks were also subject to the necessary operations for microsection preparation. The finished microsections were used to conduct the planed studies (hardness evaluation and studying the welded joint metal structure in as-welded state and after high-temperature tempering at 730 °C/3 h).

Hardness measurements were performed by Vickers method to GOST 2999–75. Load on the indenter was 5 kg. For each microsection, HV_5 value was obtained in 3–8 arbitrary points within the upper deposited layers. Such a locality of the pricks corresponds better to the procedure of hardness measurement during acceptance testing of the real products (weld face side). A greater number of measurements were performed on the microsection in as-welded state, and a smaller number — in as-heat treated state, when the range of scattering of HV_5 values was rather narrow.

The type of the structure of welded joint metal was studied in optical microscope NEOPHOT-32 with ×25–×1000 magnification. Control measurements of microhardness were performed with PMT-3 hardness meter at 0.1 kg load on the indenter.

Table 2. Modes of manual arc welding

Mode number	Electrode diameter, mm	Current, A	Arc voltage, V	Average value of actual welding speed, 10^{-3} m/s	Average heat input value, kJ/cm
1	3.2	90–100	22	3.11	5.21
2	4.0	150–160	23	3.55	7.78
3	5.0	230–240	24	4.30	10.2

Table 3. Average values of weld metal hardness, depending on the welding thermal mode

Welding mode	Q, kJ/cm	T_p, °C											
		50			160			270			360		
1	5.21	368	230	293	366	234	289	370	238	286	334	237	299
2	7.78	357	229	289	335	228	276	327	234	282	318	236	297
3	10.2	333	225	287	332	226	279	321	230	275	318	241	294
Tone denotes weld metal hardness in the state after: ● welding						(white)							
● heat treatment at 730 °C/3 h						(dark grey)							
● heat treatment at 690 °C/h						(light grey)							

RESULTS OF DUROMETRIC STUDIES

Change of weld metal hardness, depending on the thermal mode and tempering temperature is of a complex nature (Table 3). In as-welded state weld metal of 363–396 HV_5 hardness was produced under experimental conditions. Increase of the amount of heat applied to the metal during welding (both due to T_p, and due to Q) leads to lowering of weld metal hardness.

High-temperature tempering at optimal temperature of 730 °C leads to lowering of weld metal HV_5 to 221–246 units. For this case, however, the nature of hardness distribution is different in that higher average HV_5 values correspond to higher T_p for each welding mode. With Q increase, HV_5 drop is preserved for all the preheating temperatures, except for 360 °C.

Now, tempering at the temperature of 690 °C resulted in an intermediate level of weld metal hardness of 268–303 HV_5. All these values are considerably higher than those of the boundary limits according to [1].

RESULTS OF METAL STRUCTURE INVESTIGATIONS

Visual observation of weld formation during welding without preheating allowed revealing the deposited metal cracking susceptibility. Under the conditions of the weakest thermal mode 1-50, starting from the middle of groove height and up to the middle of the penultimate layer, crack initiation was consistently observed almost along then entire weld length, moving from layer to layer (Figure 1, *a*). Increase of Q noticeably reduces the cracking susceptibility, but does not completely eliminate it. So, at 2-50 thermal mode short cracks were observed in individual beads (Figure 1, *b*). In case of maximal Q (3-50 mode) no cracks were visually observed during welding. Further metallographic study of the respective microsections in the latter case did reveal cracks of ~3 mm size in the weld metal along the weld height (Figure 1, *c*). In addition to cracks, which were visually observed, the metal of welds produced in weak thermal modes, contains a large quantity of microscopic discontinuities of the type of tears, the size of which is of the order of grain or subgrain dimensions (Figure 2, *a*). Similar weld defects were also found for 1-160 thermal mode (Figure 2, *b*). No such microtears were revealed in the metal of welds produced in other welding thermal modes.

No cracklike defects were found in the fusion zone or the HAZ of any the welded joints.

In as-welded state the weld metal consists of a mixture of α-phase and carbide precipitates, typical for the bainitic-martensitic structure. Structures are characterized by a great diversity, depending on the thermal mode of welding, bead position along the weld height and kind of repeated heat treatment, to which a particular area of the metal was exposed during multipass welding. The preheating temperature and heat input determine the cooling rate of welded joint metal, depending on which a structure of different dispersity and with different ratio of the components, namely bainite and martensite, as well as with different degrees of martensite self-tempering, is formed. For two "adjacent" thermal modes the structural differences of the metal can be hardly noticeable. They, however, are clearly visible for thermal modes with an essentially different amount of heat introduced into the metal (Figure 3).

Welding in 1-50 and 2-50 modes forms the most dispersed homogeneous acicular composition of martensite, which practically is in a "structureless" state (weakly etched light-colored areas), and bainite (dark-coloured areas) (Figure 3, *a*). With increase of metal heat content due to preheating and arc thermal power the changes in the weld metal are reduced to structure coarsening: morphological type of α-phase gradually changes from fine- to coarse-acicular one, degree of carbide phase coagulation becomes higher, and a more clearer network of secondary boundaries appears (Figure 3, *b*). For the cases of modes with simultaneously high Q and T_p, areas with large grains of polygonal ferrite can be found in the weld (Figure 3, *c*).

Self-tempering of martensite, forming in the range of 300–400 °C, leads to an almost complete removal of excess carbon from oversaturated α-solid solution. The degree of tetragonality of its lattice becomes so low that it is no longer measurable by X-ray structural analysis, so that the lattice almost does not differ from the BCC lattice of ferrite. In the oversaturated α-solid

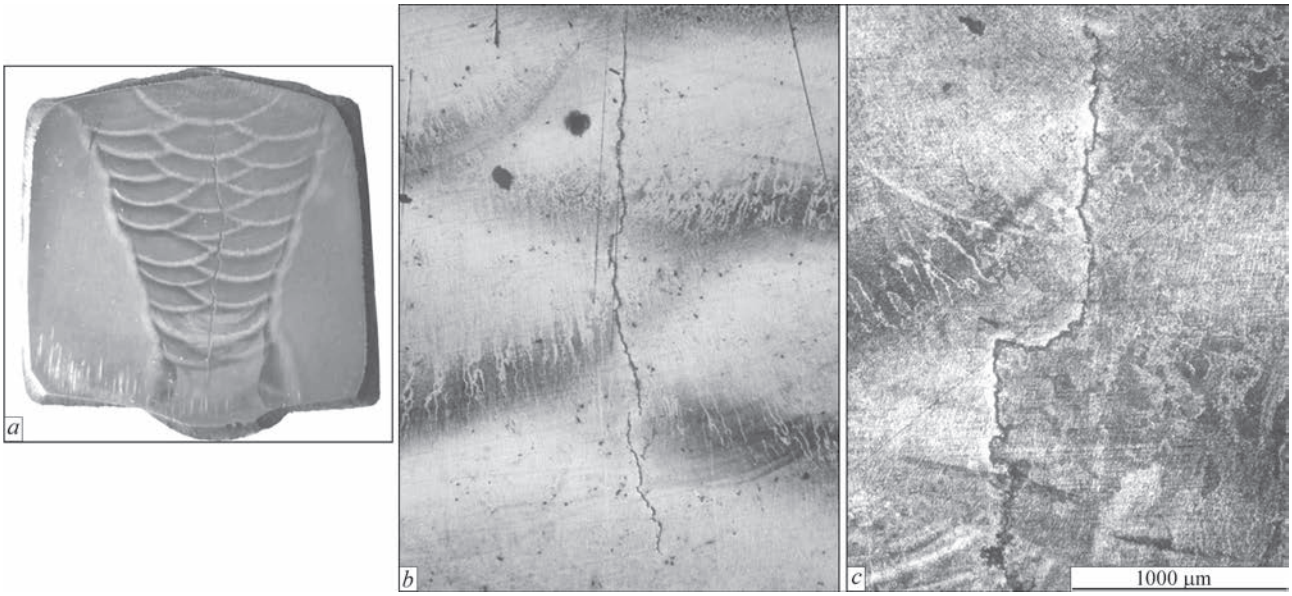

Figure 1. Cracks in the metal of welds made by welding without preheating, as-welded state: *a* — 1-50 thermal mode; *b* — 2-50 thermal mode, ×32; *c* — 3-50 thermal mode, ×50

solution, tempered at <300 °C, the degree of tetragonality of the lattice stays within the limits of sensitivity of the physical method of its evaluation [14]. Therefore, the structure of deposited metal in the state after welding with T_p = 50–270 °C contains (in addition to bainite) also martensite with different degree of self-tempering. As to the structure after welding with preheating to 360 °C, it is more appropriate to consider bainite, ferrite and carbide phases.

The structure of metal of the weld produced at $T_p >$ > 200 °C usually contains several percent of residual austenite γ_{res}, which can be present in the form of very small areas (microphases) on the grain boundaries, between bainite α-plates, and martensite laths, and thus, it can visually inconspicuous. In 200–300 °C temperature range γ_{res} decomposition proceeds with lower bainite formation [14]. Therefore, γ_{res} presence in the metal of welds made with preheating up to 270 and 360 °C is improbable.

One of the notable features of metal of all the welds observed exclusively in as-welded state, are areas of cast structure in the form of columnar crystallites, with a light-coloured fringe along their boundaries (Figure 4). The structure of the metal of light-coloured fringes along the boundaries is identified as martensitic-bainitic one, resulting from recrystallization of boundary areas in the intercritical temperature range, whereas the crystal "body" during soaking at a temperature above A_1 did not undergo recrystallization. There are the following reasons for the above identification:

- structure with light-coloured fringes around the columnar crystallites is never found in the cast zone of the last pass, or in the cast zones of the lower layers, which were not exposed to reheating up to temperatures above A_1;
- extent of such structural areas is limited (~5 mm), and their configuration follows the fusion line of the deposited beads (Figure 1, *b*);
- at a large magnification the metal structure of the light-coloured fringes (Figure 4, *b*) is not characteristic for ferrite, instead the relief shape is indicative of the product of $\gamma \rightarrow \alpha$-transformation by a shear diffusionless mechanism;
- metal microhardness is 477–518 $HV_{0.1}$ for light-coloured fringes; 384–416 $HV_{0.1}$ for middle part of columnar crystallites (data for 1-50 welding thermal mode);

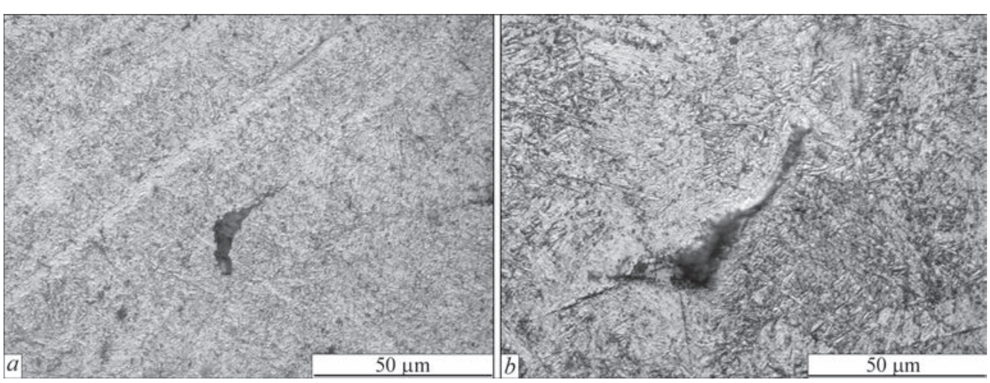

Figure 2. Microscopic discontinuities in the metal of welds made in weak thermal modes, ×1000: *a* — 2-50 mode; *b* — 3-270 mode

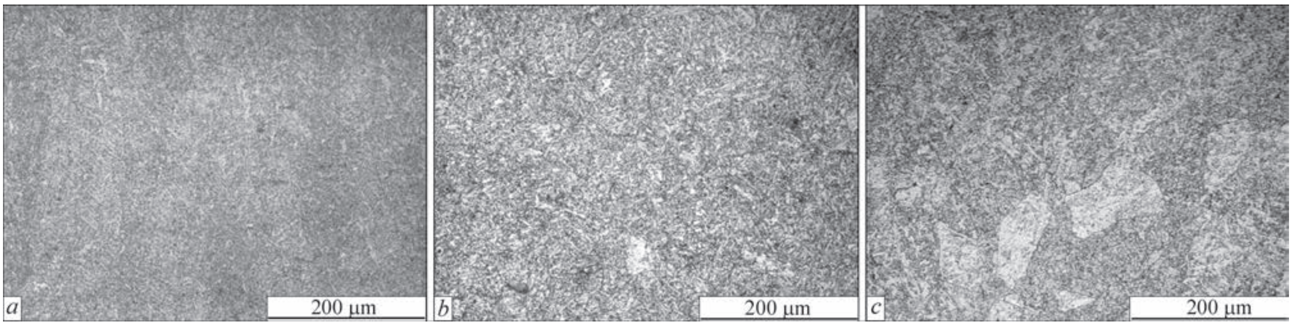

Figure 3. Type of weld metal structure, depending on thermal mode, ×250: *a* — 2-50 mode, ×100; *b* — 3-270 mode; *c* — 3-360 mode

- in as-heat treated state the light-coloured fringes are not revealed by etching, which is due to their structure type becoming similar to acicular structure of the crystallite body, due to carbide phase precipitation during high-temperature tempering.

Boundary delineation in incomplete recrystallization subzone allows evaluation of average size of the cast structure crystallites. It is interesting to note that their width depends little on the thermal mode of welding, being equal to 100 to 200 μm. Thus, increase of crystallite size with heat input rise is almost not characteristic for cast metal of this system.

Postweld tempering at 730 °C temperature leads to decomposition of oversaturated α-solid solution of martensite into ferrite and carbide precipitates. Heat treatment almost does not change the appearance of bainite areas, except for a certain increase of the quantity of the carbide phases.

A remarkable feature of the weld metal, observed exceptionally in as-tempered state, is its structural heterogeneity in the form of colonies of recrystallized ferrite grains of a large size (50–250 μm), as well as individual (single) grains of the same type in the bulk of acicular ferritic-carbide structure (Figure 5). Remnants of bainitic-martensitic structure are observed occasionally, as though locked between the adjacent ferrite grains. Proneness to this type of structural heterogeneity depends on the welding thermal mode. It is observed in the metal of welds made in thermal modes 1-50, 1-160 and 2-50. Coarse-grained ferrite is also present on macrocrack lips (Figure 5, *b*). During crack propagation, these metal areas are known to undergo intensive plastic deformation with local oversaturation by hydrogen, which tends to accumulate in the stretched zones. This leads to an assumption that ferrite appearance is associated with local deformation of metal microvolumes at the cooling stage of the welding thermal cycle, and/or during their heating at heat treatment, decomposition of unstable carbide phases in deformed volumes, hydrogen and carbon diffusion, as well as, probably, the process characteristic for hydrogen corrosion of steels (decarbonization of the solid solution due to reactions of formation of CH_4 type compounds and distribution of the latter over the crystalline lattice defects, boundaries of grains and subgrains). This kind of structural heterogeneity has a negative influence on long-term strength of the metal, because of the difference in mechanical properties of ferrite grains (163–190 $HV_{0.1}$) and surrounding dispersed acicular structure (248–268 $HV_{0.1}$) so that it is desirable to avoid it.

DISCUSSION OF INVESTIGATION RESULTS

Obtained HV_5 values of the weld metal indicate that lowering of the preheating temperature during product welding, even to 50 °C, cannot be the cause for exceeding the hardness standard values [1] (240 for the average value and 256 for individual measurements). None of the individual hardness values in the state after optimal heat treatment (730 °C/3 h), and none of the average values exceed the specified limits. Average value of 241 HV_5 for 3–360 thermal mode characterized by the highest heat input, is an exception.

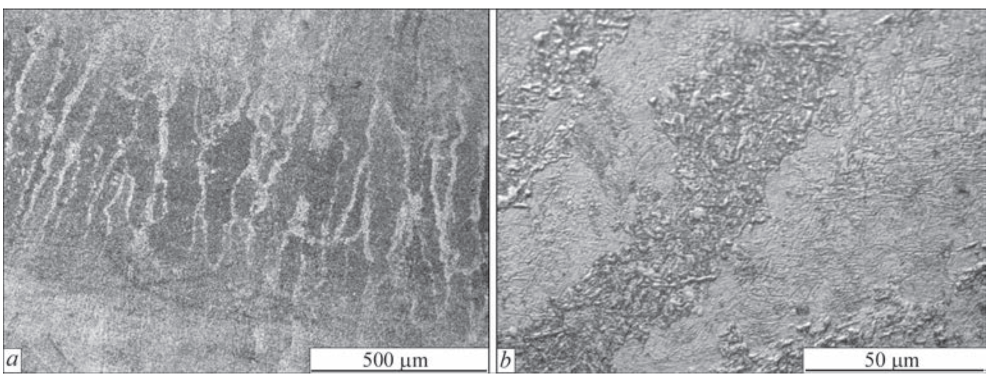

Figure 4. Structure of cast metal areas with light-coloured fringes along columnar crystallite boundaries: *a* — 2-160 mode, ×100; *b* — 3-160 mode, ×1000

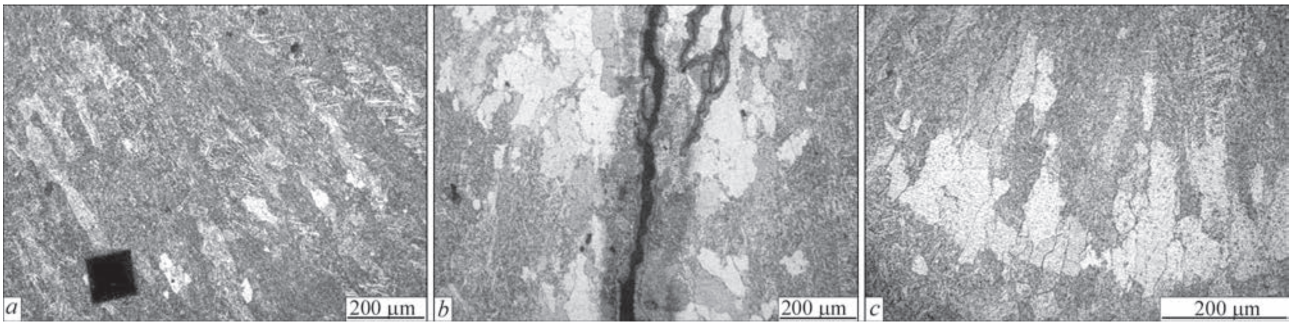

Figure 5. Structural heterogeneity of metal of as-tempered welds: *a* — individual ferrite grains in acicular structure matrix, ×125; *b* — colony of ferrite grains on the crack lips, 1-50 mode, ×125; *c* — ferrite grain colony, equidistant from the bead fusion line, 1-160 mode, ×200

An essentially higher HV_5 level for metal of all the welds tempered at 690 °C, on the whole, is an expected result for the alloying system of Cr–Mo–V steel weld, which during tempering goes through the stage of dispersion hardening. So, the noncompliance of the actual process of heat treatment of real welded products with the optimal conditions: for instance, when the product temperature (or of its part) has for a long time been in the range of 690–730 °C, not having reached the maximum of the above range, or duration of keeping at maximal temperature turned out to be shorter than the required one, should be considered the most probable cause for increased hardness of weld metal in as-heat treated state. Note that the company catalog of welding consumables [10] gives, as a reference, the level of mechanical properties and impact energy in the state after tempering by 680 °C/8 h mode for deposited metal of Boehler Fox DCMV electrodes of EN ISO 3580-A – E ZCrMoV1 B 4 2 H5 type, guaranteed by the manufacturer. However, when requirements to weld metal hardness are specified, one should not be guided by such additional information, assigning a lower temperature of welded joint tempering, or interpret them as admissibility of its random deviations in the range of 730–680 °C.

Detection of macrocracks during welding shows that level of T_p = 40–60 °C is lower than critical T_p value. Welding of Cr–Mo–V steels with electrodes of EN ISO 3580-A – E ZCrMoV1 B 4 2 H5 type is not allowed at this preheating temperature, irrespective of *Q*, because of unsatisfactory technological strength of the weld metal.

As is known, initiation and propagation of a brittle crack in the welded joint metal are due to the action of residual welding stresses and presence of factors, accelerating exhaustion of the metal ductility margin. One of such factors is the presence of defective areas (pores, nonmetallic inclusions, their clusters, etc.). Microtears detected in a considerable quantity in the weld made in 1-160 mode, being the ready center of fracture and mechanical stress concentration, impair the frequency distribution of the above-mentioned microscopic objects, promoting initiation and propagation of cracks. Even under the condition that these centers will not develop in the form of cracks during welding or postweld tempering, this factor even for a well-tempered metal, will probably have a marked negative influence on its long-term strength and ductility characteristics. For these reasons, 1-160 thermal mode should be also considered inadmissible.

For a more detailed determination of critical parameters of thermal mode, it is advantageous to consider the obtained results in comparison with the known quantitative characteristics, which are of criterial value as to cold cracking susceptibility of hardened steel welded joints under the welding conditions. For instance, the risk of cold cracking in the metal of a steel welded joint is considered to be high, if temperature M_e of the end of its martensite transformation is equal to 290 °C, and lower [15], and the volume fraction of martensite in its structure reaches 50 % and higher [16]. Moreover, 350 *HV* is considered to be a critical value of metal hardness, above which the risk of cold cracking becomes higher [16].

By the results of experiments (Table 3, as-welded state) average HV_5 value for the weld metal is higher than 350 units for thermal modes 1-50, 1-160, 1-270 and 2-50. For 3-50 mode, both the average and individual values are lower than 350 HV_5, which, however, was not a guarantee of crack absence (Figure 1, *c*). Similarly, 1-270 weld metal has a rather homogeneous structure without cracks or microtears, although its hardness is equal to 358–386 HV_5. This comparison shows that 350 *HV* and, probably, other proposed characteristics cannot be regarded as absolute criteria for all the possible alloying systems of hardened steels and welding conditions (welded joint rigidity, rates of heating and plastic deformation of the metal, diffusible hydrogen, etc.). We still assume that derived by generalization of a considerable volume of experimental data, these characteristics (particularly, when applied together) are suitable for tentative evaluation of cold cracking susceptibility and determination of the required conditions for their prevention during welding.

The quantity and type of final structural components in the metal of the weld and HAZ can be determined by the thermokinetic diagrams of austenite decomposition (γ), derived for continuous cooling of the metal. Let us consider (Figure 6) the diagram of 15Kh1M1FLsteel [4] in the assumption that the differences in element weight fractions do not have any essential influence on the transformation kinetics, types and quantity of their products in cast steel and in experimental weld metal.

Metal cooling rate w_{cool} during welding is one of the determinant factors of the influence on the structure of the metal of weld and HAZ of 15Kh1M1FL steel welded joints. The temperature of the start and end of transformations, as well as m values depend on w_{cool}. When w_{cool} ~ 100 °C/s, martensite is absent in the structure. At still lower w_{cool} values (≤ 0.4 °C/s), precipitation of structurally free ferrite can occur along the bainite grain boundaries (undesirable manifestation of structural heterogeneity). When w_{cool} ~ 100 °C/s, the steel structure is completely martensitic. Decomposition of γ at intermediate w_{cool} values characteristic for arc welding, leads to formation of bainitic-martensitic structure. γ-α-transformation starts at temperatures of the lowest γ resistance, which, depending on w_{cool}, make up the range from 655 to 450 °C. The bainite transformation region is located higher than 400–430 °C limit (upper bainite), which, in its turn, also depends on w_{cool}. Below 400–430 °C temperatures, transformation takes place with martensite formation. The lower curve of temperatures M_e of the end of martensite transformation, which are equal from 400 to 250 °C, depending on w_{cool}, corresponds to completion of γ-α-transformations. In keeping with the diagram, critical rate of cooling during welding of 15Kh1M1F steel, when all the three criteria are fulfilled (m > 50 %; M_e = 290 °C and 350 HV), should be chosen from w_{cool} range between 25 and 36 °C/s.

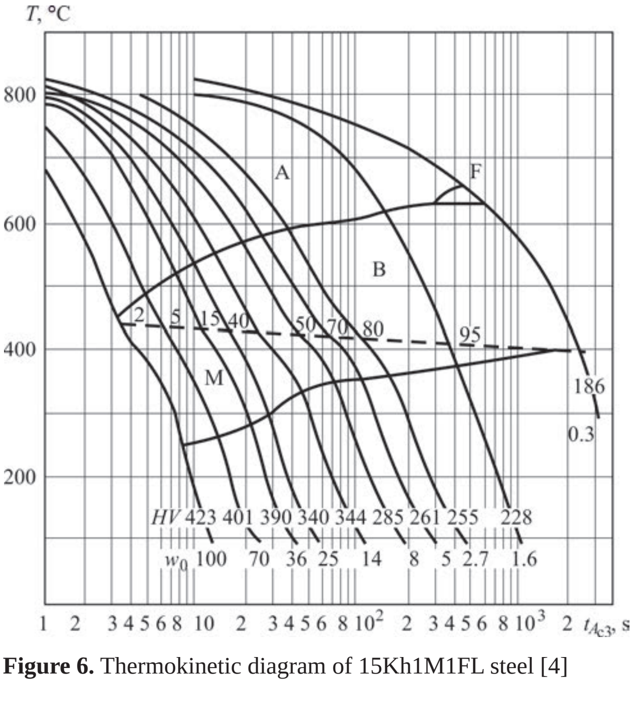

Figure 6. Thermokinetic diagram of 15Kh1M1FL steel [4]

For the conditions of manual arc welding of relatively thick-walled joints, the instantaneous cooling rate at the moment, when the metal of the weld and HAZ has reached a temperature of the lowest resistance of austenite, T_{min} can be calculated by the following formula [13]:

$$w_{cool} = 2\pi\lambda(T_{min} - T_0)^2/(q/V_w), \qquad (1)$$

where π is the pi number — 3.14159 …; λ is the metal heat conductivity, which can be taken to be 35 W/(m·°C) (for 15Kh1M1F steel in the range of 500–600 °C [8]); T_0 is the metal initial temperature (before the pass deposition), K; q is the effective thermal power of the arc, W; V_w is the arc movement speed, m/s.

Value T_{min} is determined by a curve which separates the austenite and bainite regions (Figure 6). In terms of T_{min} (w_{cool}) dependence for weak thermal modes, when high w_{cool} are anticipated (welding with concurrent self-heating to 50 °C), T_{min} was taken equal to 500 °C. For the rest of the modes T_{min} was assumed to be 550 °C. Calculation results (Table 4) allow a more accurate characterization of thermal modes. In keeping with Figure 6 and the above considerations, value w_{cool} = 33 °C/s agrees well with the concept of criticality of the respective thermal modes.

For final determination of the set of admissible thermal modes, we will take into account some other limitations, which follow from the results of this work. In terms of long-term strength of the weld metal in the state after optimal heat treatment, it is desirable to ensure a homogeneous acicular structure of the ferritic-carbide mixture. Welds produced in modes 1-270, 2-160, 2-270, 3-160, 3-270 have these characteristics. Polygonal ferrite grains in the matrix of a dispersed ferritic-carbide mixture are an undesirable kind of structural inhomogeneity. In welds made without preheating and with preheating to 360 °C, ferrite colonies and single ferrite grains are present. Taking into account this fact, as well as hardness values of 1-360, 2-360 and 3-360 welds after tempering at 730 °C/3 h (Table 3), and considering appropriate the recommendations of [3], we will limit the maximum of optimal preheating temperature by the level of 300 °C.

Current maximum admissible for 5 mm electrodes corresponds to welding at the heat input of 10.2 kJ/cm. Here, greater spattering of large electrode metal drops is observed, which firmly adhere to the plate surface and which require more time for removal. Therefore, it is not recommended to assign I_w higher than ~ 90 % of the maximal admissible one, to which Q ~ 9 kJ/cm corresponds.

Hardness of weld metal produced in 2-160 mode is lower than 350 HV, and it has a favourable dispersed structure (without macro- or microdefects or ferrite grains), however, the calculated value w_{cool} = 43 °C/s exceeds the critical one. Trying to prevent the ap-

Table 4. Calculated cooling rate of the metal at the moment of the lowest austenite resistance during multipass welding

Welding mode	Q, kJ/cm	T_p, °C			
		50	160	270	360
		$w_{cool}(T_{min}$ = 500 °C)	$w_{cool}(T_{min}$ = 550 °C)	$w_{cool}(T_{min}$ = 550 °C)	$w_{cool}(T_{min}$ = 550 °C)
1	5.21	85	64	33	15
2	7.78	57	43	22	10.2
3	10.2	44	33	17	7.8

Tone denotes w_{cool} values, corresponding to welding thermal modes: admissible (no tone); critical (light tone); inadmissible (dark tone)

pearance of undesirable features and microdefects in the production practice of welding, it is rational to somewhat increase T_p for this Q level. Required T_p (initial metal temperature) can be calculated, proceeding from (1). Taking the data of cooling graph (Figure 6): w_{cool} = 36 °C/s and T_{min} = 525 °C, we obtain T_p = 169 °C, and assume ~ 170 °C.

Nomogram (Figure 7) can be proposed as a summary of analysis of the results of this work (and taking into account the data of [3]). The area limited by *abcdef* polygon, including the dashed contour line, is the geometric locus of points, the combinations of the coordinates of which correspond to admissible values of Q and T_p during welding. The *fed* solid line is the locus of points, the combinations of the coordinates of which correspond to critical thermal modes. Below and to the left of the solid line lies the inadmissible mode region. Higher and to the right of *abcd* dashed line is the region of admissible modes, which, however, are undesirable for the above-mentioned reasons. To the left of the region of *af* contour is also the area of admissible, but undesirable thermal modes, which corresponds to low-power welding modes with a low deposition rate, poorer bead formation and higher probability of appearance of defects of the type of lacks of fusion and slagging.

Assigning one of the parameters initially, it is easy to define the optimal range and critical value of the other. Proceeding from known Q and electrode diameter, U_a, V_w parameters can be taken tentatively (Table 2), and I_w can be found from the known formula for heat input calculation [5, 13].

In the context of generalization of the work results we will formulate the main technological recommendations for producing welded joints of thick-walled assemblies from Cr–Mo–V steels with application of EN ISO 3580-A – E ZCrMoV1 B 4 2 H5 type electrodes and allowing for the probability of deviation of welded product T_p below the optimal range:

- at the stage of development of the welding technology, as well as to check the actually applied welding thermal mode for admissibility/criticality the nomogram (Figure 7) can be used together with the accompanying explanations in the text;
- 270–300 °C should be regarded as the optimal range of product preheating temperature under the ordinary conditions; at optimal preheating temperature it is possible to apply all the common methods of welding with electrodes of any diameter;
- 160 °C temperature should be regarded as the critical preheating temperature, below which performance of welding operation (bead deposition) is not allowed;
- during the cold season, when the probability of deviations of welded product T_p below the optimal range become higher, it is better to select 4 or 5 mm electrodes for welding; it is allowed to use 3.2 mm electrodes to a limited extent, or under the condition of welding at as high heat input as possible. For this purpose, it is desirable to assign the welding current near the upper admissible limit (while ensuring acceptable bead formation and spattering level), de-

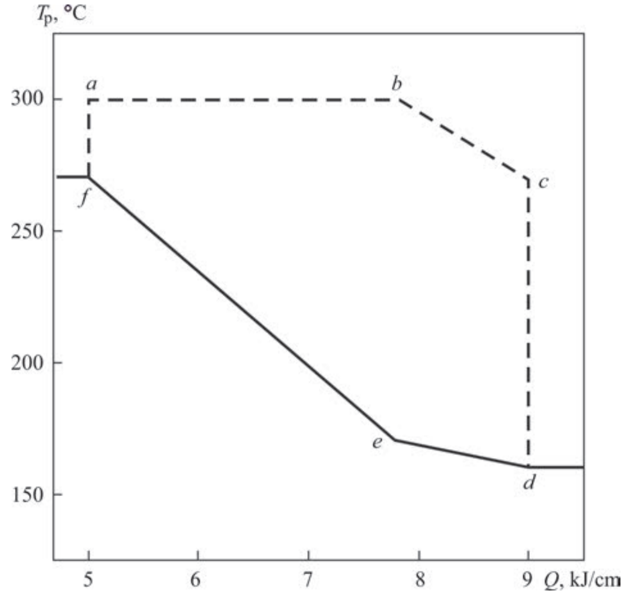

Figure 7. Nomogram of thermal modes of welding heat-resistant steels with coated electrodes of EN ISO 3580-A – E ZCrMoV1 B 4 2 H5 type

crease the arc movement speed, apply transverse oscillations of the electrode, etc. Moreover, it is allowed to perform product preheating or intermediate heating with a margin – up to temperatures somewhat higher than the optimal one (300–360 °C);

● in order to guarantee achieving an average hardness value of the weld metal after heat treatment ≤240 *HV*, excess heat input during welding (high-power modes simultaneously with metal preheating up to temperatures higher than the optimal range) should be avoided; welded joint tempering parameters should be equal to: temperature not lower than 730 °C, soaking duration of not less than 3 h; together with that it is necessary to ensure the homogeneity of heating temperature in all the product points or of the welded joint control zone (in case of local heat treatment).

CONCLUSIONS

1. The optimal range of preheating temperature of thick-walled assemblies from heat-resistant chromium-molybdenum-vanadium steels, welded by coated electrodes of EN ISO 3580-A – E ZCrMoV1 B 4 2 H5 type is 270–300 °C. Preheating temperature of 160 °C is critical under the above-mentioned conditions. Below the critical preheating temperature the probability of appearance of micro- and macrodefects of weld metal and unfavourable features of its microstructure becomes higher, which does not allow producing serviceable high-quality welded joints.

2. Meeting the hardness standards (≤240 *HV*) of metal deposited with electrodes of EN ISO 3580-A – E ZCrMoV1 B 4 2 H5 type is ensured by welding in modes without excess heat input. In addition, the following postweld tempering parameters should be ensured: not lower than 730 °C temperature, and not less than 3 h time of product soaking at this temperature.

3. Technological recommendations on producing welded joints of chromium-molybdenum-vanadium steels with electrodes of EN ISO 3580-A – E ZCrMoV1 B 4 2 H5 type, taking into account the probability of deviation of the preheating temperature below the optimal range were developed, as well as the nomogram of admissible and critical welding thermal modes, which were transferred for practical application to JSC “Ukrainian Energy Machines”.

REFERENCES

1. Tsaryuk, A.K., Ivanenko, V.D., Protsenko, N.O. et al. (2016) Standard of organizations of Ukraine SOU VEA. 200.1.1/01:2016: *Welding, heat treatment and control of tube systems of boilers and pipelines during installation and repair of power equipment. Organization of works and maintenance.* Kharkiv, Folio [in Ukrainian].
2. German, S.I. (1972) *Electric arc welding of heat-resistant steels of pearlite class.* Moscow, Mashinostroenie [in Russian].
3. Khromchenko, F.A., Lappa, V.A. (1991) Influence of thermal conditions of welding on cracking resistance of welded joints of 15Kh1M1F steel under conditions of low-cycle creep. *Svarochn. Proizvodstvo,* **12**, 33–35 [in Russian].
4. Tsaryuk, A.K., Ivanenko, V.D., Volkov, V.V. et al. (2009) *Repair welding of turbine housing parts from heat-resistant steels without postweld heat treatment.* In: Problems of service life and safety of structures, constructions and machines. Kyiv, PWI, 519–524 [in Ukrainian].
5. ISO/TR 17671-2:2002 (E): *Welding — Recommendations for welding of metallic materials.* Pt 2: Arc welding of ferritic steels.
6. Efimenko, N.G., Atozhenko, O.Yu., Vavilov, A.V. et al. (2014) Structure and properties of welded joints of 15Kh1M1FL steel at repair of casting defects by transverse hill method. *The Paton Welding J.*, **2**, 44–48.
7. Zemzin, V.N., Shron, R.Z. (1978) *Heat treatment and properties of welded joints.* Leningrad, Mashinostroenie [in Russian].
8. Zubchenko, A.S., Koloskov, M.M., Kashirskiy, Yu.V. (2003) *Grades of steels and alloys.* Moscow, Mashinostroenie [in Russian].
9. Protsenko, N.A. (2017) Introduction of harmonized international and European standards into welding production of Ukraine. *Avtomatich. Svarka,* **11**, 47–57.
10. Wissenswertes für den Schweißer (2006) *Handbuch der Böhler Sweißtechnik.* Austria GmbH.
11. Welding Filler Metals (2005) *Welding guide of Böhler Thyssen Schweisstechnik.* Deutschland GmbH.
12. ISO 6847:2013 (E): *Welding consumables — Deposition of a weld metal pad for chemical analysis.*
13. (1978) *Welding in mechanical engineering:* Refer. Book. Vol. 1. Moscow, Mashinostroenie [in Russian].
14. Novikov, I.I. (1978) *Theory of heat treatment of metals.* Moscow, Metallurgiya [in Russian].
15. Pokhodnya, I.K., Shvachko, V.I. (1997) Physical nature of hydrogen induced cold cracks in welded joints of high-strength structural steels. *Avtomatich. Svarka,* **5**, 3–10 [in Russian].
16. Makarov, E.L. (1981) *Cold cracks in welding of alloyed steels.* Moscow, Mashinostroenie [in Russian].

ORCID

S.I. Moravetskyi: 0000-0002-5807-8340,
A.K. Tsaryuk: 0000-0002-5762-5584,
V.Yu. Skulskyi: 0000-0002-4766-5355,
M.O. Nimko: 0000-0002-9672-4921

CONFLICT OF INTEREST

The Authors declare no conflict of interest

CORRESPONDING AUTHOR

S.I. Moravetskyi
E.O. Paton Electric Welding Institute of the NASU
11 Kazymyr Malevych Str., 03150, Kyiv, Ukraine.
E-mail: box.55@ukr.net

SUGGESTED CITATION

S.I. Moravetskyi, A.K. Tsaryuk, V.Yu. Skulskyi, M.O. Nimko (2023) Thermal conditions of coated electrode welding of heat-resistant low-alloy steels. *The Paton Welding J.*, **9**, 21–30.

JOURNAL HOME PAGE

https://patonpublishinghouse.com/eng/journals/tpwj

Received: 12.06.2023
Accepted: 09.10.2023

DOI: https://doi.org/10.37434/tpwj2023.09.05

THERMAL PROCESSES AND EVOLUTION OF STAINLESS STEEL STRUCTURE IN FRICTION STIR WELDING WITH A TOOL FROM pcBN

A.L. Maistrenko[1], M.P. Bezhenar[1], S.D. Zabolotnyi[1], V.A. Dutka[1], M.O. Cherviakov[2], A.M. Stepanets[1], I.O. Gnatenko[1], M.O. Tsysar[1]

[1]V. Bakul Institute for Superhard Materials of the NASU
2 Avtozavodska Str., 04074, Kyiv, Ukraine
[2]E.O. Paton Electric Welding Institute of the NASU
11 Kazymyr Malevych Str., 03150, Kyiv, Ukraine

ABSTRACT

It is shown that application of superhard materials based on cubic boron nitride for manufacture of working components of the tool for realization of friction stir welding processes allows ensuring the tool thermomechanical resistance. Computer modeling of the temperature field in the tool, and in steel parts during friction stir welding of stainless steels with a tool based on polycrystalline boron nitride (pcBN) was performed. Agreement between the numerical and experimental results of temperature distribution in the tool movement zone is shown. Strength of welded joints of stainless steel parts was determined, and evolution of weld structure was analysed.

KEYWORDS: structure evolution, friction stir welding, tool, kiborit, strength, modeling, stainless steels, temperature field

INTRODUCTION

As is known, the process of friction stir welding (FSW) is conducted at temperatures much lower than melting temperature of the metals and alloys being welded. It results in an essential lowering of residual stresses and temperature deformations, and evolution of the joint zone microstructure takes place that has a positive influence on ensuring the part material strength in their joint zone. Initially, this method was successfully used for welding magnesium- and aluminium-based alloys [1]. Magnesium alloys turned out to be a material readily weldable by FSW method, as the welding process is conducted at low temperatures (200–260 °C) with application of steel tools [1–3]. In friction stir welding of aluminium alloys the observed characteristic temperatures in the welding zone were in the range of 300–400 °C. Realization of the process of FSW of copper-based materials is performed already at temperatures of 600–700 °C that requires application of hard-alloy tools [4]. For welding steels and high-temperature alloys, however, in welding of which the temperature of 600–1000 °C is observed, a tool with already much higher thermomechanical resistance is required, in particular, based on special hard alloys or polycrystalline materials based on cBN [5, 6]. In order to substantiate the optimal design of the tool and produce a sound welded joint of the parts, as a result of FSW, it is rational to first of all perform mathematical modeling of the thermal state of the tool and the parts during welding [5–7].

Over the last twenty years, FSW method has been used for welding heat-resistant steels and alloys. Realisation of the process of FSW of stainless steels of austenitic-ferritic type and high-temperature alloys requires application of a tool from heat-resistant materials, which include special hard alloys and polycrystalline materials based on cubic boron nitride (pcBN) [8, 9].

V. Bakul Institute for Superhard Materials of the NASU is working on development and application of tools for FSW for different metals and alloys [1–4, 7]. Here, the properties of materials used for tool manufacture, should be much higher than the mechanical characteristics of the materials being welded or surfaced. More over, the tool, particularly, its working part (pin), should preserve a high wear resistance and heat resistance at high temperatures. These materials should retain their properties at rather high temperatures and cyclic loads, which are due to the forces applied to the tool during circular bending in welding or surfacing.

The objective of the work is to develop a tool from polycrystalline boron nitride (pcBN) for friction stir welding of stainless steels, analysis of thermal processes in welding and evaluation of the mechanical characteristics of the welded joints.

MATERIALS AND INVESTIGATION PROCEDURES

Polycrystalline superhard materials based on cBN are known in the world market as tool pcBN materials. The tendencies in development of studies in the field of creation of polycrystalline superhard materials based on CBN can be illustrated in the case of products of a number of foreign firms, in particular Element Six and MegaDiamond Companies [10, 11]. In Kiborit material of this class [8, 9], where the main phase is cBN (about

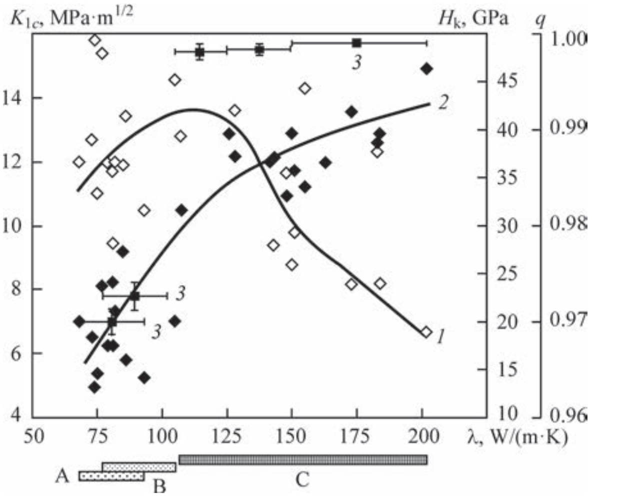

Figure 1. Crack resistance (*1*), hardness (*2*) and relative density (*3*) of polycrystals obtained by reaction sintering of CBN powder with 2 wt.% Al [9]

84 %), which is a determinant factor for formation of the structure of a composite material with a continuous frame and high hardness. Kiborit of all the grades is produced by reaction sintering of cBN with Al under high pressure conditions in hard-alloy high-pressure apparatuses (HHA) of "anvil with recess" design of "toroid" type [8, 9]. Special features of the properties of pcBN-based composites consist in their high hardness and crack resistance, chemical resistance and predominantly tribochemical wear mechanism. In the first case, there is more than 80 % cBN in the material composition, hardness is ensured by cBN frame, and crack resistance is high due to the binder along the grain boundaries (Table 1) [9]. Materials with more than 95 % cBN content in the structure have higher hardness. An example of such a material is Kiborit-1, developed at ISM of the NASU. A feature of the structure is absence of a continuous binding frame (binder composition is AlN and AlB_{12}, quantity is 3 wt.%; it is arranged in the form of inclusions along the grain boundaries). Kiborit-2 material — pcBN is produced by the method of preimpregnation of compacted cBN powder by aluminium with subsequent reaction sintering at a high pressure [8, 9]. Sintering parameters of Kiborit-2 material are as follows temperature of 1600–1750 K and pressure of up to 4.5 GPa. Here, additional evolution of the energy of chemical reaction in the working volume, alongside the external heating energy, should be noted. For such a process, steel HHA are the best, [12], one of the advantages of which is the large working volume, allowing production of large-sized samples of 32 mm diameter and 15 mm height in presses with 20 MN force (Table 2).

Table 1. Physico-mechanical properties of some Kiborit grades [9]

Characteristics	Kiborit-1	Kiborit-2	Kiborit-3
CBN quantity, %	96–97	84	70–75
Specific weight, g/cm^3	3.40–3.45	3.35–3.38	3.60
Knoop hardness at 10 N load, GPa	32–36	28–30	27
Crack resistance K_{1c}, MPa·m$^{1/2}$	8–13.5	10.5	10.5
Compressive strength, GPa	3.2	2.9	2.9
Tensile strength, GPa	0.37	-	-
Modulus of elasticity, *E*, GPa	880	-	-
Poisson's ratio	0.16		
Heat conductivity λ, W/(m·K)	150	70	70
Heat resistance up to temperature, K	1400	1400	1400
Resistance to oxidation in air to temperature, K	1200	1200	1200
TEC, $\alpha \cdot 10^{-6}$ K^{-1}	–	4.9–7.9	–
Plate diameter, mm	6.35–12.7	9.6–31.8	9.6–31.8

Figure 1 shows the changes in relative density (ρ), hardness (*H*k) and crack resistance (K_{1c}) in polycrystalline materials of the considered type for three groups (A, B, C) [9].

New Kiborit application is the work tool for friction stir welding. Rotating tools of this type consist of a shoulder and protruding pin — Figure 2. In welding the pin is immersed into the blank, and the shoulder is pressed to the surface. Friction at tool rotation generates heat, which is sufficient for transition of the materials being joined into an elasto-plastic state.

Kiborit-1 was produced by reaction sintering of cubic boron nitride powder (up to 98 %) with aluminium [8, 9]. Presence of other additives in the charge and high sintering parameters led to obtaining in the composition of Kiborit-1 binder also higher β-AlB_{12} boride, alongside AlN and AlB_2. A combination of high hardness Hk (36–38 GPa) and high heat conductivity (100–150) W/m·K with sufficiently high level of crack resistance (≥ 8 MPa·m$^{1/2}$) of Kiborit-1 enabled

Table 2. Mechanical properties of the studied materials [13]

Steel	*E*, GPa	$\sigma_{0.2}$, MPa	σ_t, MPa	δ, %	T_m, °C
08Kh18N10T (AISI 321 analog)	193	196	470	40	1400–1455
AISI 304 (08Kh18N10 analog)	196	205	510	40	1400–1455
EP-718 (KhN45MVTYuBR) (acc.to TU 14-1-3905-85)	205	550	1240	30	1260–1336
EI 698 (Kh73MBTYu)	200	705	1150	16	1370–1400

its application in blade tools. Development of superhard polycrystalline Kiborit-2 material is based on the principles of creation of a material with a continuous structure of CBN frame and reaction sintering with aluminium. The difference consisted in such a control of sintering parameters, which ensured increase of "CBN–another phase" contact surface at preservation of continuous CBN frame in the structure [9]. The given results show that hardness of the real polycrystals, containing from 65 to 96 % CBN and AlN-based binder, in all the cases is somewhat lower than the calculated one in the assumption of additive dependence on the phase composition.

Thus, we have the possibility of choosing from the composites of Kiborit series an appropriate material for application in the tools for friction stir welding of steels. It was exactly Kiborit-2, which was selected for tool manufacture, based on its high heat-resistance (1200 °C), as well as because this material has maximal crack resistance $K_{1c} = 10.5$ MPa·m$^{1/2}$, which is important at cyclic circular bending of the pin, and diameter and height dimensions of the blank of 32×15 mm, which allowed manufacturing tools with pin height of 5–6 mm and should diameter of 25 mm (Figure 2, *a*).

Stainless steels of AISI type (08Kh18N10 analog), 08Kh18N10T (AISI 321 analog), 03Kh20N16AG6, 02Kh18MBV and heat-resistant EP-718 (KhN-45MVTYuBR) and EI-698 (KhN73MBTYu) alloys [13]. Mechanical properties of some of them are given in Table 2. Figure 2, *b* shows the appearance of the weld in welding AISI 304 steel.

MEASURING THE FORCE COMPONENTS IN WELDING OF STEELS

Investigations on friction stir welding of steels with measurement of the components of the force acting on the tool, were performed in the bench mounted on the table of vertical milling machine 654, fitted with measuring sensors and software of HBM Company (Figure 3). Welding modes: tool rotation speed of 800 rpm^{-1} and feed rate of 20–50 mm/min. The tool is mounted at 88° angle relative to the part surface. Samples of 3–4 mm thickness were studied (Table 3). Welding of the studied steel samples was performed in a special bench, fitted with a system of sensors, which measure the vertical and shear components of the force, applied to the end effector (Figure 3, Table 3). It is found that the average force components, irrespective of the rotation frequency and speed of welding with the tool with the conical pin stay on the same level for all the studied steel samples of the same thickness (Table 2).

TEMPERATURE MEASUREMENT IN THE WELDING ZONE

Temperature measurement in the welding zone was performed with an infrared imager Fluke-ir25 with 5 s resolution at different moments of the tool movement along the sample (Figure 4).

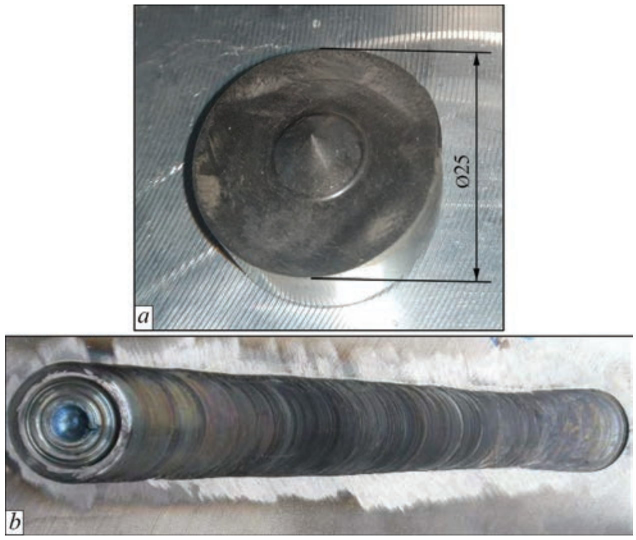

Figure 2. General view of the tool from polycrystalline boron nitride for welding stainless steels (*a*) and general view of the weld in AISI 304 steel welding (*b*)

TEMPERATURE FIELD MODELING AT FSW OF STAINLESS STEELS

Mathematical modeling of the temperature field in the parts being welded during FSW was performed. A 3D stationary model was selected, which is based on a nonlinear equation of heat conductivity. Redistribution of heat sources over the surfaces of the tool pin contact with the parts being welded is taken into

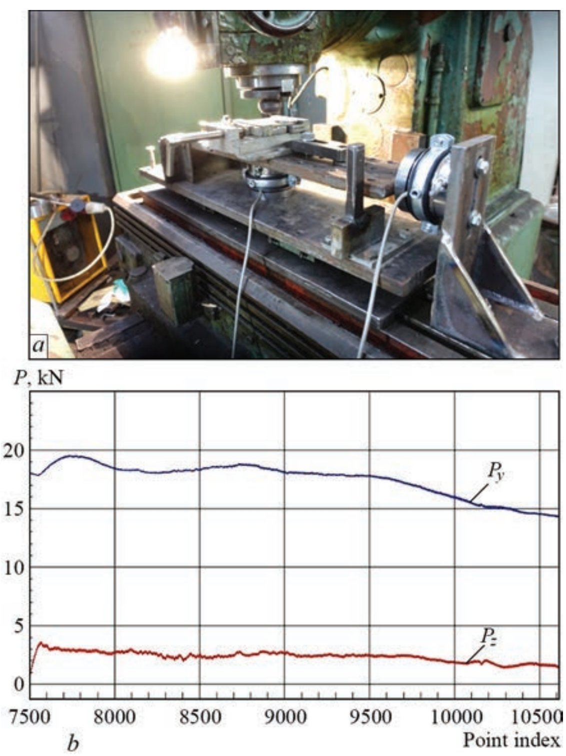

Figure 3. General view of a bench for studying the process of friction stir welding of steels (*a*), graph of the change of the components of a force acting on the tool (*b*)

Table 3. Results of measuring the force components (FSW) of samples of the studied stainless steels

Sample material	Sample thickness, mm	Horizontal component P_z, N		Vertical component P_y, N	
		Average	max	Average	max
03Kh20N16AG6	4	2385	3423	17597	19545
AISI 304 (08Kh18N10 analog)	3	1226	2766	11992	15780

account. Heat exchange with ambient air on the part free surfaces is also allowed for.

The material of the parts being welded is AISI 304 stainless steel. Two plates of 200×100×3 (4) mm size were welded by FSW along the plate larger size. The welding tools were made from Kiborit-2 material. Temperature dependencies of thermophysical properties of AISI 304 steel on temperature were taken into account: heat capacity C_p, thermal conductivity coefficient λ, density ρ, yield limit σ_y [14–16].

MATHEMATICAL MODEL OF THE TEMPERATURE FIELD

A stationary mathematical model was considered for description of the temperature field in FSW zone [17]:

$$C_p\rho(\vec{u}\ \mathrm{grad}\,T) = \mathrm{div}(\lambda\ \mathrm{grad}\,T), \quad (1)$$

where T is the temperature; C_p, ρ, λ are the specific heat capacity, density and thermal conductivity coefficient, respectively; $\vec{u}$ is the vector of the speed of the part forward movement relative to the tool.

Respective boundary conditions are assigned on the surfaces of the tool and parts (plates), as well as on the surface of contact of the tool and the plates. Heat sources act on the surface of contact of the pin, shoulder and plates, which are due to friction and plastic deformation of the plate material in this contact zone.

Heat sources due to friction are active on the shoulder contact surface. The capacity of these heat sources is calculated by the following formula

$$q_s = \begin{cases} \dfrac{2\pi r n \mu F}{A_s}, \text{ at } T < T_m, \\ 0, \text{ at } T \geq T_m, \end{cases} \quad (2)$$

where r is the distance from a point of this contact surface to the axis of rotation of the shoulder with the pin; n is the number of shoulder rotations per minute; μ is the friction coefficient; F is the axial force, acting on the pin with the shoulder; A_s is the area of the surface of shoulder contact with the parts; T_m is the temperature of plate material melting.

Figure 5 shows the results of calculations of temperature distributions in the components of the tool structure and AISI 304 steel plate being welded. Figure 6 gives a comparison of experimental and calculated temperatures. The given maximal values of experimentally measured temperatures are unfortunately limited by instrument characteristics and difficult access of the instrument to the welding zone, but it means that these are not the maximal acting temperatures in the welding zone, just acting maximal temperatures in the measured (limited) section.

INVESTIGATION RESULTS AND THEIR DISCUSSION

Experimental determination of temperature distribution in the welding zone of the studied steels was conducted. Results of temperature distributions in the measured welding zones of the studied steels beyond the tool shoulder are given in Figure 7.

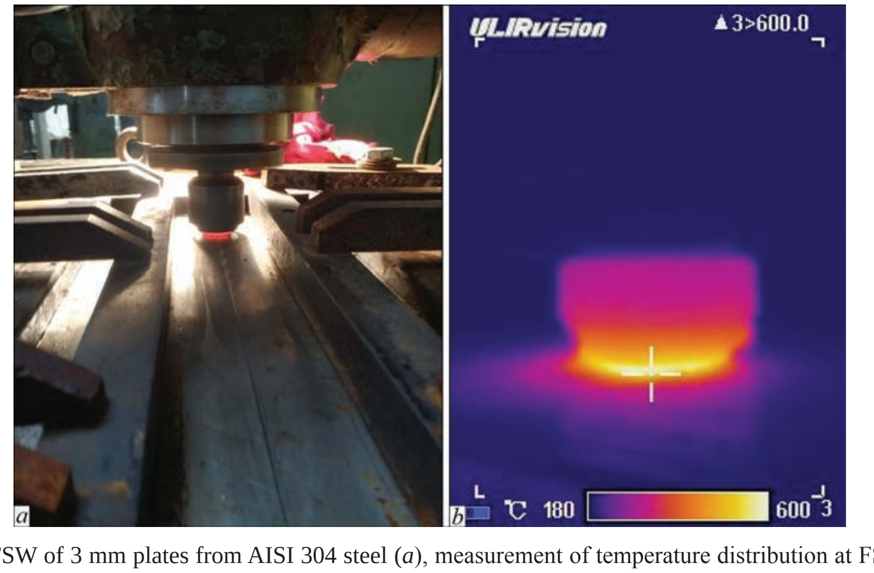

Figure 4. Images of FSW of 3 mm plates from AISI 304 steel (*a*), measurement of temperature distribution at FSW of stainless steel (beyond the tool shoulder) (*c*)

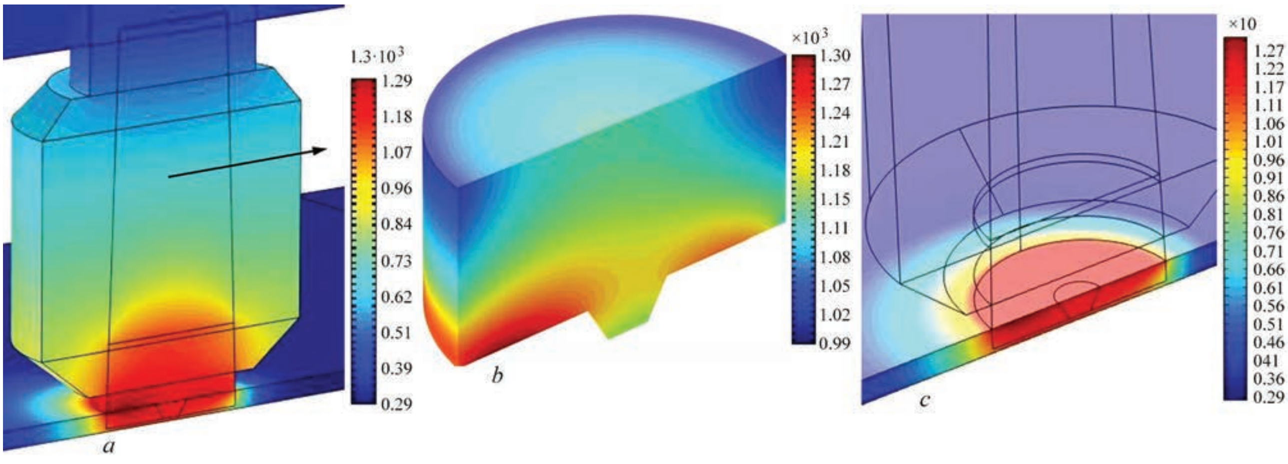

Figure 5. Pattern of the temperature field calculated in different parts of the computational domain (maximal temperature — 1303 K): *a* — in the plate, tool and tool fixtures (arrows show the direction of the tool forward movement); *b* — in the tool; *c* — in the plate being welded

Maximal studied temperature of welding the steel samples varied from 500 to 800 °C (Figure 7), temperature of welding 4 mm thick samples being practically 1.5 times higher than that of 3 mm samples, which is due to greater work of plastic deformations in the welding zone. Note also that the average temperature in welding of the studied steels is equal to T_{av} = 712 °C, i.e. the mean temperature of welding steels of austenitic-ferritic class corresponds to equation T_w = (0.45–0.62) T_m, unlike the known temperature range of welding magnesium and aluminium alloys, which corresponds to T_w (0.4–0.5)T_m ratio.

Metallographic investigations of welded samples were performed on polished microsections etched in $HCl + HNO_3$ solution for 5 min. Microstructure images obtained in optical microscope XUM-102 at ×500 magnification are shown in Figure 8. Individual grain sizes were determined using LevenhukLite software, and they are given directly in the images.

In welding 08Kh18N10T steel, the grain size practically does not change, as the size of individual grains in the welding zone is in the range of 10–20 μm, and in the initial metal it is 5–15 μm. Grain size in the welding zone of 02Kh18MBV steel is 10–50 μm, and in the material being welded it is 50–150 μm, i.e. grain size in the weld is reduced relative to the initial metal by 3 to 5 times. Growth of individual grains is observed in the zone of welding 03Kh20N16AG6 steel. So, while in the base metal grain size is 2–10 μm, in the weld zone is increased to 10–50 μm. Grain size in weld metal of AISI 304 steel (08Kh18N10T) is 20–60 μm, and in the base metal grain size reaches 40–100 μm, i.e. in welding AISI steel grain size refinement by 1.6 to 2.0 times occurs in the welded joint zone.

Base on metallographic analysis of the change of grain size in the combined weld, the ratio of grain size in the weld of EP-718 alloy to grain size in the base metal decreases practically 2 times, and the size of

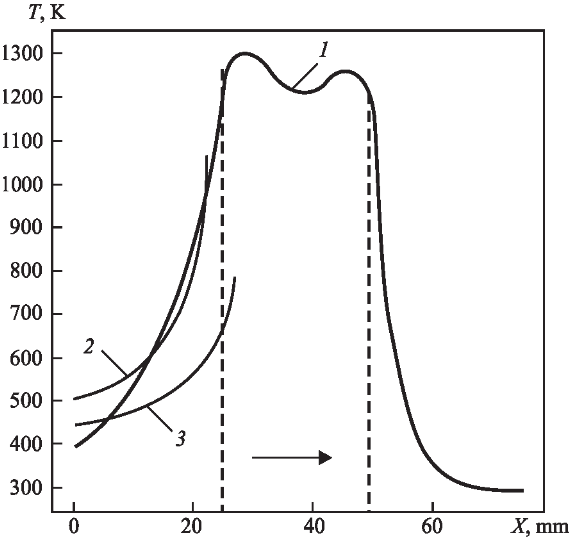

Figure 6. Comparison of calculated (*1*) and experimental (*2, 3*) temperatures along the line of welding the steel plates. Coordinate *X*, mm is the scale bar of the welded steel sample. The arrow shows the direction of tool movement. Dashed lines are the tool shoulder limits (*2* — Kh18N10T steel — 4 mm; *3*— AISI 304 steel — 3 mm)

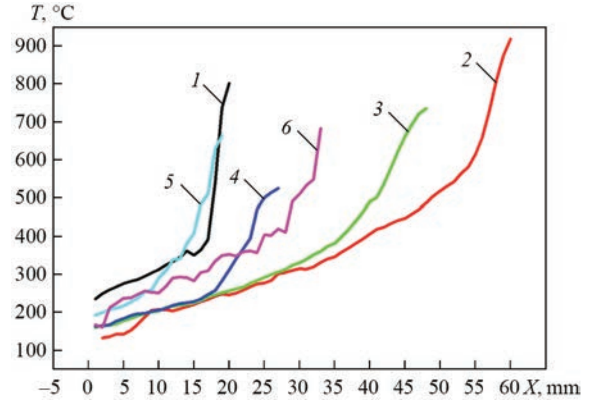

Figure 7. Experimentally determined temperature distributions behind the tool shoulder during FSW: thickness of 08Kh18N10T steel plate (*1*) — 4 mm; 02Kh18MBV steel (*2*) — 4 mm; 03Kh20N16AG6 steel (*3*) — 4 mm; AISI 304 steel (*4*) — 3 mm; EP-718 (*5*) — 4.3 mm; KhN73MBTYu steel (*b*) — 4.3 mm; *X* — coordinate is the scale bar of the steel sample being welded

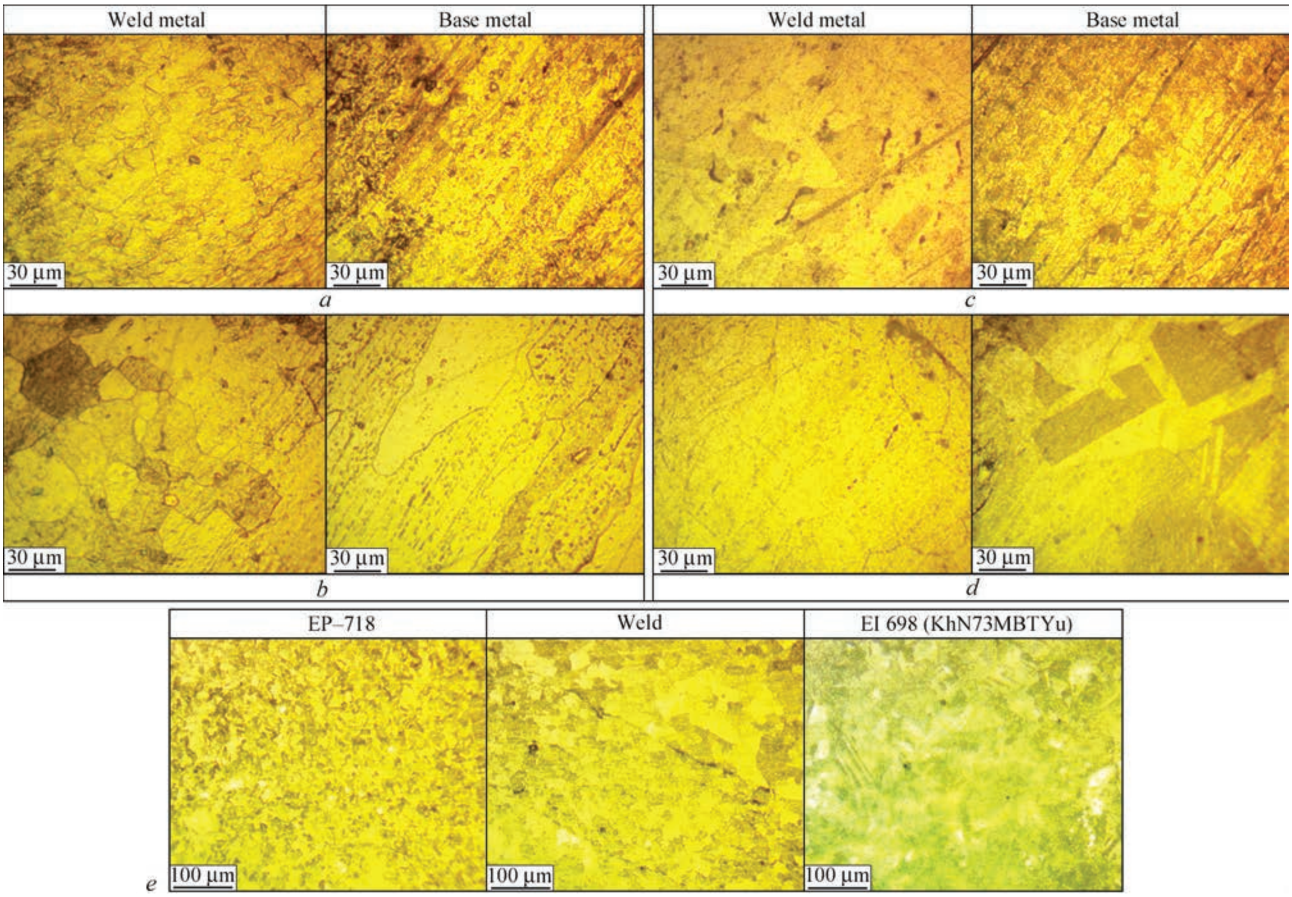

Figure 8. Evolution of weld structure in the studied steels (×500): 08Kh18N10T (*a*); 02Kh18MBV (*b*); 03Kh20N16AG6 (*c*); AISI 304 — 08Kh18N10 steel analog (*d*), EP 718 — EI 698 (*e*)

Table 4. Strength of the studied steels in the initial state and of their welded joints

Матеріал	Sample type	σ_y, MPa	σ_t, MPa	$\sigma_t^з/\sigma_t^о$
08Kh18N10T	Base metal	194	474	–
	Welded joint	135	280	0.59
02Kh18MBV	Base metal	429	707	–
	Welded joint	183	385	0.54
03Kh20N16AG6	Base metal	403	758	–
	Welded joint	275	390	0.51
AISI 304	Base metal	202	511	–
	Welded joint	171	349	0.68

grains in EI 698 steel weld is reduced 3 times relative to grain sizes in the base metal.

STRENGTH OF FSW JOINTS OF THE STUDIED STEELS

Tensile testing of material welded samples was performed in servohydraulic machine MTS-318.25. All the samples of the studied metals for strength determination were cut out in one direction — orthogonally to the welded plate axis. Strength of the studied steel welded joints relative to that of base metal of these steels was determined. It should be noted that the ratio of welded joint to base metal strength varied in the range from 0.51 to 0.68 (Table 4), i.e. strength lowering is quite significant, which determines the need to optimize the kinematic and force parameters of FSW process, which will ensure higher strength of the welded joints. Therefore, optimization of kinematic and force parameters of the welding process, which should ensure the high strength of the welded joint, requires a long and careful research, which is the next goal in the development of this area of technology.

CONCLUSIONS

1. A tool from polycrystalline boron nitride (pcBN) was developed for FSW of stainless steels and high-temperature nickel alloys. Test tools were manufactured from pcBN Kiborit-2 for realization of the process of FSW of structural components from up to 4 mm stainless steels and high-temperature alloys.

2. A model of the thermal process of friction stir welding of stainless steel was proposed and temperature distributions in the tool and parts being welded were calculated.

Investigations of thermal processes during welding showed that, depending on the thickness of samples being welded, the maximal temperature in the studied steel welding zone varied from 500 to 900 °C, which is approximately equal to (0.45–0.62)T_m.

3. A metallographic study was performed of the mean size of weld grain, compared to the sample base metal was performed. So, the mean size of grains in the zone of

welding 08Kh18N10T steel is in the range of 10–20 μm, and in the initial metal it is 5–15 μm, i.e. it remains without any significant changes. Mean size of grains in the welding zone of 02Kh18MBV steel reaches 10–50 μm, and in the weld material it is 50–150 μm, i.e. the grain size in the weld is reduced from 3 to 5 times relative to that of the base metal. In the zone of 03Kh20N16AG6 steel weld, a slight growth of the sizes to 10–50 μm is observed relative to the base metal with grain size of 2–10 μm. Grain size in the weld of AISI 304 steel reaches 20–60 μm, compared to base metal with grain size of 40–100 μm. Therefore, in welding a refinement of grain size from 1.6 to 2.0 times is found in the welded joint zone. Mean grain size in the weld of a mixed joint of EP-718 and EI-698 alloys is reduced from 2 to 3 times, relative to that of grains in the base meal of these alloys.

4. The ratio of strength of the studied material welded joints and that of the base metal varied in the range from 0.51 to 0.68, which determines the need to conduct more profound studies, aimed at optimization of FSW kinematic and force parameters, which will provide a higher strength of welded joints of this type.

REFERENCES

1. Majstrenko, A.L., Lukash, V.A., Zabolotny, S.D. et al. (2016) Application of friction stir method for welding of magnesium alloys and their structure modifying. *The Paton Welding J.*, **5–6**, 68–74. DOI: https:// doi.org/10.15407/tpwj2016.06.11
2. Maistrenko, A.L., Lukash, V.A., Usenko, B.O. et al. (2019) Welding of aluminium curvilinear panels by friction stir welding method. In: *Abstr. of Pap. of All-Ukrainian Int. Conf. on Problems of Welding and Related Technologies (17–19 September, 2019, Mykolaiv-Koblevo)*, 85–86.
3. Gnatenko, I.O., Oliinyk, N.O., Ilnytska, G.D. et al. (2019) Influence of friction stir welding on corrosion resistance of high-strength aluminium alloys. Rock destruction and metal-working tool: Technique and technology of its fabrication and application. Issue 22. Kyiv, ISM, 469–476 [in Russian].
4. Grigorenko, G.M., Adeeva, L.I., Tunik, A.Yu. et al. (2015) Application of friction stir welding method for repair and restoration of worn-out copper plates of MCCB moulds. *The Paton Welding J.*, **5–6**, 55–58.
5. Zhu, X.K., Chao, Y.J. (2004) Numerical simulation of transient temperature and residual stresses in friction stir welding of 304L stainless steel. *J. of Materials Proc. Technology*, **146**, 263–272.
6. Al-moussawi, M., Smith, A., Young, A. et al. (2016) An Advanced Numerical Model of Friction Stir Welding of DH36 Steel. In: *Proc. of 11th Inter. Symp. of Friction Stir Welding. Cambridge, UK.* https://www.researchgate.net/publication/305330065
7. Majstrenko, A.L., Nesterenkov, V.M., Dutka, V.A. et al. (2015) Modeling of heat processes for improvement of structure of metals and alloys by friction stir welding method. *The Paton Welding J.*, **1**, 2–10.
8. Novikov, M.V., Shulzhenko, O.O., Bezhenar, M.P. et al. (1998) *Method of sintering of composite material based on cubic boron nitride*. Pat. 25281A, Ukraine, Int. Cl. C04B35/5831. Fil. 21.07.97, Publ. 25.12.98 [in Ukrainian].
9. Novikov, N.V., Shulzhenko, O.O., Bezhenar, N.P. et al. (2001) Kiborit: Manufacture, structure, properties, application. *Sverkhtvyordye Materialy,* **2**, 40–51 [in Russian].
10. *Megadiamond pcBN Products for Industrial Tooling*. USA, The Publication of Megadiamond.
11. *Introduction to De Beers PCD and pcBN cutting tool materials*: 1.2.3. The Publication of De Beers Industrial Diamond Division.
12. Bezhenar, N.P., Romanenko, Ya.M., Konoval, S.M. et al. (2018) Kiborit: New materials and new fields of application. In: *Proc. of 6th Int. Samsonov Conf. on Materials Science of Refractory Compounds (Kyiv, Ukraine, 22–24 May 2018)*.
13. Zubchenko, A.S. (2003) Grades of steels and alloys. Moscow, Mashinostroenie [in Russian].
14. Bentz, D.P., Prasad, K. (2007) *Thermal Performance of Fire Resistive Materials I. Characterization with Respect to Thermal Performance Models*. Edition: NISTIR 7401. Publ., U.S. Department of Commerce.
15. Bentz, D.P., Flynn, D.R., Kim, J.H., Zarr, R.R. (2006) A slug calorimeter for evaluating the thermal performance of fire resistive materials. *Fire and Materials*, 30(**4**), 257–270.
16. Bogaard, R.H., Desai, P.D., Li, H.H., Ho, C.Y. (1993) Thermophysical properties of stainless steels. *Thermochimica Acta*, **218**, 373–393.
17. Nandan, R., Roy, G.G., Lienert, T.J., DebRoy, T. (2006) Numerical modelling of 3D plastic flow and heat transfer during friction stir welding of stainless steel. *Sci. and Technol. of Welding and Joining*, 11(**5**), 526–53.

ORCID

A.L. Maistrenko: 0000-0001-5479-326X,
S.D. Zabolotnyi: 0000-0003-1287-8454,
M.O. Cherviakov: 0000-0003-4440-7665,
I.O. Gnatenko: 0000-0002-9466-0215,
M.O. Tsysar: 0000-0002-4494-9109

CONFLICT OF INTEREST

The Authors declare no conflict of interest

CORRESPONDING AUTHOR

A.L. Maistrenko
E.O. Paton Electric Welding Institute of the NASU
11 Kazymyr Malevych Str., 03150, Kyiv, Ukraine.
E-mail: almaystrenko46@gmail.com

SUGGESTED CITATION

A.L. Maistrenko, M.P. Bezhenar, S.D. Zabolotnyi, V.A. Dutka, M.O. Cherviakov, A.M. Stepanets, I.O. Gnatenko, M.O. Tsysar (2023) Thermal processes and evolution of stainless steel structure in friction stir welding with a tool from pcBN. *The Paton Welding J.*, **9**, 31–37.

JOURNAL HOME PAGE

https://patonpublishinghouse.com/eng/journals/tpwj

Received: 28.06.2023
Accepted: 09.10.2023

DOI: https://doi.org/10.37434/tpwj2023.09.06

DIFFUSION WELDING OF MAGNESIUM ALLOY MA2-1 THROUGH A ZINC INTERLAYER

Yu.V. Falchenko, L.V. Petrushynets, V.Ie. Fedorchuk, V.A. Kostin, O.L. Puzrin

E.O. Paton Electric Welding Institute of the NASU
11 Kazymyr Malevych Str., 03150, Kyiv, Ukraine

ABSTRACT

The paper gives the results of investigations on vacuum diffusion welding of MA2-1 magnesium alloy. Different technological measures were used in welding: unsupported welding, welding with application of forming matrices, welding without interlayers and with a zinc interlayer. It is found that it is not possible to produce the joint in unsupported welding without an interlayer at 400 °C temperature and process duration less than 60 min. Increase of welding temperature or time leads to considerable grain growth. Application of 250 μm zinc interlayer and of the following welding mode: T = 320 °C, P = 10 MPa, t = 30 min allows producing the joint. Analysis of chemical composition in different areas of the joint zone shows that development of diffusion processes in the butt during welding results in pore formation with magnesium content on the level of 17.8–20.12 wt.% in the zinc interlayer at 2–3 μm distance from magnesium/zinc contact line. In the central part of the joint zone the metal chemical composition is close to pure zinc composition. Application of forming matrices and an interlayer of zinc in the solid-liquid state in welding in the following mode: T = 340 °C, P = 10 MPa, t = 30 min. allows producing sound joints due to localisation of plastic deformation in the butt joint. Results of metallographic investigations showed formation in the butt joint of common grains and remains of the interlayer in the form of dispersed particles of 15–50 μm size, with chemical composition of Mg–4.53Al–0.20Mn–63.49Zn, wt.%, having an irregular elongated shape.

KEYWORDS: vacuum diffusion welding, magnesium alloy, interlayer, microstructure, microhardness

INTRODUCTION

Magnesium is one of the most common elements in the earth's crust. It is the most lightweight material of all the structural metals. Its density of 1.74 g/cm^3 is four times lower than that of steel and by a third lower than that of aluminium. Owing to its low density and high specific mechanical properties, magnesium is becoming ever wider accepted in different industries, such as automotive (steering wheels, seat frames, steering column housing, driver airbag housing, steering wheels, etc.), aerospace (parts of turbofan engine box, engine compressor housing, transmission case, etc.), medicine (implants), electronic equipment (housing for mobile phones, computers, laptops, cameras and portable media players), sport (archery bow handles, tennis rackets, golf clubs, bicycle frames, and roller skate chassis), manual tools (chain saw housings, housings of gears and hand tool motors, handles of hand shears and hand drills) [1, 2].

An essential increase of the production of magnesium and its alloys requires development of effective joining methods. It is known that fusion welding leads to softening of magnesium alloys in the joint zone, formation of welds with a coarse-crystalline structure, and it is accompanied by appearance of pores, microinclusions of oxide films and cracks, formation of which is caused by metal melting and subsequent solidification [3, 4].

Diffusion welding is an attractive technology in this respect, which allows avoiding defects, often appearing at application of fusion welding methods. According to literature sources, in welding without interlayers at a temperature below 420 °C, the diffusion processes in the butt are slowed down, the contact line is clearly visible; and shear strength of such samples is low. Application of a higher temperature (450–490 °C) in combination with a longer welding duration (90–120 min) leads to excess grain growth, and, consequently, to deterioration of the joint mechanical properties [5, 6].

Application of interlayers allows producing sound joints; however, the welding temperature remains high. So, welding through a silver interlayer is performed at 480–500 °C [7, 8], through a copper interlayer — at 480–530 °C [9, 10], through nickel interlayer — at 515–520 °C [11, 12].

Given examples point to the need to apply interlayers, which alongside surface activation, would allow conducting the process at lower temperatures. Pure zinc interlayers can be regarded as one of such promising materials.

The objective of the study was to determine the influence of a zinc interlayer in diffusion welding of MA-1 magnesium alloy on formation of structure and properties of the welded joints.

MATERIALS AND PROCEDURE

Vacuum diffusion welding (VDW) of MA2-1 magnesium alloy (Mg – 3.8–5.0Al – 0.8–1.5Zn –

0.3–0.7Mn, wt.%) [13] was conducted in P-115 unit at the temperature of 250–560 °C, 10 MPa pressure, 15–60 min process duration, and vacuum in the chamber was maintained on the level of $1.33\cdot10^{-3}$ Pa. Welding of 15×10×1.5 mm plates was conducted both in an unsupported state and using forming matrices. Welding in unsupported state envisages free deformation of the samples during the welding thermodeformational cycle. With this welding scheme, deformation of the entire sample takes place. In welding using forming matrices (forced deformation) conditions are in place for plastic deformation localization in the sample joint zone. The oxide film was removed from the sample contact surfaces by mechanical scraping, which was followed by degreasing them in ethyl alcohol. Pure zinc foil 250 μm thick was used as an interlayer.

Microstructural studies of the welded joints were conducted on transverse microsections in metallographic optical microscope Neophot-32 and scanning electron microscope JEOL JSM-840 in secondary-electron imaging mode (SEI). Electron microscope is fitted with a combined system for energy dispersive microanalysis INCA PentaFet-x3. Microsections were prepared by a standard procedure on high-speed polishing grinders, using diamond pastes of different dispersion. Sample polishing was conducted to 14th class of surface cleanliness. Grain size was determined by a linear method with application of a micrometer eyepiece, using from 10 to 20 fields of vision. Hardness of phase components was measured by Vickers in M-400 hardness meter of Leco Company. The load was 1N (100 gr), load application time was 10 s.

RESULTS AND THEIR DISCUSSION

MA2-1 alloy in the initial state has a fibrous structure with a uniform size distribution of grains. Grains of 22–25 μm size prevail in the metal structure, but individual regions with grain size of 10–15 μm are observed (Figure 1). In keeping with the scientific sources, the grain structure is α-solid solution [14]. Grain boundaries are thicker, secondary phase ($Mg_{32}(Al, Zn)_{49}$ or Mg_4Al_3), probably, evolves along them [15]. Traces of rolling texture are preserved in the sample central part. As a result of chemical heterogeneity of the material, a small region with dark precipitates is observed in the sample center. Hardness distribution over the microsection plane is rather nonuniform: it is 501–591 MPa in the area of chemical heterogeneity, 451–453 MPa in the center without precipitates, and 473–507 MPa along the sample ends at 100–150 μm distance from the edge.

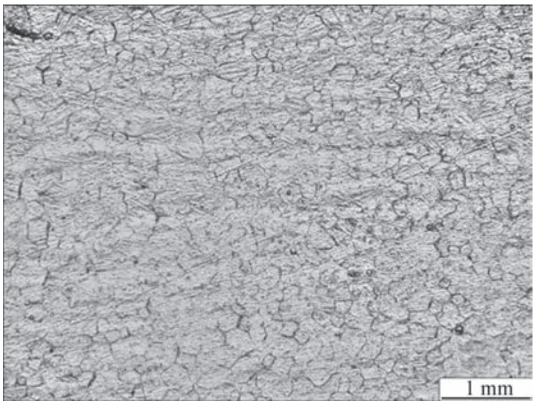

Figure 1. Microstructure of MA2-1 alloy in the initial state

Experiments were conducted on vacuum diffusion welding of MA2-1 alloy in an unsupported state without interlayer application. It is shown that the joint cannot be produced at welding duration of less than 60 min at 400 °C temperature: samples break at the microsection preparation stage. Note that at process duration of 15 min, interaction between the sample contact surfaces was absent. With increase of holding time individual adhesion areas began to be observed between the surfaces being welded (Figure 2, *a*). Grain size here is predominantly equal to 35–100 μm, and individual grains of 200–320 μm size are present. Material microhardness varies in the range of 438–566 MPa, its value being 502 MPa on the joint line.

Welding temperature rise even to 560 °C does not allow producing sound welded joints (Figure 2, *b*). After the welding thermodeformational cycle 150–350 μm is the predominant grain size for MA2-

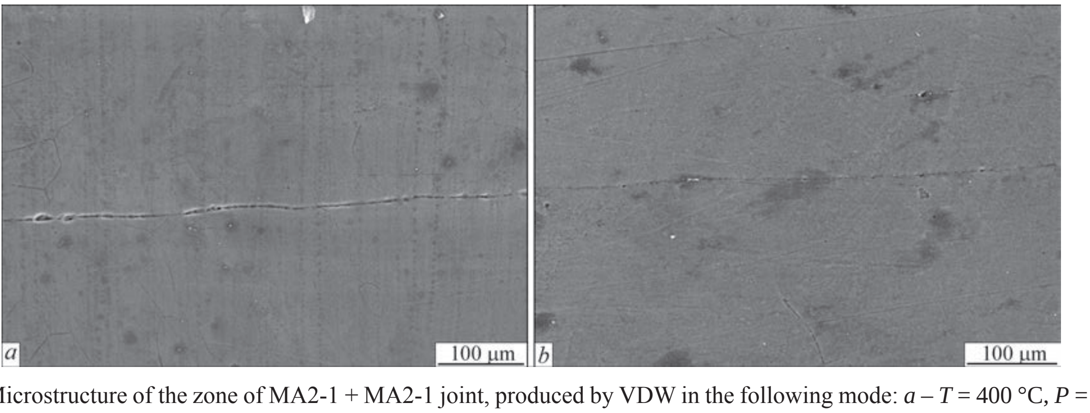

Figure 2. Microstructure of the zone of MA2-1 + MA2-1 joint, produced by VDW in the following mode: *a* – T = 400 °C, P = 10 MPa, t = 60 min; *b* - T = 560 °C, P = 10 MPa, t = 15 min

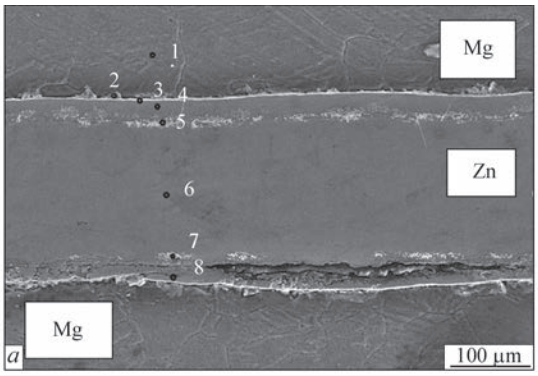

Spectrum number	Element content, wt.%			
	Mg	Al	Mn	Zn
1	99.39	–	0.09	0.52
2	66.41	0.91	0.21	32.47
3	62.06	1.14	0.28	36.52
4	20.12	–	–	79.88
5	3.27	0.15	0.31	96.27
6	2.26	–	–	97.74
7	–	–	0.10	99.90
8	17.80	–	–	82.13

b

Figure 3. Microstructure (*a*) and chemical composition (*b*) of the zone of MA2-1 + Zn + MA2-1 joint produced by VDW in the following mode: $T = 320$ °C, $P = 10$ MPa, $t = 30$ min

1 alloy, individual clusters of 60–100 μm grains and separate grains, growing through the entire sample thickness, are observed. Note a marked degradation of the joint metal: after high-temperature impact of the welding mode, brittle fracture of the magnesium alloy is in place, as a result of intensive grain growth. Microhardness of such joints is more uniform, and it varies from 371 MPa in the joint zone to 458 MPa closer to the sample outer boundaries. It is attributable to complete development of the recrystallization process and disappearance of texture traces with simultaneous homogenization of the chemical composition.

It is known that interlayer application in diffusion welding allows localizing plastic deformation in the butt joint [16]. That is why interlayers in the form of foil were used in further studies.

Zinc of 250 μm thickness was selected as an interlayer. Zinc application allows an essential lowering of process temperature to 320 °C. In keeping with the equilibrium state diagram, several eutectic reactions are observed in magnesium-zinc system at 340 and 368 °C temperatures. Increase of welding temperature up to a value higher than the eutectic reaction temperature leads to component melting and zinc penetration throughout the entire thickness of the sample, resulting in further brittle fracture of the sample. Welding at lower temperatures of 250–300 °C does not provide the conditions for joint formation.

Figure 3 shows the microstructure (*a*) and chemical composition (*b*) of the joint zone of samples produced in the following mode: $T = 320$ °C, $P = 10$ MPa, $t = 30$ min.

After welding the interlayer thickness is ~200 μm. The results of metallographic investigations lead to the conclusion that welding magnesium to magnesium with zinc interlayer application is quite promising, as it allows the joints to be produced at relatively low temperatures. It should be noted, however, that a chain of longitudinal pores forms in joint zone from both sides as a result unbalanced diffusion flows. Analysis of the chemical composition of different regions of the joint zone shows that pores form in the zinc interlayer at 2–3 μm distance from magnesium/zinc contact line with magnesium content on the level of 17.8–20.12 wt.%, which corresponds to

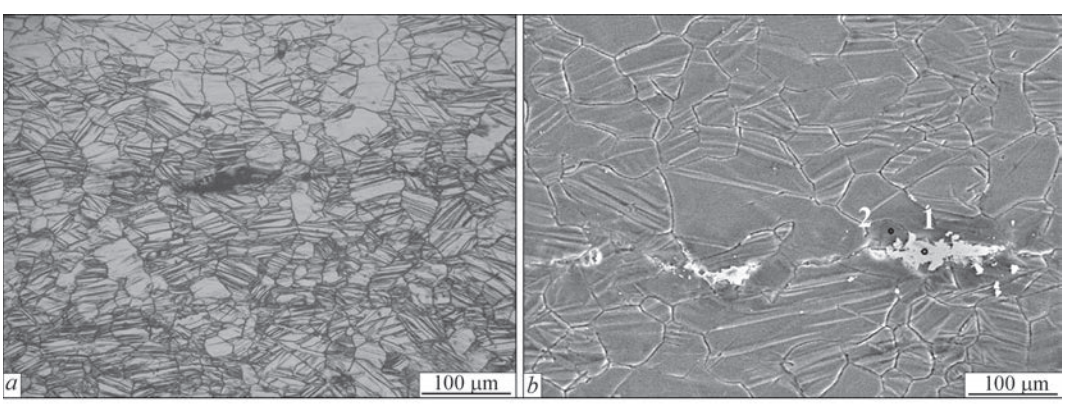

Spectrum number	Element content, wt.%			
	Mg	Al	Mn	Zn
1	31.77	4.53	0.20	63.49
2	98.71	2.51	0.06	1.72

c

Figure 4. Microstructure (*a*) and chemical composition (*b*) of the zone of MA2-1 + Zn + MA2-1 joint produced by VDW in forming matrices in the following mode: $T = 340$ °C, $P = 10$ MPa, $t = 30$ min

$MgZn_2$ phase [17]. In the central part of the joint zone (point 6), the metal chemical composition is close to that of pure zinc (Zn – 2.26Mg, wt.%).

Variation in grain size was detected in the metal structure with a large number of twins located at 500 μm distance from the weld deeper in the metal with finer grain of 30–100 μm. At greater depth the grains are of 100–200 μm size with isolated twins. Joint microhardness is rather uniform, except for 20 regions, where $MgZn_2$ phase formed. Here, microhardness is increased to 580 MPa, compared to 330–458 MPa for other sample regions.

Further studies were conducted in welding in forming matrices, which ensure plastic deformation localizing in the sample joint zone during the thermodeformational cycle of welding. Figure 4 shows the microstructure (*a*, *b*) and chemical composition (*c*) of the joint zone of samples produced in forming matrices in the following mode: $T = 340$ °C, $P = 10$ MPa, $t = 30$ min.

In this case, zinc is practically completely removed from the butt joint. The cause for that is the welding process proceeding in the solid-liquid state. As shown by microstructural analysis, growing of common grains through the joint zone takes place in the butt joint, which is indicative of active running of the diffusion processes. Isolated dispersed inclusions of an irregular shape, oriented in the direction of the metal flow, are observed in the butt joint. Inclusion size is 15–50 μm. White inclusions in Figure 4, *b* are $Mg_{51}Zn_{20}$ phase, according to [17]. Mean grain size in the magnesium alloy is mostly equal to 15–60 μm, with separate grains of up to 200 μm. Microhardness along the joint zone is nonuniform, varying in the range of 594–660 and 330–479 MPa for regions with $Mg_{51}Zn_{20}$ phase inclusions and without it, respectively. It can be assumed that such a microhardness distribution will not have a negative impact on the joint mechanical properties, as intermetallic inclusions are of a dispersed nature. Microhardness in the base metal is 371–526 MPa. Evaluation of the joint bending strength was performed, which showed that the bend angle of samples with a zinc interlayer, produced by diffusion welding in forming matrices, is equal to 180°, unlike samples produced without using the interlayer, which fail at microsection preparation stage.

CONCLUSIONS

Proceeding from the derived results, we can conclude that it is difficult to produce sound welded joints in vacuum diffusion welding of MA2-1 alloy without using interlayers.

Welding performance in the mode of $T = 340$ °C, $P = 10$ MPa, $t = 30$ min, with application of forming matrices and zinc interlayer which is in the solid-liquid state, allows producing sound joints. Based on the results of metallographic studies, formation of common grains and practically complete removal of the interlayer are observed in the butt joint with appearance of dispersed particles of 15–50 μm size elongated along the joint line with chemical composition of Mg–4.53Al–0.20Mn–63.49Zn, wt.%. The nature and detailed explanation of the mechanism of joint formation through an interlayer which is in a solid-liquid state, under the impact of local plastic deformation in the butt joint, requires further studies.

REFERENCES

1. Manoj Gupta, Nai Mui Ling Sharon (2011) *Magnesium, magnesium alloys, and magnesium composites*. Hoboken, New Jersey, John Wiley & Sons, Inc.
2. Gialanella, S., Malandruccolo, A. (2020) *Aerospace Alloys*. Springer, Cham.
3. Min, D., Shen, J., Lai, S., et. al. (2009). Effect of heat input on the microstructure and mechanical properties of tungsten inert gas arc butt-welded AZ61 magnesium alloy plates. *Materials Characterization*, 60(**12**), 1583–1590. DOI: http://doi.org/10.1016/j.matchar.2009.09.010
4. Abbas, M., Khan, A., Ali, M. et. al. (2014) Effect of weld current and weld speed on the microstructure and tensile properties of magnesium alloy specimens during tungsten inert gas. *Technical J.*, 19(**II**), 35–39.
5. Fei, Lin, Tiepeng, Li, Lulu, Sun, Qingsen, Meng. (2012) A study on vacuum diffusion bonding of as-extruded AZ31 magnesium alloy. *Applied Mechanics and Materials*, 121–126(**10–14**). DOI: https://doi.org/10.4028/www.scientific.net/AMM.121-126.10
6. Fei, Lin, Jie, Li, Hongwei, Zhao et. al. (2013) Experimental research on vacuum diffusion bonding of as-extruded AZ61 magnesium alloy. *Advanced Materials Research*, **788**, 34–37. DOI: https://doi.org/10.4028/www.scientific.net/AMR.788.34
7. Zhang, Weixiang, Du, Shuangmin (2013) Investigation into Cu-interlayered diffusion bonding trial of AZ31B alloy. *Advanced Materials Research*, 167–171(**631–632**). DOI: https://doi.org/10.4028/www.scientific.net/AMR.631-632.167
8. Torun, O., Karabulut, A., Baksan, B. et. al. (2008) Diffusion bonding of AZ91 using a silver interlayer. *Materials and Design*, **29**, 2043–2046. DOI: https://doi.org/10.1016/j.matdes.2008.04.003
9. Reza, Ghavami, Ayoub, Halvaee, Amir, Hadian (2019) Effect of bonding temperature on interface properties of AZ31 magnesium alloys joined by transient liquid phase using silver interlayer. *Materials Research Express*, **6**, 1–9. DOI: https://doi.org/10.1088/2053-1591/ab44df
10. Sun, D.Q., Liu, W.H., Gu, X.Y. (2004) Transient liquid phase bonding of magnesium alloy (Mg–3Al–1Zn) using copper interlayer. *Mater. Sci. and Technol.*, 20(**12**), 1595–1598. DOI: https://doi.org/10.1179/174328413X13789824293506
11. Jin, Y.J., Khan, T.I. (2012) Effect of bonding time on microstructure and mechanical properties of transient liquid phase bonded magnesium AZ31 alloy. *Materials and Design*, **38**, 32–37. DOI: https://doi.org/10.1016/j.matdes.2012.01.039
12. AlHazaa, A.N., Khalil Abdelrazek Khalil, Muhammad A. Shar (2016) Transient liquid phase bonding of magnesium alloys AZ31 using nickel coatings and high frequency induction heat sintering. *J. of King Saud University Science*, **28**, 152–159. DOI: https://doi.org/10.1016/j.jksus.2015.09.006
13. GOST 14957–76: *Wrought magnesium alloys. Grades* [in Russian].
14. Morozova, G.I. (2008) Phase composition and corrosion resistance of magnesium alloys. *Metallovedenie i Termich. Obrab. Metallov*, **3**, 8–12 [in Russian].

15. Shi, Z.Z., Zhang, W.Z. (2013) Prediction of the morphology of $Mg_{32}(Al, Zn)_{49}$ precipitates in a Mg–Zn–Al alloy. *Intermetallics*, **39**, 34–37. DOI: https://doi.org/10.1016/j.intermet.2013.02.023
16. Piskun, N.V., Falchenko, Yu.V., Petrushinets, L.V. (2020) Formation of the structure and mechanical properties of joints of TiAlNb intermetallic alloy in diffusion welding. *The Paton Welding J.*, **2**, 2–8. DOI: https://doi.org/10.37434/tpwj2020.02.01
17. Okamoto, H. (1994) Comment on Mg–Zn (magnesium-zinc). *J. of Phase Equilibria*, **15**, 129–130. DOI: https://doi.org/10.1007/BF0266770

ORCID

Yu.V. Falchenko: 0000-0002-3028-2964,
L.V. Petrushynets: 0000-0001-7946-3056,
V.Ie. Fedorchuk: 0000-0002-9929-3231,
V.A. Kostin: 0000-0003-0625-2113,
O.L. Puzrin: 0000-0002-2677-4667

CONFLICT OF INTEREST

The Authors declare no conflict of interest

CORRESPONDING AUTHOR

Yu.V. Falchenko
E.O. Paton Electric Welding Institute of the NASU
11 Kazymyr Malevych Str., 03150, Kyiv, Ukraine.
E-mail: falchenko@paton.kiev.ua

SUGGESTED CITATION

Yu.V. Falchenko, L.V. Petrushynets, V.Ie. Fedorchuk, V.A. Kostin, O.L. Puzrin (2023) Diffusion welding of magnesium alloy MA2-1 through a zinc interlayer. *The Paton Welding J.*, **9**, 38–42.

JOURNAL HOME PAGE

https://patonpublishinghouse.com/eng/journals/tpwj

Received: 05.07.2023
Accepted: 09.10.2023

DOI: https://doi.org/10.37434/tpwj2023.09.07

IMPROVEMENT OF THE TECHNOLOGY OF MANUFACTURING LOW-HYDROGEN AGGLOMERATED FLUXES USING FUSED MATERIALS

I.O. Goncharov, V.V. Holovko, A.P. Paltsevych, A.M. Duchenko

E.O. Paton Electric Welding Institute of the NASU
11 Kazymyr Malevych Str., 03150, Kyiv, Ukraine

ABSTRACT

Gas chromatography method was used to study thermal desorption of hydrogen from mineral raw materials, used in manufacture of agglomerated welding fluxes. The good prospects for application of fused materials in the charge composition in agglomerated flux manufacture were established. Increase of fused material content in the composition of agglomerated flux charge leads to lowering of the flux susceptibility to sorption of environmental moisture. At increase of the content of fused material in the agglomerated flux charge from 15 up to 40 % the diffusible hydrogen content in the deposited metal decreases from 3.5 to 2.6 cm^3/100 g in submerged-arc welding with these fluxes.

KEYWORDS: hydrogen, automatic arc welding with agglomerated fluxes, low-alloy steels

INTRODUCTION

Metal structures from high-strength low-alloy (HSLA) steels have been ever wider introduced into production over the recent years [1, 2]. In high-strength steel welding the metal under the influence of the thermal cycle can form structures which, on the one hand promote considerable strengthening of the metal, and on the other hand, increase its cold cracking susceptibility [3, 4]. Metal ability to resist cold crack initiation and propagation becomes higher with lowering of diffusible hydrogen concentration in it. Conditions were determined, under which the risk of cold cracking in welded joints is minimized. So, in the case of limiting the metal cooling rate to 10 °C/s in the temperature range of 600–500 °C and diffusible hydrogen content to 4 cm^3/100 g in the deposited metal, the level of stresses, which the metal of the HAZ of welded joints on steels with carbon equivalent C_e = 0.35–45 % can withstand without cold cracking, is equal to 90 % of its yield limit [5].

Considering the analysis of changes in the requirements to strength and ductility of high-strength low-alloy steels, a vast majority of the authors come to the conclusion that these requirements cannot be met when welding with the currently available fused fluxes [6, 7]. Thus, there is no alternative to the choice of agglomerated fluxes in high-strength steel welding. Their wide introduction in Ukraine is held back by absence of modern industrial production. In works [8, 9] the authors, while noting the advantages of agglomerated fluxes, also mention their inherent disadvantages, which are determined by their manufacturing method: higher susceptibility to environmental moisture sorption, lower strength of flux granules and dependence of flux quality on the quality of raw materials used in its manufacture. As regards the latter shortcoming, it needs an additional explanation. Owing to absence of pyrometallurgical and high-temperature processes in the liquid slag in agglomerated flux manufacture, it is impossible to lower the content of such impurities as sulphur, phosphorus, structural moisture and organic compounds in the charge material composition. Considering the higher level of requirements to the content of impurities in welding HSLA steels, the quality of agglomerated fluxes is largely determined by the quality of raw materials used in their manufacture. The high-quality raw materials necessary for agglomerated flux manufacture is either absent or very expensive in Ukraine. This is exactly the cause for absence of industrial production of agglomerated fluxes in Ukraine – the country where the first agglomerated fluxes were developed. On the other hand, at manufacture of fused fluxes there are capabilities for melt refining to remove impurities, and a high-capacity industrial production of fused fluxes is available, Ukraine taking the first place by the volumes of their manufacture until recently. It creates opportunities for development of a new technology of agglomerated flux manufacture, based on application of fused materials. In work [10] a conclusion is made about using fused materials, made by duplex-process technology, in the charge in manufacture of low-hydrogen agglomerated fluxes. Such materials have a low total content of sulphur, phosphorus and hydrogen. Thermal desorption of hydrogen from them occurs at up to 800 °C temperatures.

The objective of this work was determination of the influence of adding fused materials to the charge composition on their susceptibility to sorption of environmental moisture, and diffusible hydrogen content in the deposited metal in welding with the developed agglomerated fluxes.

PROCEDURES FOR STUDYING HYDROGEN CONTENT IN RAW MATERIALS AND DIFFUSIBLE HYDROGEN IN THE DEPOSITED METAL

Total content of hydrogen in raw materials was determined by the chromatographic method, having a high sensitivity to hydrogen, and resolution with respect to O_2, N_2, CH_4, CO, CO_2, H_2O [11]. It allows determination of both the total hydrogen content in the studied materials, and the process of hydrogen desorption at their heating up to the temperature of 1100 °C.

Diffusible hydrogen content in weld metal was determined by chromatographic analysis to GOST 23338°91 with application of OB 2781P gas analyzer. Sample heating temperature was 150 °C, which allowed reducing the hydrogen measuring time. The objectivity of the results of measuring the volume of diffusible hydrogen is due to the fact that hydrogen, which evolved from the sample in a sealed metal chamber, is measured by gas chromatography method. The reliability of the results of measuring the diffusible hydrogen content is confirmed by numerous comparative tests with mercury analysis method to ISO Standard 3690:2018 [12].

Samples for analysis of diffusible hydrogen content in the deposited metal were produced by bead deposition on a composite sample from 10G2FB steel with application of welding wire of Sv-10G1NMA grade at DCRP in the following mode: I_w = 550–600 A, U_a = 32–34 V, V_w = 36 m/h. Sample preparation and determination of diffusible hydrogen content in the deposited metal was performed to ISO 3690:2018.

INVESTIGATION OF HYDROGEN CONTENT IN RAW MATERIALS FOR AGGLOMERATED FLUX MANUFACTURE

Technology of agglomerated flux manufacture, unlike that of fused flux manufacture, has limited capabilities for lowering their hydrogen content. Raw materials are the main source of hydrogen in manufacture of agglomerated welding fluxes. That is why it is important to use non-traditional raw materials with limited hydrogen content. Conducted analysis of wastes of Ukrainian industrial enterprises showed that from such materials the most suitable for flux manufacture is granulated slag from silica manganese production and slag crust, which forms in welding large-diameter pipes. Table 1 gives their compositions.

These materials are remelted products and contain only a small amount of hydrogen, namely slag crust — 25 cm^3/100 g; and granulated slag from silica manganese production — 198 cm^3/100 g. Hydrogen is present in them in the form of moisture absorbed on their surface, which is readily removed by baking at up to 300 °C temperature.

Analysis of hydrogen content was performed in raw materials which can be used in manufacture of agglomerated fluxes for welding. Investigations showed that hydrogen content is more than 1500 cm^3/100 g in G-OO alumina, and 6300 cm^3/100 g is periclase. Considering the high content of hydrogen in these materials, its content was also studied in other materials, which contain magnesium and aluminium oxides. In particular, conducted investigations showed that hydrogen content in white corundum of 25 A grade is equal to 92 cm^3/100 g, and in periclase powder for PPE-88 electric furnaces it is 1156 cm^3/100 g. Such a hydrogen level in materials is critical in terms of their applicability for agglomerated flux manufacture. That is why the influence of raw material heat treatment on their hydrogen content was studied. Thermogravimetric and differential thermal analyses of the above-mentioned materials were also performed in the range from 20 to 1000 °C. Such a study was conducted in air, and its purpose was to determine whether undesirable oxidation of the raw materials will occur simultaneously with hydrogen desorption from them at their baking. It was found that for the raw materials given below heat treatment at 900 °C is optimal, allowing hydrogen content in quartz sand to be lowered from 240 to 15 cm^3/100 g, in white corundum of 25A grade — from 92 to 10 cm^3/100 g, in fluorite concentrate — from 340 to 10 to 15 cm^3/100 g, in periclase powder for PPE-88 electric furnaces — from 1156 to 10 to 15 cm^3/100 g, and in fused flux — from 60 to 10 to 15 cm^3/100 g. It is proposed to conduct baking of charge materials for agglomerated flux manufacture at the temperature of 900 °C for 1 h before granulation.

It is understandable that high-temperature baking of raw material components in agglomerated flux manufacture is rather energy efficient. Investigations of the remelted products — slag crust and slag from silica manganese production showed that they have low total content of hydrogen and lower (up to 300 °C) temperature of removal of hydrogen-containing compounds. Therefore, it is promising to apply fused materials, including those made by duplex-process technology in agglomerated flux charge, to limit their hydrogen content.

Table 1. Chemical composition of granulated slag from silica manganese production and slag crust of AN-60 welding flux

Material name	Chemical composition, wt.%									
	SiO_2	MnO	CaF_2	CaO	Al_2O_3	MgO	FeO	P_2O_5	SO_2	Rest
Slag from silica manganese production	48.0	20.0	–	14.0	8.0	5.0	0.3	0.008	1.0	3.7
Slag crust of AN-60 flux	40.0	35.0	7.0	8.0	4.0	2.0	4.0	–	–	–

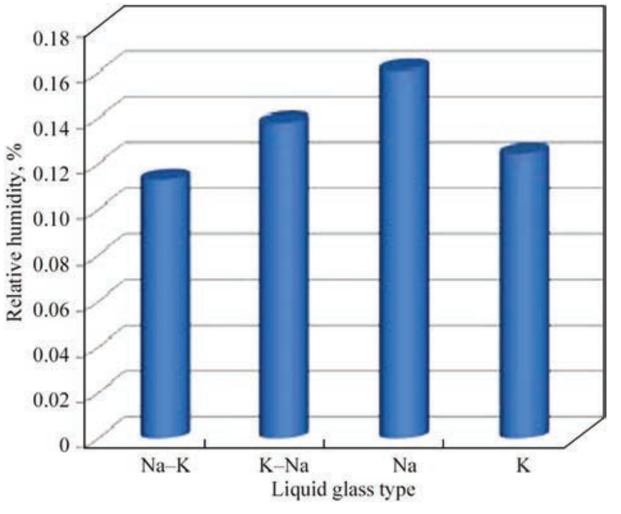

Figure 1. Influence of liquid glass type in the agglomerated flux charge on their susceptibility to moisture absorption

INVESTIGATIONS OF THE SUSCEPTIBILITY TO AMBIENT AIR MOISTURE SORPTION BY AGGLOMERATED FLUXES, HAVING FUSED MATERIALS IN THE CHARGE COMPOSITION

Technology of agglomerated flux manufacture is based on irreversibility of the process of dehydration of the liquid glass component during flux heat treatment. The final product of liquid glass dehydration is a strong, dense and moisture-resistant silicate film, having a certain resistance to environmental moisture absorption. The liquid glass type essentially influences the agglomerated flux susceptibility to moisture sorption (Figure 1).

Evaluation of the kinetics of sorption-induced moisture absorption by the fluxes was performed during which flux samples, baked at the temperature of 400 °C for 2 h before the experiment were soaked in the desicator with constant humidity of 77.6 % and temperature of 22 ± 0.5 °C. The lowest sorption capacity was demonstrated by agglomerated fluxes based on Na–K liquid glass.

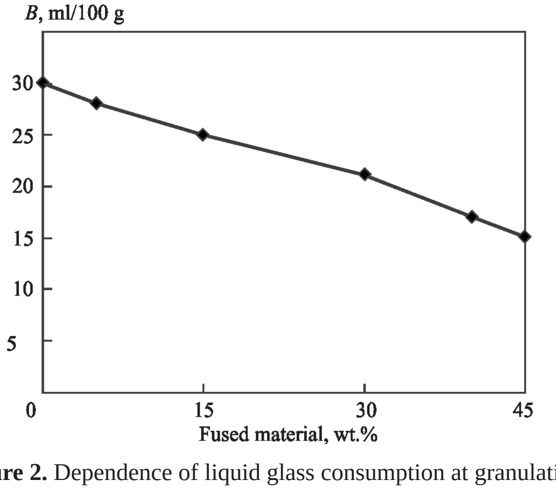

Figure 2. Dependence of liquid glass consumption at granulation of agglomerated flux on fused material content

Experimental agglomerated fluxes of $MgO–Al_2O_3–SiO_2–CaF_2–TiO_2–ZrO_2$ system were manufactured, which differed by the content of fused material in their composition. Screenings of AN-47 flux to GOST 9087 made by duplex-process, were taken as the fused material.

It was found that increase of the content of fused materials up to 45 %, in the agglomerated flux charge composition, which, in our opinion, have smaller specific surface compared to the traditional raw materials, leads to reduction of the quantity of binder required for granule formation from 30 to 15 % (Figure 2).

Content of liquid glass dry residue largely determines the agglomerated flux susceptibility to moisture absorption. This is confirmed by the results of comparative studies of fused and agglomerated fluxes based on mineral raw materials with different content of fused materials (Figure 3).

Increase of fused material content to 45 % leads to lowering of the flux sorption capacity by 46 %, and by this characteristic such flux is close to fused flux with glassy grain structure and it is superior to agglomerated aluminate basic fluxes, made by the traditional technology. In our study agglomerated OP-132 flux of Oerlikon Company, and fused manganese-silicate fluxes with pumice-like (AN-60) and glassy (AN-348A) grain structure were used for comparison.

INVESTIGATIONS OF DIFFUSIBLE HYDROGEN CONTENT IN THE DEPOSITED METAL IN WELDING WITH AGGLOMERATED FLUXES

Diffusible hydrogen content in the deposited metal was studied in welding with agglomerated fluxes of $MgO–Al_2O_3–SiO_2–CaF_2–TiO_2–ZrO_2$ system, which differed

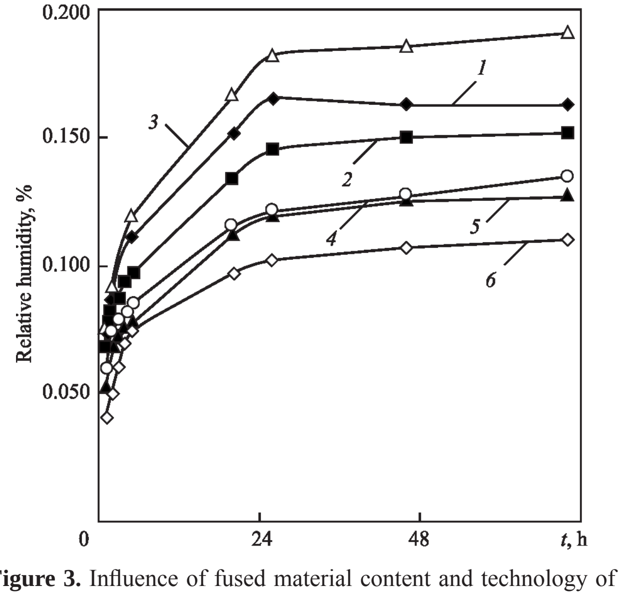

Figure 3. Influence of fused material content and technology of welding flux manufacture on flux susceptibility to sorption of environmental moisture: *1* — 15 % of fused material; *2* — 30 % of fused material; *3* — basic agglomerated aluminate; *4* — fused pumicelike manganese silicate; *5* — 45 % of fused material; *6* — fused glassy manganese silicate

Table 2. Influence of fused material content in agglomerated flux composition on diffusible hydrogen content in the deposited metal

Number	Content of fused material in the agglomerated flux charge composition	Diffusible hydrogen content $[H]_{dif. dep. metal}$, cm^3/100 g
1	15	3.2; 3.9; 3.5
2	40	2.6; 2.7; 2.3

by the content of fused material in their composition. Screenings of AN-47 flux to GOST 9087 made by duplex-process were taken as the fused material.

Investigation results are given in Table 2.

One can see from Table 2 that increase of fused material content from 15 to 40 % in the charge composition leads to reduction of the content of $[H]_{dif. dep. metal}$ below 3 cm^3/100 g. In keeping with the classification proposed by IIW, at $[H]_{dif. dep. metal}$ level below 5 cm^3/100 g welding electrodes are regarded as such which ensure a very low diffusible hydrogen content in the deposited metal [11]. Modern agglomerated fluxes of the leading world manufacturers provide $[H]_{dif. dep. metal}$ of up to 5 cm^3/100 g. Therefore, it can be considered that agglomerated fluxes, having fused materials manufactured by duplex-process in their charge composition, ensure extremely low hydrogen content in the deposited metal.

CONCLUSIONS

1. Gas chromatography method was used to study the total hydrogen content in mineral raw materials, applied in manufacture of agglomerated welding fluxes. It is proposed to conduct baking of charge materials for manufacture of agglomerated fluxes at the temperature of 900 °C for 1 h before granulation. The good prospects for application in the charge composition of wastes of Ukrainian industrial enterprises, which are remelted products and which contain a small quantity of hydrogen was established, namely slag crust of fused welding flux AN-60 (25 cm^3/100 g) and granulated slag of silica manganese production (198 cm^3/100 g). It was established that hydrogen is present in these materials in the form of moisture absorbed on the surface, which is readily removed by baking at up to 300 °C temperature.

2. It is found that increase of the content of fused materials in the charge composition of agglomerated fluxes up to 45 % leads to reduction of the quantity of binder required for flux granules formation from 30 to 15 %.

3. Increase of the content of fused material in the composition of agglomerated flux charge to 45 % leads to lowering of sorption capacity of the fluxes by 46 % and by this characteristic such fluxes are close to fused fluxes with glassy grain structure and are superior to agglomerated aluminate basic fluxes, made by the traditional technology.

4. With increase of the content of fused material in the composition of the agglomerated flux charge from 15 to 40 % the diffusible hydrogen content in the deposited metal in welding with agglomerated fluxes drops from 3.5 to 2.6 cm^3/100 g.

REFERENCES

1. Morrison, W.B. (2000) *Past and future development of HSLA steels. HSLA steels.* Beijing The Metallurgical Industry Press.
2. Komizo, Yu-ichi. (2006) Progress in structural steels for bridge and linepipe. *Transact. of JWRI*, **1**, 1–7.
3. Poznyakov, V.D. (2023) *Welding technologies for repair of metal structures.* Kyiv, PWI [in Ukrainian].
4. Tianli, Zhang, Zhuoxin, Li, Frank, Young et. al. (2014) Global progress on welding consumables for HSLA steel. *ISIJ Inter.*, **8**, 1472–1484.
5. Poznyakov, V.D. (2017) Welding technologies for production and repair of metal structures from high-strength steels. *Visnyk NANU,* **1**, 64–72 [in Ukrainian].
6. Golovko, V.V., Potapov, N.N. (2010) Peculiarities of agglomerated (ceramic) fluxes in welding. *Svarochn. Proizvodstvo,* **6**, 29–34 [in Russian].
7. Pokhodnya, I.K. (2003) Welding consumables: State-of-the-art and tendencies of development. *Svarochn. Proizvodstvo,* **6**, 26–40 [in Russian].
8. Bublik, O.V. (2009) Advantages and disadvantages of agglomerated (ceramic) fluxes in comparison with the fused fluxes of identical purpose. *Svarochn. Proizvodstvo,* **2**, 27–30 [in Russian].
9. Golovko, V.V. (2012) Agglomerated fluxes in local welding production (Review). *The Paton Welding J.,* **2**, 33–35.
10. Goncharov, I.O., Holovko, V.V., Paltsevych, A.P. et al (2023) Technologies for producing low-hydrogen fused fluxes. *The Paton Welding J.,* **7**, 37–42. DOI: https://doi.org/10.37434/tpwj2023.07.05
11. Pokhodnya, I.K., Yavdoshchyn, I.R., Paltsevych, A.P. et al. (2004) *Metallurgy of arc welding. Interaction of metals with gases.* Kyiv, Naukova Dumka [in Ukrainian].
12. ISO 3690:2018: *Welding and allied processes — Determination of hydrogen content in arc weld metal*.

ORCID

I.O. Goncharov: 0000-0003-2915-0435,
V.V. Holovko: 0000-0002-2117-0864,
A.P. Paltsevych: 0000-001-8640-7909

CONFLICT OF INTEREST

The Authors declare no conflict of interest

CORRESPONDING AUTHOR

I.O. Goncharov
E.O. Paton Electric Welding Institute of the NASU
11 Kazymyr Malevych Str., 03150, Kyiv, Ukraine.
E-mail: goncharovia@ukr.net

SUGGESTED CITATION

I.O. Goncharov, V.V. Holovko, A.P. Paltsevych, A.M. Duchenko (2023) Improvement of the technology of manufacturing low-hydrogen agglomerated fluxes using fused materials. *The Paton Welding J*., **9**, 43–46.

JOURNAL HOME PAGE

https://patonpublishinghouse.com/eng/journals/tpwj

Received: 19.06.2023
Accepted: 09.10.2023

DOI: https://doi.org/10.37434/tpwj2023.09.08

PROPERTIES OF WC–Co–Cr COATINGS, DEPOSITED BY MULTICHAMBER DETONATION DEVICE AND THEIR APPLICATION

O.V. Kolisnichenko, Yu.M. Tyurin

E.O. Paton Electric Welding Institute of the NASU
11 Kazymyr Malevych Str., 03150, Kyiv, Ukraine

ABSTRACT

Coatings from WC–Co–Cr AMPERIT®554.074 powder were deposited using a multichamber detonation device. Investigations of coating microstructure and phase composition were conducted, using scanning electron microscopy and X-ray structural analysis. Dense coatings form at spraying by this method, which consist of inclusions of tungsten carbide phases, uniformly distributed in Co–Cr matrix. Coating porosity is equal to ~0.2 %, microhardness is 10.4 ± 1.2 GPa. Experience of application of multichamber detonation device for deposition of wear-resistant coatings from WC–Co–Cr powder is shown, both at the stage of part reconditioning and at design of components of various mechanisms.

KEYWORDS: thermal spraying, detonation device, hard alloy, coating, microstructure, wear, porosity, hardness, industrial application

INTRODUCTION

Metal-ceramic coatings, spray-deposited by thermal methods, are an efficient solution of a wide range of problems as regards extension of the service life of parts of machines and various devices [1, 2]. Coatings based on tungsten carbide and chromium carbide are often used to improve the wear resistance in friction pairs, abrasive, corrosion and erosion wear in pumping and compressor and turbine equipment, pipeline and stop valves, parts for pulp and paper, textile and aviation industries, etc. Moreover, spraying of hard alloy coatings is believed to be an alternative to galvanic chrome plating, because of strict environmental standards and problems with consumption during the process of galvanic coating deposition [3]. Metal-ceramic coatings are applied predominantly by high-velocity oxyfuel (HVOF) method and detonation spraying (DS) [4–6], due to lower temperature of powder particles in the combustion product flow and shorter flight time, compared to plasma methods. It allows avoiding a considerable content of brittle phases, as well as lowering of the degree of carbide decomposition during spraying, while preventing a decrease of hardness and wear resistance. In addition, higher particle velocities in high-velocity processes ensure better quality coating with higher cohesion, adhesion, and low porosity. At present, in view of ever growing requirements to the quality of metal-ceramic coatings, work is in progress both on development of the new, and optimization of the current technologies of thermal spraying. Alongside HVOF and DS, such technologies as cold gas-dynamic spraying (CS) and method of high-velocity air-fuel spraying (HVAF) are ever wider used for metal-ceramics deposition [7, 8]. The direction of detonation spraying of metal-ceramic coatings is also developing [9]. As one of the numerous variants of the design of detonation guns for thermal spraying PWI developed a multichamber valveless detonation device (MCDD). The objective of this work is investigation of the microstructure and properties of coatings of WC–Co–Cr system, produced by MCDD, as well as the possibility of its application for coating deposition on products for various industries.

EQUIPMENT, MATERIALS AND PROCEDURES FOR INVESTIGATIONS

WC–Co–Cr powder (86 %–10 %–4 %) (H.C.Stark) with 15–45 μm particles size (AMPERIT®554.074 grade) was used for coating deposition on the surface of 12Kh18N10T steel samples. Investigations of powder microstructure, elemental composition and morphology (Figure 1, Table 1) were conducted in scanning electron microscope QUANTA 200 3D. Energy dispersive X-ray analyzer of EDAX Company, built into the scanning electron microscope, was used to obtain the spectra of the characteristic X-ray radiation of the powder sample surface.

Coatings were sprayed with multichamber detonation device (MCDD) [10]. This device realizes the mode of detonation combustion of a gas mixture in specially profiled chambers. The device is schematically shown in Figure 2.

Accumulation of combustion energy from the two chambers (cylindrical and circular) in the barrel ensures formation of a high-velocity jet of the combustion products, which accelerates and heats the powder

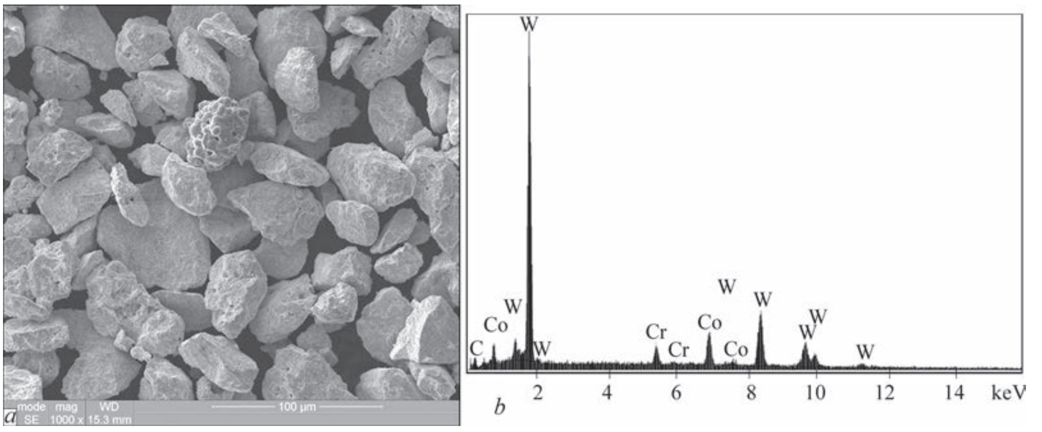

Figure 1. Powder of AMPERIT®554.074 grade: *a* — surface morphology of WC–Co–Cr powder; *b* — spectrum of characteristic X-ray radiation of the powder surface

Table 1. Elemental composition of WC–Co–Cr powder

Powder	Elements, wt.%/at.%			
	C	Cr	Co	W
WC–Co–Cr	4.77/36.94	3.57/6.39	9.60/15.16	82.05/41.51
Note. wt.% is the element weight fraction; at.% is the element atomic fraction.				

being sprayed [11]. In the device a continuous feeding of the combustible gas mixture and powder is realized, which allows initiation of the detonation combustion process at a high frequency of 20 Hz and higher. Figure 3 shows MCDD for spraying of coatings, located in a soundproof box, fitted with equipment for controlling the technological process. The equipment consists of a sprayer, standard powder feeder with feeding of up to 3 kg/h of powder, standard low pressure gas panel (max. 0.3 MPa) for feeding oxygen, propane-butane, air and automated control system.

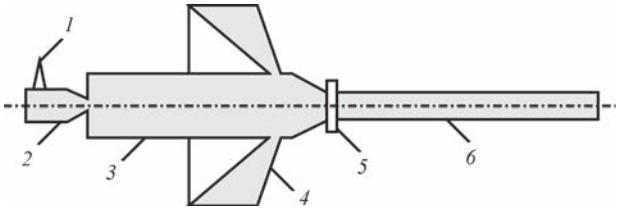

Figure 2. Schematic of a multichamber detonation device; *1* — spark plug; *2* — prechamber; *3* — cylindrical combustion chamber*; 4* — circular combustion chamber; *5* — powder feed; *6* — barrel

Figure 3. Device for coating deposition using MCDD

During spraying the speed of movement of the sprayed sample relative to the detonation device barrel was equal to 2000 mm/min, distance to the sample was 50 mm, powder consumption was 1/5 kg/h, transport gas flow rate (nitrogen) was 1 m^3/h, detonation frequency was 20 Hz. Table 2 gives the data on consumption of the combustible gas mixture components.

Structural-phase analysis of samples of the powder and sprayed coating from WC–Co–Cr was conducted by X-ray diffraction method in the range of 2θ angles from 20 up to 100° with step-by-step scanning $\Delta(2\theta) = 0.05°$ and 7 s exposure time in the point, using DRON-UM1 diffractometer (in monochromatic CuK_α-radiation, $\lambda = 0.154059$ nm), which provides integral information about a layer of the thickness of several microns. Graphite single crystal was used as a monochromator.

Transverse microsections were prepared to study the powder coatings on samples. Coating microstructure was examined using scanning electron microscope Quanta 200 3D. Porosity was determined by

Table 2. Flow rates of combustible mixture components

Flow rate of combustible mixture components, m^3/h		
Oxygen	Propane (70 %) + butane (30 %)	Air
2.7*/2.6**	0.66*/0.62**	1.7*/1.6**
*Cylindrical combustion chamber. **Circular combustion chamber.		

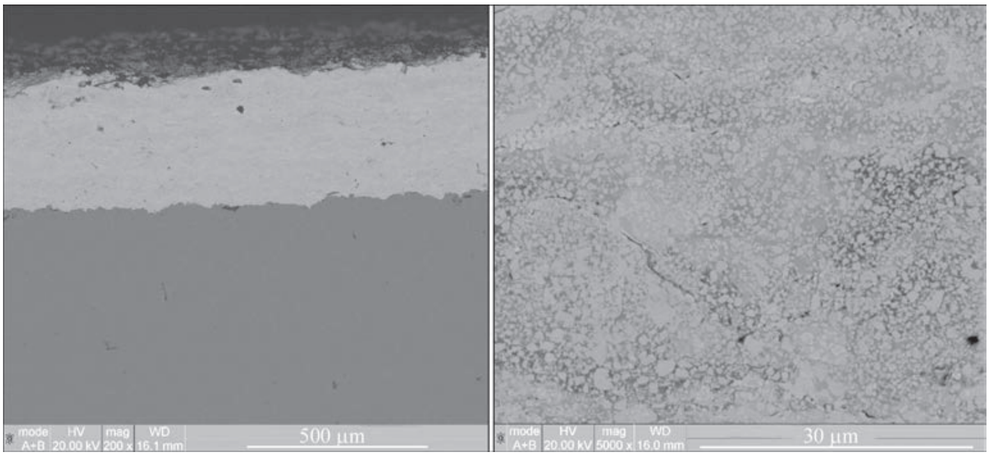

Figure 4. Image (SEM) of transverse microsection of WC–Co–Cr coating

the metallographic method with elements of qualitative and quantitative analysis of pore geometry, using optical inverted microscope Olympus GX51. Volume fraction of pores and structural components was determined using ATLAS software in several fields of vision. Microhardness is determined in keeping with DSTU ISO 6507-1:2007 in M-400 microhardness meter of LECO Company by Vickers test at 300 g load on the indenter.

Wear resistance of WC–Co–Cr coating was studied by tribometry methods using computer-controlled automated friction machine (Tribometer, CSM Instruments) by a standard ball-on-disc testing scheme to ASTM G-99 standard. The sample was mounted in a holder, and a rod was fastened normal to the sample plane, its end carrying a 6 mm dia ball from aluminium oxide. Testing was conducted in air (ambient air temperature of 30 °C, humidity of 23.8 %) at 10 N load and 10 cm/s linear speed, friction path was 1000 m.

INVESTIGATION RESULTS AND DISCUSSION

Figure 4 shows a scanning electron microscopy image at different magnification of surface microstructure of a transverse microsection of a sample with WC–Co–Cr coating.

Thickness of the deposited coatings on the examined samples was equal to approximately 370 ± 10 μm. No cracks or delamination areas were observed on the transverse section images.

Structural studies showed that the coatings consist of uniformly distributed carbide particles of 0.5 to 2 μm diameter and Co-Cr matrix interlayers of up to 1 μm thickness. In the coating micrographs the carbide particles are presented in the form of light-coloured areas with angled edges, unmelted during spraying, accordingly; the gray zone corresponds to the matrix, rich in Co and containing Cr, W and C. Black areas are pores. The histogram of pore size distribution in the coating is given in Figure 5. Porosity of WC–Co–Cr coating is equal to ~0.2 %.

X-ray structural analysis was conducted for a more detailed identification of phases, both in the initial powder and in the coating. X-ray structural analysis of the initial powders revealed that in the initial WC–Co–Cr powder (AMPERIT®554.074 grade, particle size composition of 45 + 15 μm) the main phase is WC (~80 %). Up to 12–14 % of Co_3W_3C phase was also found, its presence being probably related to processes occurring in powder manufacturing (bulk material sintering and sintered sponge grinding). The balance are Co_6W_6C and Co-Cr metal matrix (Figure 6, *a*). Analysis of coating roentgenographs (Figure 6, *b*) deposited using MCDD, showed that structure formation in this case is similar to phase formation processes, occurring when other methods of high-velocity thermal spraying are used [12]. New W_2C (~18 %) and W (~6 %) phases appear in the coating simultaneously with the main WC phase (~60 %). Their presence leads to the conclusion that the processes of WC grain dissolution and decarbonisation take place. During spraying the high-temperature products of detonation combustion heat the powder. Here, the decarbonisa-

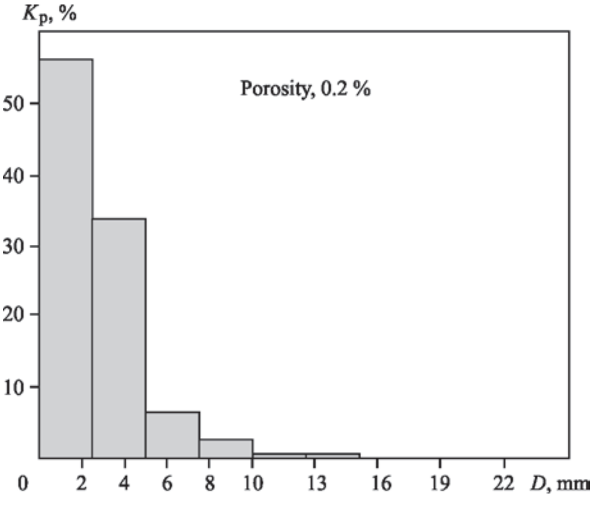

Figure 5. Pore size distribution

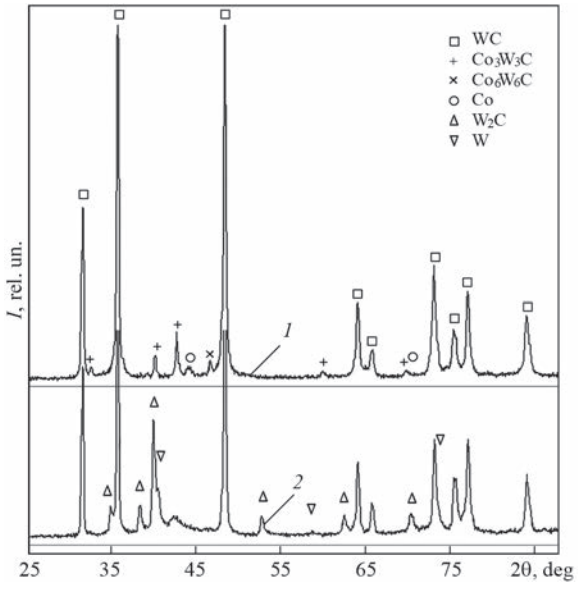

Figure 6. Analysis of coating roentgenograph: *a* — roentgenograph of initial WC–Co–Cr powder; *b* — coating roentgenograph

tion mechanism begins developing from melting of Co–Cr metal binder, as it has a lower melting temperature than that of WC carbides. Here, the boundaries of WC grains begin dissolving in the molten metal. As a result, carbon interacts with oxygen in the combustion products. At the moment of collision with the sample surface, the particles quickly cool down. W_2C layers form in the matrix from the oversaturated solid solution around the existing WC carbide particles. No Co peak (as in the powder) is found in the matrix. Despite the fact that W_2C hardness is higher than that of WC, presence of a more brittle W_2C phase, surrounding the WC particles, leads to lowering of wear resistance [6]. Moreover, enrichment of Co–Cr binding phase by tungsten and carbon increases its hardness and leads to strength decrease. In the roentgenograph a halo is present between angles $2\theta = 37–45°$, which is indicative of the fact that Co–Cr matrix can be in an amorphous-nanocrystalline state, which is determined by high cooling rates, inherent to the spraying process with application MCDD application.

Microhardness measurements were conducted over the entire coating cross-section. Obtained $HV_{0.3} = 10.4 \pm 1.2$ GPa value corresponds to hardness level in the coatings produced by various high-velocity spraying processes [4].

Intensity of wearing of the sample and the counterbody as a result of the conducted friction tests (Figure 7) was evaluated by the following formula:

$$W = V/(Pl),$$

where W is the wear intensity, $mm^3 \cdot n^{-1} \cdot m^{-1}$; V is the removed material volume, mm^3; P is the load, n; l — is the friction path, m.

Testing showed that the friction coefficient is equal to 0.527 ± 0.029 on average. Coating wear rate is $1.125 \cdot 10^{-5}$ $mm^3 \cdot n^{-1} \cdot m^{-1}$, and that of the counterbody is $4.603 \cdot 10^{-6}$ $mm^3 \cdot n^{-1} \cdot m^{-1}$.

EXAMPLES OF INDUSTRIAL APPLICATION OF THE COATING

High physical-mechanical and service properties of coatings from WC–Co–Cr powder, applied by MCDD, were confirmed in practice. For instance, it is rational to apply such coatings for reconditioning of stop valve components: gate valves, ball valves, wedge plugs, etc. (Figure 8, *a*). Metal-ceramic coatings have proven themselves well at reconditioning of parts for pulp and paper industry and polygraphy: scrapers, rollers, traction and support plates, valves and paper drawing shafts (Figure 8, *b*).

Application of metal-ceramic coatings is not limited only to part reconditioning sector. The produced coatings also allow development of fundamentally new engineering solutions for machine parts already at their design stage. As an example, Figure 9 shows parts from light alloys with a wear-resistant coating, spray-deposited by MCDD. WC–Co–Cr coating on

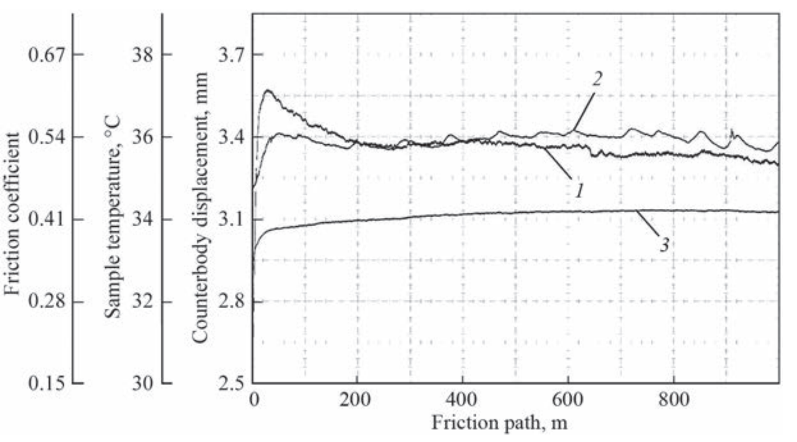

Figure 7. Friction parameters: *1* — friction coefficient; *2* — sample temperature; *3* — counterbody movement in the direction normal to the tested sample surface

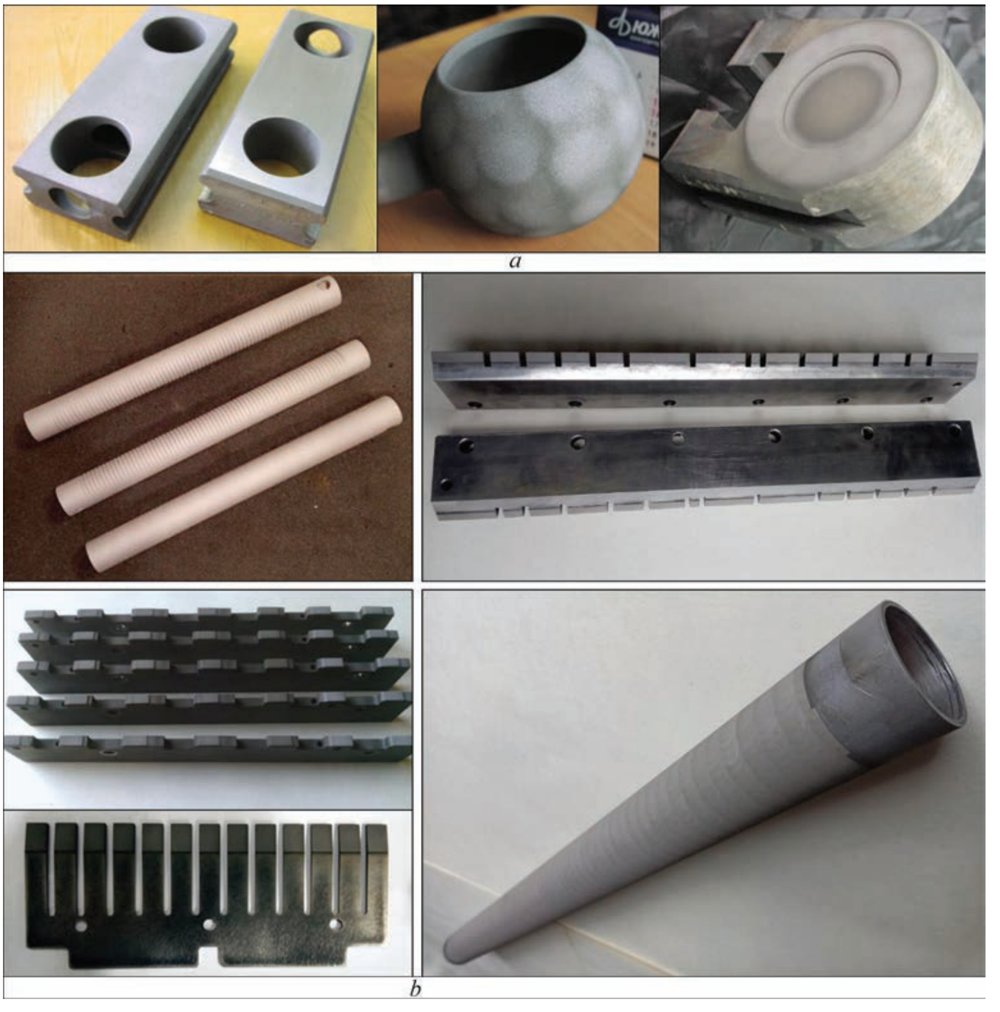

Figure 8. Parts with coating from WC–Co–Cr powder: *a* — stop valve parts; *b* — parts for pulp and paper industry and polygraphy

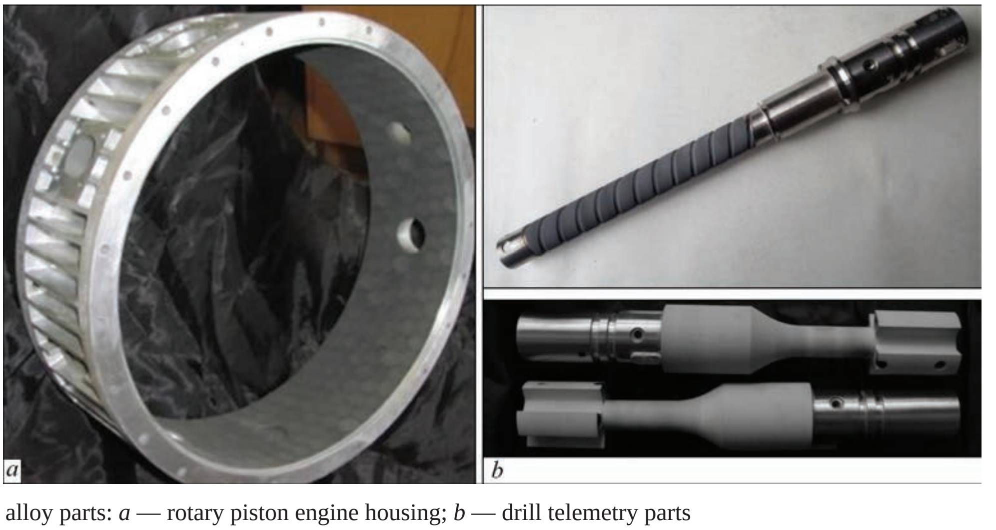

Figure 9. Light alloy parts: *a* — rotary piston engine housing; *b* — drill telemetry parts

the inner surface of rotary piston engine housing from an aluminium alloy allowed a considerable extension of its service life at weight reduction. Fulfilment of this condition is one of the most important elements during design of light flying vehicles. Application of a hard-alloy coating on titanium parts for drilling telemetry is geodesy enabled protecting them for intensive hydroabrasive wear and thus increasing the period between rather costly repair-adjustment operations.

Several examples of application of hard alloy coatings are considered. Now the range of problems solved is rather large and it is constantly expanded. Detonation spraying methods are also improved, and new samples of equipment are developed, which opens up new prospects and technology application spheres.

CONCLUSIONS

A multichamber detonation device was used to realize high-velocity thermal deposition of coatings from WC–Co–Cr powders.

X-ray diffraction analysis showed that coating formation with MCDD application is accompanied by the processes of partial decarbonisation of the carbides and formation of hard, but brittle phases, which is also characteristic for other HVOF and detonation methods of coating deposition, which are widely accepted.

Hardness of the produced coatings of $HV_{0.3}$ = = 10.4 ± 1.2 GPa and low porosity of ~0.2 % allow their application for prevention of abrasive, corrosion and erosion wear of the surfaces of various parts of machines and plants.

The effectiveness of WC–Co–Cr coatings deposited with MCDD application on the parts of various industrial devices has been confirmed by their practical application.

REFERENCES

1. Ang, A.S.M., Howse, H., Wade, S.A. et. al. (2016) Development of processing windows for HVOF carbide-based coatings. *J. of Thermal Spray Technol.*, **25**, 28–35. DOI: https://doi.org/10.1007/s11666-015-0318-z
2. Berger, L.M. (2015) Application of hardmetals as thermal spray coatings. *Int. J. of Refractory Metals and Hard Materials*, **49**, 350–364. DOI: https://doi.org/10.1016/j.ijrmhm.2014.09.029
3. Sun, B., Fukanuma, H., Ohno, N. (2013) Investigation and characterization of HVAF WC–Co–Cr coatings and comparison to galvanic hard chrome coatings. In: *Proc. of the Inter. Thermal Spray Conf. 2013 (May 13–15, 2013, Busan, Republic of Korea)*, 389–394.
4. Borisov, Yu.S., Astakhov, E.A., Murashov, A.P. et al. (2015) Investigation of structure and properties of thermal coatings of WC–Co–Cr system produced by high-velocity methods of spraying. *The Paton Welding J.*, **10**, 25–28. DOI: https://doi.org/10.15407/tpwj2015.10.04
5. Singh, L., Chawla, V., Grewal, J.S. (2012) A review on detonation gun sprayed coatings. *J. of Minerals and Materials Characterization and Engineering*, 11(**03**), 243. DOI: http://dx.doi.org/10.4236/jmmce.2012.113019
6. Picas, J.A., Punset, M., Baile, M.T. et. al. (2009) Properties of WC–Co–Cr based coatings deposited by different HVOF thermal spray processes. *Plasma Processes and Polymers*, **6**, 948–953. DOI: https://doi.org/10.1002/ppap.200932402
7. Torkashvand, K., Gupta, M., Björklund, S. et. al. (2021) Influence of nozzle configuration and particle size on characteristics and sliding wear behavior of HVAF-sprayed WC–Co–Cr coatings. *Surf. and Coat. Technol.*, **423**, 127585. DOI: https://doi.org/10.1016/j.surfcoat.2021.127585
8. Granata, M., Gautier di Confiengo, G., Bellucci, F. (2022) High-pressure cold spray coatings for aircraft brakes application. *Metals*, 12(**10**), 1558. DOI: https://doi.org/10.3390/met12101558
9. Bamola, R., Ewell, T., Robinson, P. et. al. (2016) Coatings deposited using a valve-less detonation system. In: *Proc. of the Int. Thermal Spray Conf. 2016 (May 10–12, 2016, Shanghai, P.R. China)*, 127–131. DOI: https://doi.org/10.31399/asm.cp.itsc2016p0127
10. Tyurin, Yu.M., Kolisnichenko, O.V. (2008) *Method of detonation spraying of coatings and device for its realization*. Pat. 8383, Ukraine.
11. 11.Kolisnichenko, O.V., Tyurin, Yu.N., Tovbin, R. (2017) Efficiency of process of coating spraying using multichamber detonation unit. *The Paton Welding J.*, **10**, 18–23. DOI: https://doi.org/10.15407/tpwj2017.10.03
12. Garfias Bulnes, A., Albaladejo Fuentes, V., Garcia Cano, I. et. al. (2020) Understanding the influence of high velocity thermal spray techniques on the properties of different anti-wear WC-based coatings. *Coatings*, 10(**12**), 1157. DOI: https://doi.org/10.3390/coatings10121157

ORCID

O.V. Kolisnichenko: 0000-0003-4507-9050,
Yu.M. Tyurin: 0000-0002-7901-7395

CONFLICT OF INTEREST

The Authors declare no conflict of interest

CORRESPONDING AUTHOR

O.V. Kolisnichenko
E.O. Paton Electric Welding Institute of the NASU
11 Kazymyr Malevych Str., 03150, Kyiv, Ukraine.
E-mail: okolis@i.ua

SUGGESTED CITATION

O.V. Kolisnichenko, Yu.M. Tyurin (2023) Properties of WC–Co–Cr coatings, deposited by multichamber detonation device and their application. *The Paton Welding J.*, **9**, 47–52.

JOURNAL HOME PAGE

https://patonpublishinghouse.com/eng/journals/tpwj

Received: 18.07.2023
Accepted: 09.10.2023